Ultrasonic flow stimulation and particles removal in a porous material

Pietro Poesio

Ultrasonic flow stimulation and particles removal in a porous material

Ultrasonic flow stimulation and particles removal in a porous material

Proefschrift

ter verkrijging van de graad van doctor
aan de Technische Universiteit Delft,
op gezag van de Rector Magnificus prof. dr. ir. J.T. Fokkema
voorzitter van het College voor Promoties,
in het openbaar te verdedigen
op maandag 6 december 2004 om 13.00 uur

door

Pietro POESIO
Ingegnere Meccanico, Università degli Studi di Brescia
geboren te Desenzano del Garda, Italië.

Dit proefschrift is goedgekeurd door de promotoren:
Prof. dr. ir. G. Ooms
Prof. dr. ir. M.E.H. van Dongen

Toegevoegd promotor: Dr. ir. D.M.J. Smeulders

Samenstelling promotiecommissie:

Rector Magnificus,	voorzitter
Prof. dr. ir. G. Ooms,	Technische Universiteit Delft, promotor
Prof. dr. ir. M.E.H. van Dongen,	Technische Universiteit Eindhoven, promotor
Dr. ir. D.M.J. Smeulders,	Technische Universiteit Delft, toegevoegd promotor
Prof. dr. Ing. G.P. Beretta,	Università degli Studi di Brescia
Prof. dr. P.K. Currie,	Technische Universiteit Delft
Prof. dr. ir. F.T.M. Nieuwstadt,	Technische Universiteit Delft
Prof. dr. V. N. Nikolaevskiy,	Institute of Earth Physics, RAS

The work presented in this thesis was supported financially by FOM.

ISBN 90-6464-109-9

Printed by Ponsen & Looijen, The Netherlands.

Stellingen behorende bij het proefschrift van Pietro Poesio

1. De invloed van hoog frequent geluid op de stroming van een vloeistof door een poreus materiaal kan verklaard worden uit de afname van de vloeistofviscositeit als gevolge van de temperatuursverhoging veroorzaakt door de dissipatie van de akoestische energie. (Dit proefschrift)

2. Akoestische "streaming" kan gemeten worden in een vloeistof die door een poreus materiaal stroomt, ofschoon het effect zwak is. (Dit proefschrift)

3. Brugvorming door deeltjes is een belangrijk vervuilingmechanisme tijdens de stroming van een vloeistof met kleine deeltjes door een poreus materiaal. (Dit proefschrift)

4. Ultrasone stimulatie kan effectief gebruikt worden om de permeabiliteit van het gesteente van een oliereservoir in de buurt van een boorput te verbeteren en daardoor de productiviteit te verhogen. (Dit proefschrift)

5. In de studie van een turbulent stromende suspensie dient in veel gevallen het zwaartekrachtseffect veroorzaakt door het dichtheidsverschil tussen de deeltjes en de vloeistof in rekening te worden gebracht.

6. Voor een olie/water kern/ring stroming door een pijpleiding kan de opwaartse kracht op de kern, te wijten aan het dichtheidsverschil tussen de twee vloeistoffen, gecompenseerd worden door de kracht op de kern ten gevolge van secondaire stromingen veroorzaakt door rimpels op het olie/water tussenoppervlak welke de vorm hebben van slangengolven. (G. Ooms and P. Poesio, Phys. Rev. E. 68, 066301, 2003.)

7. Brekingsindex "matching" geeft de mogelijkheid om (gebruikmakende van "particle image velocimetry") gelijktijdig het snelheidsveld in beide fasen van een vloeistof-vloeistof stroming of een deeltjes-vloeistof stroming te meten. Het is daarom een unieke techniek om een dieper inzicht te verschaffen in de fysica van zulke stromingen.

8. Soms is een eenvoudig model dat de voornaamste eigenschappen van een verschijnsel beschrijft beter dan een gedetailleerd model, waarvan de resultaten zo gecompliceerd zijn dat ze een goed begrip van het verschijnsel verhinderen.

9. Academisch onderzoek kan zeer nuttig zijn bij het oplossen van technologische problemen uit de industrie. Het probleem is een gemeenschappelijke taal te vinden.

10. Nederlanders zijn bijna altijd op tijd. Italianen zijn nooit te laat, of te vroeg. Zij komen eenvoudigweg, wanneer zij dat van plan zijn.

Deze stellingen worden verdedigbaar geacht en zijn als zodanig goedgekeurd door promotor, prof. dr. ir. G. Ooms.

Propositions going together with the thesis of Pietro Poesio

1. The influence of high-frequency acoustic waves on the flow of a liquid through a porous material can be explained by the viscosity decrease of the liquid due to the temperature increase caused by the dissipation of acoustic energy. (This theses)

2. Acoustic streaming can be measured in a liquid flowing through a porous material, although the effect is weak. (This theses)

3. Particle-bridge formation is an important fouling mechanism during the flow of a liquid with small particles through a porous material. (This theses)

4. Ultrasonic stimulation can be used effectively to improve the permeability of the near wellbore region of an oil reservoir and therefore to enhance the productivity. (This theses)

5. In the study of a turbulently flowing suspension the gravity effect caused by the density difference between the particles and the fluid has to be taken into account in many cases.

6. For oil-water core-annular flow through a pipeline the buoyancy force on the core, due to the density difference between the two liquids, can be counterbalanced by the force on the core due to secondary flows caused by ripples at the oil-water interface that have the shape of "snake" waves. (G. Ooms and P. Poesio, Phys. Rev. E. 68, 066301, 2003.)

7. Refractive index matching provides the possibility to measure simultaneously (using particle imaging velocimetry) the velocity field in both phases of a liquid-liquid flow or a solid -liquid flow. It is, therefore, a unique technique to provide a deeper insight in the physics involved in such flows.

8. Sometimes a simple model that describes the main features of a phenomenon is better than a detailed one, whose results are so complicated that it prevents a good understanding of the phenomenon.

9. Academic research can be very useful when solving technological problems from industry. The problem is to find a common language.

10. Dutchman are almost always on time. Italians are never too late, or too early. They simply arrive when they intend to.

These propositions are considered defendable and as such have been approved by the supervisor, prof. dr. ir. G. Ooms.

Ad Angelo, Linda
e Monica

Contents

Summary

An experimental and theoretical investigation has been made of the influence of high-frequency acoustic waves on the flow of a liquid through a porous material. The experiments have been performed on Berea Sandstone cores. Two acoustic horns were used with frequencies of 20 kHz and 40 kHz, and with maximum power output of 2 kW and 0.7 kW respectively. Also a temperature measurement of the flowing liquid inside the core was made. A high external pressure was applied in order to avoid cavitation. The acoustic waves were found to produce a significant effect on the pressure gradient at constant liquid flow rate through the core samples. During the application of acoustic waves the pressure gradient inside the core decreases. This effect turned out to be due to the decrease of the liquid viscosity caused by an increase in liquid temperature as a result of the acoustic energy dissipation inside the porous material. Also a theoretical model has been developed to calculate the dissipation effect on the viscosity and on the pressure gradient. The model predictions are in reasonable agreement with the experimental data.

The influence of high-frequency acoustic waves on the flow of a liquid through a porous material has been studied in more detail. Particular attention was paid to the phenomenon of acoustic streaming of the liquid in the porous material due to the damping of the acoustic waves. The experiments were performed on Berea sandstone cores. Two acoustic horns were used with frequencies of 20 kHz and 40 kHz, and with maximum power output of 2 kW and 0.7 kW respectively. A high external pressure was applied in order to avoid cavitation. A microphone was used to measure the damping of the waves in the porous material and also temperature and pressure measurements in the flowing liquid inside the cores were carried out. To model the acoustic streaming effect Darcy's law was extended with a source term representing the momentum transfer from the acoustic waves to the liquid. The model predictions for the pressure distribution inside the core under acoustic streaming conditions are in reasonable agreement with the experimental data.

A study has been made of the removal of small particles from a porous material by means of ultrasonic irradiation. The fouling particles were assumed to be attached to the pore walls due to colloidal forces. To that purpose a microscopic theoretical model has been developed to calculate the force of a traveling acoustic wave on a spherical particle attached to the wall of a smooth, cylindrical pore inside the porous material. This force was compared with the adhesion force between a small particle and a pore wall. From the comparison between the two forces the conditions were found, at which particles are detached from pore walls and removed from the porous material. The transformation of the results gained from the microscopic model to macroscopic property (permeability) of the porous material was made by means of the Kozeny relation. The aim was to be able to understand and predict qualitatively the influence of relevant parameters on the ultrasonic cleaning process. Predictions made with the theoretical model were compared with data from experiments carried out with ultrasound to remove particles from Berea sandstone. The agreement is reasonable.

Next the formation and ultrasonic removal of fouling particles bridges, blocking the pore throats in a porous material, were studied experimentally for the case of a natural sandstone. The influence of the liquid velocity, particle concentration and the ratio of the particle diameter to pore diameter on the level of fouling was as expected from the formation of particles bridges inside the sandstone. Attention was also given to the removal of the fouling particle structures by means of high-frequency acoustic waves.

The possibility to remove particles bridges was investigated numerically starting from a single

pore blocked by two spherical particles. First the adhesion force between a particle in a particles bridge and the pore wall material was calculated. Then the effect of acoustic waves on the particle bridge was determined. The comparison between the adhesion force and the acoustic detaching force determines whether a particles bridge will be removed or not. A sensitivity study was carried out to check the influence of different parameters such as wave amplitude, flow rate, aspect ratio and frequency. We developed an upscaling procedure to translate results obtained at (microscopic) pore level to the permeability at the macroscopic level. A reasonable agreement is found.

The fouling of a porous material by external particles and the optimal way to clean it by means of high-frequency acoustic waves were investigated carefully. Particular emphasis was given to the fouling by mud particles of the near wellbore region of an oil reservoir. Therefore we used in the experiments a natural sandstone as porous material and mud particles as fouling particles. To generate fouling mud particles were flushed through a sandstone core. Next the core was treated with very short bursts of ultrasound and the change in permeability was measured after each burst. Experiments were carried out under different acoustic-cleaning conditions to investigate the influence of the relevant parameters on the cleaning process. For instance, the amplitude of the acoustic waves, the duration of the bursts and the time between the bursts were varied. During the ultrasonic cleaning process brine flowed through the core. The influence of this flow was studied by changing the flow rate. Also the influence on the cleaning process of the temperature, pressure and initial core permeability was investigated. The experimental results show that short bursts of acoustic energy are more efficient for cleaning than long bursts or a continuous application of ultrasound (for the same total amount of acoustic energy). The overall conclusion is, that the optimal way of ultrasonic cleaning is by applying many very short bursts of low amplitude and a short rest time between the bursts while keeping the liquid (brine) flow at a very low velocity. More acoustic energy is needed to clean a core with a high initial permeability than a core with a low one. At low pressure cavitation occurs and prevents the generation of ultrasonic bursts.

A rather fundamental study of particles bridge formation was carried out. To that purpose the behavior of small particles in a linear shear field at low but finite Re-number was studied. We were interested in the hydrodynamic interaction between the particles and in the conditions under which they collide. The flow field around the particles were computed as function of time by means of the lattice-Boltzmann technique. The total force and torque acting on each particle was computed at each time step and the position of the particles was updated. The trajectories and the particle induced disturbances were studied for a variety of conditions. As mentioned special attention was given to the conditions that lead to collision of the particles and to particles bridge formation at the entrance to a pore throat.

Samenvatting

Er is een experimenteel en theoretisch onderzoek uitgevoerd betreffende de invloed van hoogfrequente akoestische golven op de stroming van een vloeistof door een poreus materiaal. De experimenten werden uitgevoerd aan kernen van Berea zandsteen. Twee akoestische hoorns werden gebruikt met frequenties van 20 kHz en 40 kHz, en met een maximum vermogen van 2 kW en 0.7 kW respectievelijk. De temperatuur van de stromende vloeistof binnen de kern werd gemeten. Een hoge druk werd toegepast om cavitatie te voorkomen. Bij een constant vloeistofdebiet door de kern bleken de akoestische golven een aanzienlijk effect op de drukgradiënt in de vloeistof binnen de kern te hebben. Gedurende de toepassing van akoestische golven nam de drukgradiënt af. Dit effect bleek veroorzaakt te worden door de afname van de vloeistofviscositeit als gevolg van de toename van de vloeistof temperatuur veroorzaakt door de akoestische energie dissipatie binnen het poreuze materiaal. Er werd ook een theoretisch model ontwikkeld om het effect van de energie dissipatie op de viscositeit en op de drukgradiënt te berekenen. De voorspellingen van dit model stemden redelijk overeen met de meetresultaten.

De invloed van de hoogfrequente akoestische golven op de stroming door een poreus materiaal werd daarna in meer detail bestudeerd. Speciale aandacht werd daarbij besteed aan het verschijnsel van de akoestische streaming in het poreuze materiaal veroorzaakt door de demping van de akoestische golven. De experimenten werden weer uitgevoerd aan Berea zandsteen kernen, en dezelfde akoestische hoorns als hiervoor genoemd werden gebruikt. Een microfoon werd gebruikt om de demping van de akoestische golven in het poreuze materiaal te meten. Ook werden de temperatuur en de druk van de stromende vloeistof in de kern gemeten. Om het akoestische streaming effect te modelleren werd de Darcy vergelijking uitgebreid met een bron term, die de impulsoverdracht van de akoestische golven naar de vloeistof representeert. De model voorspellingen voor de vloeistofdruk binnen de kern onder akoestische streaming condities bleken in redelijke overeenstemming met de meetresultaten.

Een onderzoek werd daarna gemaakt van het verwijderen van kleine vaste, interne deeltjes uit een poreus materiaal door middel van ultrasone bestraling van het materiaal. Deze interne deeltjes werden binnen het materiaal vrijgemaakt door een verandering van de samenstelling van de vloeistof. Er werd daarbij verondersteld, dat de vervuilende deeltjes aan de wanden van de porin gehecht waren vanwege collodale krachten. Een theoretisch model op microscopische schaal werd ontwikkeld om de kracht te berekenen uitgeoefend door een lopende akoestische golf op een bolvormig deeltje dat aan de wand gehecht is van een gladde, cilindrische porie binnen het poreuze materiaal. Deze kracht werd vergeleken met de adhesie kracht tussen een klein deeltje en de poriewand. Uit het vergelijk van de twee krachten werden de condities gevonden, waaronder deeltjes van poriewanden losgemaakt worden en vervolgens uit het poreuze materiaal. De vertaling van de resultaten van het microscopische model naar een macroscopische eigenschap (permeabiliteit) van het poreuze materiaal werd gemaakt met behulp van de Kozeny relatie. Het doel van dit gedeelte van het onderzoek was om de invloed van enige relevante parameters op de ultrasone verwijdering van deeltjes te begrijpen en kwalitatief te voorspellen. Modelvoorspellingen werden vergeleken met resultaten van metingen uitgevoerd tijdens het ultrasoon verwijderen van deeltjes uit Berea zandsteen. De overeenkomst was redelijk.

Vervolgens werd de vorming and ultrasone verwijdering van vervuilende deeltjesbruggen die de porin in een poreus materiaal blokkeren, experimenteel bestudeerd voor een natuurlijke zandsteen. De invloed van de vloeistofsnelheid, deeltjesconcentratie en de verhouding van de deeltjesdiameter

en poriediameter bleek te zijn zoals verwacht mocht worden van de vorming van deeltjesbruggen binnen zandsteen. Er werd ook aandacht besteed aan de verwijdering van de vervuilende deeltjesbruggen door middel van hoogfrequente akoestische golven. De mogelijkheid om deeltjesbruggen te verwijderen werd numeriek onderzocht uitgaande van een enkele porie die geblokkeerd wordt door twee bolvormige deeltjes. Eerst werd de adhesiekracht tussen een deeltje in een deeltjesbrug en het materiaal van de poriewand berekend. Daarna werd de kracht van de akoestische golven op de deeltjesbrug bepaald. Het vergelijk van de adhesiekracht en de akoestische kracht bepaalt, of een deeltjesbrug verwijderd zal worden of niet. En gevoeligheidsstudie werd uitgevoerd om de invloed van de verschillende parameters, zoals de akoestische golfamplitude, vloeistofsnelheid, de verhouding van deeltjesdiameter en poriediameter en frequentie te onderzoeken. Tenslotte werd een procedure ontwikkeld om de resultaten die op microscopische schaal verkregen waren te vertalen naar de permeabiliteit op macroscopische schaal.

De vervuiling van een poreus materiaal door externe deeltjes en de optimale wijze om zulke deeltjes ultrasoon te verwijderen, was het volgende onderwerp van onderzoek. Speciale aandacht werd gegeven aan vervuiling door deeltjes aanwezig in een boorvloeistof, die gedurende de boorfase vanuit de boorput in het aangrenzende gebied van een olievereservoir dringen. Daarom werd gedurende de experimenten weer een natuurlijke zandsteen als poreus materiaal gebruikt en deeltjes uit een boorvloeistof als vervuilende deeltjes. Om vervuiling te verkrijgen werden de deeltjes door de zandsteenkern gestroomd. (Een groot verschil tussen vervuiling door externe deeltjes en vervuiling door interne deeltjes is, dat vervuiling door externe deeltjes alleen in een dunne laag aan de buitenkant van het poreuze materiaal aanwezig is terwijl bij interne deeltjes het gehele materiaal vervuild is.) Vervolgens werd de kern bestraald met korte pulsen van hoogfrequente akoestische golven en na iedere puls werd de verandering in permeabiliteit gemeten. Experimenten werden uitgevoerd onder verschillende akoestische condities, om de invloed van relevante parameters op de verwijdering van deeltjes te bestuderen. De amplitude van de akoestische golven, de duur van de pulsen, en de tijd tussen de pulsen werden bij voorbeeld gevarieerd. Gedurende de ultrasone behandeling stroomde een vloeistof door de kern. De invloed van de vloeistofstroming werd onderzocht door de stroomsnelheid te variren. Ook de invloed van de temperatuur, de druk en de permeabiliteit vr vervuiling werd onderzocht. De experimenten toonden aan, dat korte pulsen van akoestische energie efficinter zijn dan langdurige pulsen of een continue toepassing van ultrasone bestraling (voor dezelfde totale hoeveelheid toegepaste geluidsenergie). De algemene conclusie is dat de optimale wijze van verwijdering van externe deeltjes is door het toepassen van vele korte pulsen van lage amplitude met een korte rusttijd tussen de pulsen, waarbij de snelheid van de vloeistofstroming laag gehouden wordt. Meer akoestische energie is nodig voor het verwijderen van vervuilende deeltjes uit een zandsteen met een hoge permeabiliteit vr vervuiling dan uit een zandsteen met een lage initile permeabiliteit. Bij te lage druk treedt cavitatie op, waardoor de generatie van ultrasone pulsen onderdrukt wordt.

Tenslotte werd een tamelijk fundamentele studie van deeltjesbrug vorming uitgevoerd. Daartoe werd het gedrag van kleine deeltjes in een lineair snelheidsveld bij een vaste wand bij lage maar eindige waarden van het Reynolds getal bestudeerd. Er was speciale aandacht voor de hydrodynamische wisselwerking tussen de deeltjes en in de condities waarbij ze botsen. Het stromingsveld rondom de deeltjes werd als functie van de tijd berekend met behulp van de rooster Boltzmann techniek. De totale kracht en torsie werkend op elk deeltje werd na ieder tijdstap bepaald en de nieuwe positie van de deeltjes berekend. De deeltjesbanen en de verstoring van het stromingsveld veroorzaakt door de deeltjes werden voor verschillende omstandigheden onderzocht. Speciale aandacht werd daarbij besteed aan de condities, die tot deeltjesbotsingen en tot deeltjesbrug vorming bij de ingang tot een porie leiden.

Chapter 1

Introduction

1.1 Introduction

Oil is retained under certain geo-chemical conditions in sedimentary rocks called reservoirs. Once oil has formed it migrates, under the action of gravity, toward the surface through permeable formations. If an impermeable layer is found, the oil is trapped and a reservoir is formed. A reservoir is, then, defined as a porous formation confined by impermeable boundaries. Once a suitable reservoir has been discovered and evaluated, wells have to be drilled in order to produce the oil.

In order to increase both the production rate and the total amount of oil that can be withdrawn from a reservoir, a number of techniques is applied. The ensemble of these techniques is called stimulation. Classical stimulation techniques are injection of acid or solvent, injection of steam and hydraulic fracturing. New techniques have been proposed and investigated. Tambini (2003) reviews non-conventional stimulation techniques and he mentions, among others, acoustic stimulation. It is claimed that acoustic stimulation can be used to stimulate the total reservoir by using waves with a frequency in the range of 500 Hz. However, there is no real evidence to prove this assertion. In this thesis we will only deal with the acoustic stimulation of the near wellbore region of an oil reservoir. For this application ultrasonic waves are used with a frequency in the range of 15 kHz or higher.

There are, in principle, several explanations for the near wellbore stimulation of a reservoir. A possible explanation is, that the ultrasonic waves heat up the oil and decrease its viscosity. Or the acoustic waves can increase the effective permeability of the porous rock (for instance due to peristaltic transport, see Aarts & Ooms (1998)). We refer to this explanation as: flow stimulation. Another explanation is that the high frequency acoustic waves remove fouling particles that tend to accumulate in the near wellbore region. This explanation is referred to as: ultrasonic cleaning.

There are two reasons for the fouling by small particles of the near wellbore region. For instance, the particles penetrate from the bore mud into the rock formation during the exploration (drilling) phase. A SEM-picture of mud particles invasion is shown in Fig. 1.1. Reduction in permeability can also be induced by internally generated particles during the production phase. After oil starts to be produced, water, or steam, is injected from the injection well. Due to the change in salinity the chemical composition of the rocks changes and small particles are generated inside the rock.

1.2 Literature review

The first use of ultrasounds to improve oil recovery dates back to 1950s and 1960s. Sherborne (1954) proposed the use of ultrasounds in an oil-bearing formation during liquid flooding to enhance extraction efficiency. Bodine, in a series of patents (see Beresnev & Johnson (1994) for a full list), proposed the use of acoustic waves to clean petroleum-bearing strata, to induce additional fracturing in reservoirs and to enhance mobility or to achieve a more effective penetration

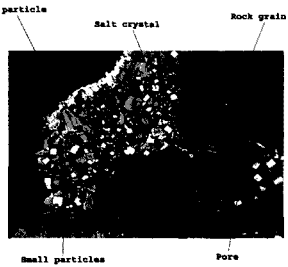

Figure 1.1: SEM-photograph of an oil bearing rock. Black holes are places where a mixture of oil and water is present. Gray grains form the solid skeleton and, in this case, they are quartz particles. Cubic elements are salt crystal resulting from the drying process necessary to take the picture.

of injected chemicals into the formation. However, these studies do not provide a physical insight into the stimulation phenomenon. The literature about field tests is reviewed in section 1.2.1. Thereafter, laboratory studies and theoretical investigations about flow stimulation in porous materials by means of acoustic waves are reviewed in section 1.2.2. Laboratory studies and theoretical investigations about ultrasonic cleaning are reviewed in section 1.2.3.

1.2.1 Field test

Few tests were carried out at relative low frequencies (down to 5 kHz). So it is very likely that, for those applications, the penetration is not limited to the first few centimeters of the formation, but a deeper penetration may be achieved. (The frequency determines the acoustic penetration into the porous rock.) Most of the literature about application of ultrasounds on oil reservoirs comes from Russian research institutes or Russian oil companies. The first ultrasonic stimulation reported was performed in 1975 in the former-USSR. An increase of oil production was achieved during the sonification of oil fields in Western Siberia. After application of acoustic waves with frequencies between 5 kHz and 50 kHz for several hours, an increase in oil flow rate was observed and it lasted between 94 and 147 days after the stimulation (dependent on the well). The application of high-frequency acoustic waves was successful in 52% of the wells treated. Unfortunately, the geological characteristics for each well were not reported. Also the exact conditions during stimulation were not reported.

Results of acoustic stimulation of an oil well in Western Siberia were also reported by Kuznetsov & Efimova (1983). One marginal well was stimulated in three stages. The producing reservoir rock was a fine-grained sandstone with siliceous clay and carbonaceous cement. A region of radius equal to 16 times the radius of the well was deliberately damaged by mud particles invasion. Results of stimulation are reported in Fig. 1.2. As result of the first phase of the application (intensity of 1.6 kW/m^2 and 16.5 kHz frequency) an increase in oil production was achieved. The production was further enhanced by increasing the intensity to 4 kW/m^2 (second phase). A sharp decrease in productivity occurred when 5 kW/m^2 waves were applied (third phase). The authors could relate this decrease to a degassing of the liquid. Nevertheless, an increase of 15% was achieved.

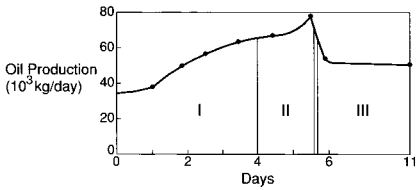

Figure 1.2: Production rate for a well stimulated by ultrasound. In the last (third) phase of the treatment a decline in production rate is observed. The authors relate this to a degassing of the reservoir (Kuznetsov & Efimova 1983).

Morris (1974) describes the use of an ultra-high frequency tool, which produced 2-s ultrasound pulses for cleaning sand and carbonate formation. The treatment lasted 2 minutes per 30 cm. Because of the high frequency the penetration depth was rather shallow: the principal effect produced in this case was purely mechanical destruction of wellbore scales. Production increase was achieved in 14 of the 21 wells treated. It remains unclear why the 33% of the wells did not show any increase in flow rate.

More recently, *Shaw Resource Service Inc.* (1992) issued a report on field tests on a piezoelectric sonic tool. The first test was performed on a single well over a period of three months in 1983. The average increase of rate of production, while the tools were in operation, was about of 19%. A success in the 40-50% of the cases was reported on the seventeen wells treated and lasted up to one month.

In October 1996, Roberts, Sharma & Maki (1998) performed tests on two different fields. The ultrasonic tool had a maximum acoustic power of 170 W and can treat an about 60 cm vertical length. The first test was performed in coal-bed methane wells in New Mexico (USA). The aim was to remove fines from the producing zones. The production company indicated that these wells had never been an economical methane producer despite several attempts to stimulate them by hydraulic fracturing. The tool was lowered to the bottom of the producing zones and the well was shut in. During the operation of the tool, the pressure was recorded each 5 minutes. The producing area was treated in 6 separate 60 centimeters intervals. No conclusive data could be drawn from these tests. Although two wells were treated, only one well was producing significantly during the treatment. Because the second well was not flowing significantly during the treatment, it is unlikely that fines were removed during the sonification.

Roberts et al. (1998) performed another field test in Texas (USA) during October 1996. In this case the wells had produced oil and the aim of the treatment was to remove the plugging due to migration of fines. Five wells were chosen for their continuous production rate decline; four of them were in the same producing field and were low-volume producers. Preliminary tests, to estimate the production rates, were carried out during the four days prior to the stimulation treatment. The production rate was monitored for 16 days after the stimulation and compared with the pre-treatment situations. The production rate showed, after a stabilization period of 4-5 days, an increase in oil production with respect to the pre-treatment situation. Water production, after a sharp rise during the initial stage, started decreasing. The cumulative production rate

of the four wells was (at the end of the 16 days) fairly stable and about the double that of the pre-treatment condition (from 35 to 70 barrels of oil per day). For the fifth well, pre-treatment test showed an anomalous high production rate (compared with the well history) and, therefore, the results for this well were inconclusive.

Kas'yanov & Shaloshov (2002) reported about a field test where ultrasonic stimulation was used to enhance the effect of chemicals. The test was carried out in three stages between October 1989 and April 1991 (location of the field is not indicated). The ultrasonic application was performed with frequencies of 13.8 kHz and 8.2 kHz and pulse sequences of 6 ms were applied. The power (electrical input into the tool) was of 12 kW. The authors reported an increase in the filtration factor (a measure of the penetration rate of the acid) to 1.3 m/day, but pre-treatment values were not given. The authors explain the positive effect of the ultrasonic treatment in the following way: as consequence of acid injection, the interaction of active reagents and rocks leads to the formation of gas, which accumulates in pores and micro-cracks (also known as gas colmatation). The effect of ultrasound is to accelerate the gas diffusion into the liquid phase, increasing the active interfacial area.

1.2.2 Flow stimulation

The first laboratory study regarding the influence of ultrasonic energy on fluid flow through a porous material was carried out by Duhon (1964). Duhon studied the characteristics of oil displacement by water in the presence of ultrasound. The author observed an increase in oil recovery from sandstone as a result of the ultrasonic excitation. Regarding the possible mechanisms responsible of the increase of oil permeability, Duhon cited cavitation and radiation pressure produced by ultrasound. Cavitation could be a consequence of low-pressure experimental set-up. Radiation pressure was a consequence of ultra-high frequencies used (1-5.5 MHz).

Fairbanks & Chen (1971) measured the percolation of oil through sandstone at different oil temperatures in the presence of a 20 kHz sound field. Increased percolation rates in the presence of ultrasound were noted at all temperatures, but were largest at temperatures between 100^{o} C and 110^{o} C. The authors do not provide a quantitative explanation of this change. Beresnev & Johnson (1994) speculated that changes in oil viscosity, caused by temperature increase, could explain the results. However, independent control of the oil physical properties and temperature variations were not carried out during the experiments. Gadiev (1977) conducted laboratory experiments in saturated, unconsolidated sand that was exposed to vibration with frequencies between 40 Hz and 15 kHz (15 kHz is the lowest frequency for near wellbore region stimulation.). As result of the excitation, an increase of oil displacement by water was observed. Gadiev reported an increase of 10-15%, but he did not provide enough details neither of the experimental set-up nor of the measurement procedure.

Cherskiy, Tsarev, Konovalov & Kuznetsov (1977) measured the permeability of core samples saturated with fresh water in the presence of a 26.5 kHz acoustic field. Differently from previous works, both pulses and continuous sonification were applied. According to their description, after the application an increase of the permeability was measured both for the pulse mode and for the continuous one. The pulse mode duty cycle was not mentioned, but it was shown to be somewhat more effective. The authors suggested the destruction of boundary water films as an explanation of the effect obtained. However, these authors did not give a satisfying description of the set-up nor of the experimental procedure. The effect of ultrasound of continuous wave acoustic field on displacement of immiscible fluids was studied by Neretin & Yudin (1981). During the displacement of hydrocarbon by water in presence of a sound field, the hydrocarbon yield increased by a factor ranging from 65% to 85%. Simkin & Surguchev (1991) observed the intense growth of oil droplets after two minutes of acoustic stimulation. Frequency and intensity were not reported. They attributed the growth to sonically induced coalescence of oil droplets.

The effect of ultrasound on viscosity of polymeric solution was also investigated by Johnston (1971). He reported a decrease of 6 times the original viscosity after 20 minutes of sonification at 880 kHz. Similar results were reported by Nosov (1965) for application of 300 kHz waves and by Sokolov & Simkiv (1981) for frequency of 18 kHz. It has to be noticed that an independent

measure of the temperature was not carried out, so it is not possible to distinguish between molecular degradation and temperature effects.

In (1994) Beresnev & Johnson, after a careful review of the literature including also publications in Russian not easily accessible, concluded that no clear evidence was available about the mechanisms responsible for the flow stimulation. They suggested that the following mechanisms might be involved:

- The acoustic wave field may considerably reduce the influence of capillarity forces on the oil percolation, resulting in an increased rate of migration through the porous material. The reason is that vibration of the solid surface reduces the adherence of the fluid to it. Mechanical vibrations destroy the surface film absorbed on the pore boundaries, increasing the effective cross section of the pores. Cavitation may also contribute to the destruction.
- Non-linear effects, such as acoustic streaming, may give the fluid extra momentum.
- Reduction of surface tension and viscosity of liquid in the ultrasonic sound field (due to energy dissipation) may give an apparent decrease in permeability.
- Changes in phase-permeability can be a consequence of sound application.
- Mechanical abrasion effect of pores may be a consequence of high frequency and high intensity acoustic fields.

It is worth mentioning, that no evidence for these explanations is provided.

In (1998), Aarts & Ooms proposed a model based on peristaltic transport. According to this model ultrasound induces a deformation of the boundaries and, hence, an increase in the flow rate. Subsequent experimental validation of this model showed that the predictions made were not in agreement with the measured values. The theory pointed to a strong influence of wall stiffness, while the experimental results obtained from different material were independent of wall stiffness.

Gorbachev, Rafikov, Rok & Pechkov (1999) argued that at frequencies larger than the critical frequency, the pore fluid behaves as a perfect fluid (non viscous fluid) and that the flow rate increases even if the pressure drop is kept constant. Maksimov & Radchenko (2002) presented a numerical study where the equations of conservation of mass, momentum and energy in presence of ultrasound in porous media were solved by a finite difference three-dimensional code. The presence of waves was included as a source term. They found that an increase of the oil flow rate in a well could last up to three months, in qualitative agreement with observation. Esipov, Fokin & Ovchinnikov (2002) argued that the enhancement of oil flow rate through a porous material could be explained taking into account a non-Newtonian behavior of the oil at reservoir conditions. In this case, the non-linearity of the medium could induce a net flow in presence of an oscillating (even weak) acoustic field. Mikhailov (2002) investigated theoretically the effect of ultrasonic stimulation on the oil/water relative permeability. According to this study, ultrasound induces an increase in oil flow rate. Nikolaevskiy & Stepanova (2002) pointed out the importance of gas, as was already noticed by Duhon (1964). To further investigate this effect, they applied ultrasound (frequency of 30 kHz) during a water-flooding test. As result of the stimulation, bubbles were generated causing a change in the flow pattern. The authors reported an increase in oil recovery factor from 42% (without ultrasounds) to 85% (for the case of ultrasound application together with surfactant).

1.2.3 Ultrasonic cleaning

Cleaning effects of ultrasound were first investigated by Abad-Guerra (1976) who focused his attention on paraffin deposition on sandstone. He studied the effects of ultrasound waves (information on frequencies or intensities was not reported) on a core whose permeability was reduced to zero by precipitating paraffin. The permeability improvement ranged from 7% to 51%. The author concluded that the principal factors causing the removal of paraffin in the formation was cavitation. Successful paraffin removal from rock using ultrasonic waves was reported by Horblit (1951)

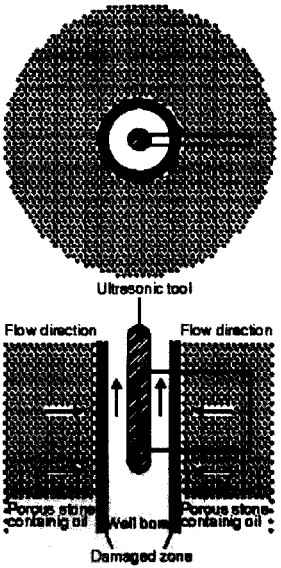

Figure 1.3: Sketch of a near wellbore region in which also the ultrasonic tool is depicted. The black box represents the piece of rock used in the experiments by Venkitaraman et al. (1995).

while Komar (1967) reported mixed results. In none of those works, information on frequency or intensity was reported.

Ultrasonic removal of near wellbore fouling caused by fines and mud solids were investigated by Venkitaraman, Roberts & Sharma (1995). The idea was to take a piece of rock as representative of the whole near wellbore region. This sample was then put in a linear set-up and damaged in different ways, similarly to what happens in a reservoir (a sketch is given in Fig. 1.3). They investigated the effect of ultrasound (between 10 and 100 kHz) on the removal of fine clay particles and mud solids (Bentonite) from samples of Berea sandstone and limestone. They conclude that:

- For both sandstone and limestone the permeability increases due to the acoustic treatment in case of mud invasion. The effectiveness of the treatment depends on several parameters such as flow rate and power. An increase in permeability is possible both when oil and water are the saturating liquid.
- The removal of fine clay particles is also possible and its effectiveness depends on the power input. The effect of ultrasonic cleaning is enhanced when sonification is carried out in static conditions (no flow rate imposed through the rock sample).

It is important to point out that no characterization of the penetration of mud solid was performed and that the experimental set-up was at low pressure allowing cavitation to play a role (as noticed also by the authors themselves)*.

Gorbachev et al. (1999) pointed out that colloidal particles coalesce and form flock-like structures within the porous medium. The flock formation is initially weakly bonded and with high porosity (~90%). As the time goes by, the bonds become stronger and the porosity reduces (~60%). The effect of acoustics is to break apart those structures (this procedure is usually called peptization). Since the time plays a critical role in the structures resistance, acoustic stimulation must be applied in the earlier stages of the exploitation. They even suggested to use acoustic techniques to prevent near wellbore region fouling.

Roberts, Venkitaraman & Sharma (2000) also studied the possibility to remove organic deposit and polymer invasion by ultrasound. They found that sonification could improve the permeability in all the cases they investigated. Their results are summarized in Tab. 1.1.

Type of Damage	Section 1 before sonification	Section 1 after sonification	Section 2 before sonification	Section 2 after sonification
Mud	0.07	0.32	1.0	1.0
Fines	0.03	0.18	0.03	0.03
Paraffin	0.40	1.20	0.40	0.85
Polymers	0.22	0.37	0.53	0.78

Table 1.1: Information about the cleaning efficiency of the ultrasonic tool used by Roberts et al. (2000). The value of the permeability, made dimensionless with the initial (unfouled) value, is shown for two sections in the core before and after the acoustic treatment. Section 1 is defined as the first 2.54 cm of the core of porous material used in the investigation. Section 2 is defined as the second 10.70 cm of the core.

Wong, v. Bas, Groenenboom & Zuiderwijk (2003) carried out experiments on the removal of mud solids, fine particles and polymers from Berea sandstone. They managed to increase the permeability of a damaged sample, but the number of experiments was small and not all the relevant parameters were reported. No explanations or interpretations were given. It is important to emphasize that in none of the laboratory experiments that have been performed a negative result was found. In all the cases reported, an increase in permeability was obtained. Some conditions gave better results than others, but for all conditions a positive result was found.

Application of ultrasound to porous material was also recently proposed to remove hydrocarbon waste from urban area. In some experiments it was shown that oil droplets could be removed from the soil (Kim & Wang 2003).

All the results reviewed so far have been obtained with a linear cell, while the real configuration is circular (see Fig. 1.3). v. Bas, Zuiderwijk, Wong, v. Batenburg, Birchak & Yoo (2004) made a first attempt to carry out experiments with a circular cell.

1.2.4 Conclusions

From the review about field studies it has become clear that ultrasonic well stimulation is not well understood. Most field applications gave inconclusive results. Often the relevant parameters were not reported, either because of confidentiality or because in field tests it is difficult to control and measure these parameters. Laboratory studies and theoretical work have investigated both the ultrasonic flow stimulation and the ultrasonic cleaning effect. Concerning flow stimulation complex situations have been studied. For instance, a two-phase flow of a non-Newtonian fluid was studied while a satisfactory explanation for the case of a single phase Newtonian fluid was

*This study is relevant for the research presented in this thesis. I will refer to it later on to discuss in more details the conclusions.

still missing. The effect of acoustic energy dissipation into heat was not studied systematically. Similarly, no attention was given to non-linear acoustic effects, such as acoustic streaming.

Concerning the ultrasonic cleaning very few careful experimental studies are reported in the literature. Some interesting experiments were carried out by Roberts and coworkers. However, the influence of only a few parameters were investigated. Most of the experiments were performed at low pressure, allowing cavitation to play a (major) role, while during the production of oil cavitation is never (or hardly) an issue. No models to predict the acoustic cleaning efficiency are presented in the literature. So at the moment there is no reliable tool to predict the cleaning efficiency and the influence of different parameters on this efficiency.

1.3 This work

The aim of this thesis is to study the ultrasonic flow stimulation and ultrasonic cleaning in detail. The literature review showed that an understanding of these phenomena based on physical mechanisms is not available.

We started with the ultrasonic flow stimulation. To that purpose the effect of ultrasonic waves on the pressure drop for the flow of a liquid through a porous material (at constant flow rate) was investigated. A set of very well controlled experiments, where all the important parameters were varied and reported, was carried out. Also a theoretical model was developed and compared with experiments. The possibility to generate a net steady flow through a porous material due to acoustic streaming was carefully investigated and modeled theoretically.

Thereafter we studied the ultrasonic cleaning in detail. Accurate experiments, during which all relevant parameters were varied and measured, were performed. Different types of fouling were investigated: fouling induced by internal particles (simulating the oil production process) and fouling induced by external particles (simulating the exploration phase). Two types of fouling were considered: fouling due to particle deposition on the walls of the pores of the porous material or fouling due to particles bridge formation blocking the throats of the pores. Theoretical models were developed and numerical simulations were carried out to study the physical mechanisms of fouling and ultrasonic cleaning.

1.4 Outline of thesis

This thesis is based on papers published or submitted for publication over the last four years. As a consequence the chapters are in principle self-contained and can be read separately. However, to help the reader to see the general path followed in the course of the study, comments are added between chapters to explain the transition from one chapter to the next one. To be able to read the thesis it is important, that the reader has some knowledge about Biot's theory (Biot 1956) for acoustic wave propagation through a porous material. Therefore a brief review of this theory is given in Appendix A and B of Chap. 3 for readers who are not familiar with it.

In Chap. 2 acoustic flow stimulation in a porous material is investigated experimentally and theoretically. It is found that ultrasonic stimulation decreases the pressure drop for the flow of a liquid through a core of Berea sandstone (at a constant flow rate) due to the increase in temperature that originates from the strong damping of the wave. Since damping of high-frequency acoustic waves is very strong in a porous material, acoustic streaming is investigated in Chap. 3. The next chapters are devoted to ultrasonic cleaning. First attention is paid to fouling caused by particles generated inside the porous material. Cleaning of such particles deposited on the pore walls is studied experimentally and theoretically in Chap. 4. In Chap. 5 permeability reduction caused by particles bridges blocking the pore throats is analyzed experimentally and the possibility to ultrasonically remove such particles bridges is investigated. In order to understand the physics that governs particles bridge formation and removal we have also carried out numerical simulations of these phenomena at the pore level. Results of this study are given in Appendix A and in Chap. 6. Finally in Chap. 7 attention is given to the ultrasonic cleaning of particles penetrated into the

porous material from outside.

The study starts with an investigation of the effect of ultrasonic waves on the flow through a porous material. As discussed in the introduction only a limited number of experiments devoted to this effect were carried out by other researchers so far. Moreover, most published experiments deal with rather complex flow situations, such as the influence of acoustic waves on a two-phase flow through a porous material. Therefore, in the next chapter accurate and detailed experimental results are reported about the influence of acoustic waves (with a frequency of 20 kHz or 40 kHz) on the single-phase flow of a brine through a Berea sandstone core (with a permeability between 100 and 300 mD). Also a theoretical model, based on an effective medium approach, is developed and its predictions are compared with the experimental data.

Chapter 2

An investigation of the influence of acoustic waves on the liquid flow through a porous material*

Abstract

An experimental and theoretical investigation has been made of the influence of high-frequency acoustic waves on the flow of a liquid through a porous material. The experiments have been performed on Berea Sandstone cores. Two acoustic horns were used with frequencies of 20 kHz and 40 kHz, and with maximum power output of 2 kW and 0.7 kW respectively. Also a temperature measurement of the flowing liquid inside the core was made. A high external pressure was applied in order to avoid cavitation. The acoustic waves were found to produce a significant effect on the pressure gradient at constant liquid flow rate through the core samples. During the application of acoustic waves the pressure gradient inside the core decreases. This effect turned out to be due to the decrease of the liquid viscosity caused by an increase in liquid temperature as a result of the acoustic energy dissipation inside the porous material. Also a theoretical model has been developed to calculate the dissipation effect on the viscosity and on the pressure gradient. The model predictions are in reasonable agreement with the experimental data.

2.1 Introduction

Fouling of the near well bore region can decrease the oil recovery from an oil reservoir dramatically. Different techniques have been developed to remove this fouling; for instance the injection of acids that dissolve the fouling particles. These techniques have undesirable side effects: they are costly, impose production shut-off or have a negative impact on the environment. Therefore in more recent years a new cleaning method has been proposed and investigated: treatment of the near well bore region with high-frequency, high-energy acoustic waves. However the results of this technique are rather variable. Acoustic cleaning causes an increase in the oil flow rate in only about 50 percent of the cases. In a number of cases it even has a negative effect on the flow rate. In order to optimize this technique it is essential to understand the physical mechanism of acoustic cleaning.

In this publication we go back even one step further. We first try to understand the influence of high-frequency acoustic waves on the flow of a liquid in a porous material without fouling. Only when we have understood this influence will we make the next step: to understand the effect of acoustic waves on fouling particles being present in the liquid in the porous material. In the review article by Beresnev & Johnson (1994) several mechanisms have been proposed for the influence

*P. Poesio, G. Ooms, S. Barake, and F.v. Bas. "An investigation of the influence of acoustic waves on the liquid flow through a porous material". *J. Acoust. Soc. Am.*, 111(5):2019–2025, 2002.

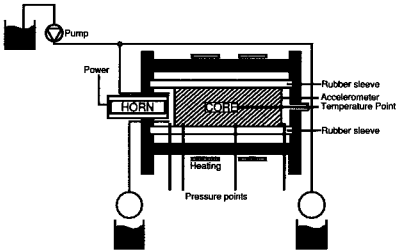

Figure 2.1: Experimental set-up with one temperature measurement.

of high-frequency acoustic waves on the flow of a liquid in a porous material. They mention, for instance, the reduction in adherence between pore wall and liquid, acoustic streaming, acoustic cavitation, in-pore turbulence, viscosity decrease due to energy dissipation, etc. Aarts & Ooms (1998) have developed a model based on a peristaltic liquid transport caused by a deformation of the pore walls due to the traveling acoustic waves.

However no certainty exists as to which mechanism is the correct one. We focus our investigation on Berea Sandstone with permeability 100 to 300 mD and on acoustic frequencies below the critical frequency, Biot (1956). We have carried out a detailed experimental and theoretical investigation of the influence of acoustic waves on the (laminar) liquid flow through a porous material. The results are given in this publication.

2.2 Experimental set-up

2.2.1 Cores

The cores that are used for the experiments are cylindrically shaped Berea Sandstone samples. They are very representative for the type of porous material in an oil reservoir. The length of the cores is 20 cm and the diameter 7.62 cm. The porosity is about 25%. The initial permeability is 100-300 mD for all samples.

2.2.2 Set-up

A core is placed in a rubber sleeve to keep it fixed during the experiment. It is then placed in a steel vessel in which down-hole conditions are simulated (up to 150 bars and $100°C$). An acoustic horn is placed at one end of the core (see Figs. 2.2.2 and 2.2).

The high pressure in the vessel makes it possible to avoid cavitation (for pressures lower than 100 bars the influence of cavitation becomes noticeable). The space between the vessel and sleeve, which is filled with water, is then pressurized to 180 bars to make the rubber sleeve completely seal off. A constant flow of brine (a 2% KCl solution in water) through the core is generated by means of a pump. So, because of mass conservation, the local superficial velocity in the core is constant. We use brine instead of plain water to avoid colloidally induced migration of fines. A flow in both directions is possible. This allows us to have the liquid flow and the acoustic wave propagating in the same direction or in opposite directions. There are four pressure measurements, two along the core (at 2.54 cm and 10.70 cm) and two at both ends of the core (see Figs. 2.2.2 and 2.2). dP_1 is

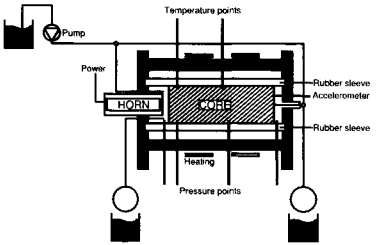

Figure 2.2: Experimental set-up with two temperature measurements.

the pressure drop over the first part of the core sample, dP_2 the pressure drop over the middle part and dP_c the total pressure drop over the core. The pressure drop over the third part dP_3 can be calculated in the following way $dP_3 = dP_c - (dP_1 + dP_2)$. For the first experiments a thermocouple was placed in the middle part of the core, approximately 10 cm deep from the side wall. To do this a hole was drilled in the core and the thermocouple is placed inside (see Fig. 2.2.2). Liquefied metal was poured in the hole to fix the thermocouple. The aim was to measure the liquid temperature in the middle part of the core during the experiments. During the first experiments we found a very interesting effect with respect to the temperature. In order to investigate this effect in more detail we installed two thermocouples at the sidewall of the porous medium, through the rubber sleeve (see Fig. 2.2). This new temperature measurement method is better than the first one, as the probes do not disturb the flow field. Results with both measurement methods will be reported in this publication. Calculations show that the temperature profile is uniform within the core. Also the temperature in front of the core can be measured. The data are sent to a digital data recorder and processed on a computer.

2.2.3 Ultrasonic equipment

The ultrasonic equipment consists of:

- a converter, which converts electricity into mechanical vibrations of a piezoelectric element;
- an amplifier, which is used to set the amplitude of the vibrations;
- an ultrasonic horn, which concentrates the mechanical vibrations onto the front side of the core sample. Two acoustic horns are applied: a Branson Module PGA 220 (a 20 kHz horn with maximum power output of 2000 W) and a Branson Module PGA 470 (a 40 kHz horn with maximum power output of 700 W). The power output can be selected as a percentage of the maximum.

2.2.4 Microphone

A microphone is placed at the end side of the core. It is used to measure the amplitude of the acoustic signal after passage through the core. In this way the damping of the signal was determined during the experiments.

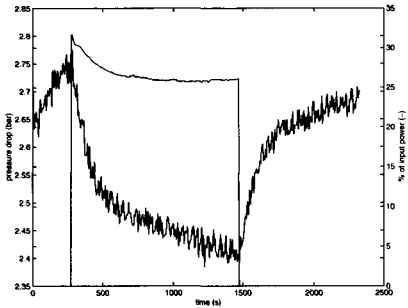

Figure 2.3: Pressure gradient over the middle part of the core (bold line) and percentage of power input (narrow line) as function of time.

2.3 Experimental procedure and results

2.3.1 Experimental procedure

A new core is used for each new series of experiments. Before performing experiments, the following steps are taken:

- **The core is flushed with CO_2 to expel all the air in the porous material. The gas flow is kept on for several minutes.**
- **After the gas flow is stopped a constant flow rate of the brine is started: the high pressure ensures that all the CO_2 dissolves into the brine.**
- **The three pressure drops, the temperature in the middle part of the core (or at the sidewall of the core) and in front of the core, and the constant flow rate of the brine are recorded.**
- **The flow rate is increased up to the maximum value that the pump can deliver to detach and remove possible fines that are present in the core sample.**

2.3.2 Experimental results

As an example of our experimental results we show in Fig. 2.3 the pressure drop over the middle part of the core dP_2/dx as a function of time during one of the experiments: x is the distance to the front end of the core.

Also the applied acoustic power is given as function of time. In this experiment the acoustic frequency is 20 kHz which is significantly lower than the critical value (230 kHz). The measurement of the pressure gradient over the middle part is accurate, as there is no influence of end-effects of the core. For this reason we will leave out of consideration in this paper results for the pressure gradients dP_1/dx and dP_3/dx over the end parts. It can clearly be seen in Fig. 2.3, that during application of acoustic power the pressure gradient over the middle part of the core decreases. During this experiment the (constant) liquid flow and the acoustic wave propagation were in opposite direction. The flow rate was 75 ml/min.

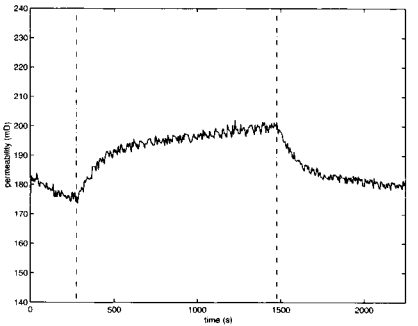

Figure 2.4: Permeability as a function of time calculated assuming a constant temperature.

From the measured flow velocity and pressure gradient as function of time we have calculated, neglecting the influence of the temperature change on the liquid viscosity, the permeability of the porous material in the middle part of the core sample as function of time by applying Darcy's law. This law is given by

$$\frac{dp}{dx} = -\frac{\mu}{K}v, \tag{2.1}$$

in which K is the permeability, μ the liquid viscosity and v the liquid velocity. As mentioned the viscosity was considered constant and computed at the initial temperature ($30°C$), measured in the core before the experiment. In Fig. 2.4 the calculated permeability for the middle part is shown as function of time. It seems, as if the high-frequency acoustic waves cause a significant increase of the (effective) permeability.

However the liquid temperature has an influence on the liquid viscosity. Therefore we repeated the calculation of the permeability of the middle part of the core, but this time taking the (known) influence of the temperature (measured in the middle part of the core) on the viscosity into account. The result is shown in Fig. 2.5, that represents the same experiment as in Fig. 2.4. The relationship between temperature and viscosity we used can be found in the form of a table in Zaytsev & Aseyev (1992). As can be seen there is no longer an influence of the high-frequency acoustic waves on the permeability. The permeability remains nearly constant. The pressure drop decrease observed during the application of acoustic waves is solely due to the decrease of the liquid viscosity, caused by the temperature increase of the liquid as a result of the acoustic energy dissipation in the porous material. This holds for all our experiments; both for case that the acoustic wave propagation and liquid flow are in opposite direction as when they are in the same direction. In the following we will compare this result with theoretical predictions.

2.4 Damping coefficient

Before we can make theoretical predictions concerning the influence of acoustic wave propagation on the liquid flow through a porous material we must know the damping of the wave inside the material. The incident acoustic wave is split in the porous medium into a slow wave and a fast wave. The damping of the slow wave is very fast and is known. However the damping of the fast

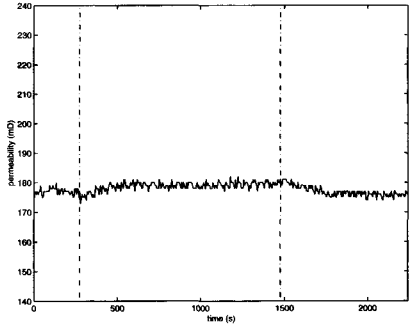

Figure 2.5: Permeability as a function of time calculated using the measured temperature.

wave is much more difficult to predict. Biot's theory (Biot 1956) predicts a damping coefficient for the fast wave which is too low for many porous materials. To the best of our knowledge no models are available that can predict a damping coefficient for the fast wave, which is in agreement with the experimental measurements. This is the reason why we decided to determine this damping coefficient for our core samples experimentally. In order to measure the attenuation we used cores of different lengths (5 *cm*, 11 *cm* and 16 *cm*) and measure the damping as function of the core length with the aid of the microphone. Since we were not able to move the microphone (it is embedded in the plunger at the end of the core), the void space (in case of the shorter cores) had to be filled in with a substitute material. We used Peek (a plastic). It can be assumed that the losses in the filling material are small compared to the losses in the porous material itself. We show an example of our experiments in Fig. 2.6. In this case a brine-saturated core was used and the experiment was carried out at room temperature. For each core length, six different power inputs were used. As expected, each set of points could be interpolated by means of an exponential curve. The averaged damping coefficient was calculated to be 8.3 m^{-1}.

2.5 Theoretical calculations

We will now calculate the influence of high-frequency acoustic waves on the flow in a porous medium and in particular pay attention to the influence of the heat generation due to the dissipation of the acoustic waves on the flow. We first calculate the temperature distribution in the core as function of time, taking into account the acoustic energy dissipation and the convective heat transport due to the liquid flow. We assume that the solid and the fluid are in thermal equilibrium: there is no heat transfer either from liquid to solid or vice-versa. To check this hypothesis we made use of the method proposed by Kaviany (1995). We may assume that the radial temperature distribution is uniform, because the rubber sleeve is a good insulating material. So we consider the temperature to be a function of the axial coordinate only. The following heat balance equation is then satisfied:

$$[\rho_f c_{p,f}\phi + (1-\phi)\rho_s c_{p,s}]\frac{\partial T}{\partial t} + \rho_f c_{p,f} v \frac{\partial T}{\partial x} = \kappa \frac{\partial^2 T}{\partial x^2} + S_{\text{heat}} \tag{2.2}$$

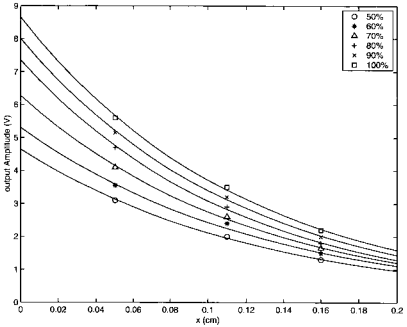

Figure 2.6: Output signal as a function of core length. T=20°C, p_{porc}=120 bars, p_{conf}=185 bars.

in which T is temperature, $c_{p,f}$ and $c_{p,s}$ are the specific heat for liquid and solid, ρ_f and ρ_s are the liquid and solid density and v is the superficial velocity of the liquid. ϕ is the porosity. κ is the effective diffusion coefficient: for simplicity it is taken equal to the average of the values for the fluid and solid. In Eq. 2.2 we did not include a term representing the heat transfer from the core sample via the side wall and the rubber sleeve to the water in the surrounding vessel. However, the heat conductivity of the rubber sleeve is very small and the heat loss to the water is (according to our calculation) therefore negligible compared to the convective heat transfer. Only when the convective heat transfer is absent (v=0), will the heat transfer through the side wall become important. The source term in Eq. 2.2 may be written:

$$S_{heat} = 2\alpha_{fast} I_{fast,0} e^{-2\alpha_{fast} x} + 2\alpha_{slow} I_{slow,0} e^{-2\alpha_{slow} x} \tag{2.3}$$

$I_{fast,0}$ and $I_{slow,0}$ are the initial values (at the front end of the core) of the intensities of the fast wave and slow wave, that are transmitted in the porous material as a result of the incident acoustic wave at the front end of the core. There is no transmitted shear wave as the incident acoustic wave is perpendicular to the porous material surface at the front end. The damping coefficients for the fast wave and the slow wave are given by α_{fast} and α_{slow}.

To calculate the intensity of the fast and the slow waves from the intensity of the incident wave we applied the procedure proposed by Wu, Xue & Adler (1990) using the Poynting vector for elastic waves in porous media. By definition the absolute value of the Poynting vector is the intensity of the wave.

As mentioned it is well-known that the damping coefficient of the fast wave is considerably larger than the value calculated using Biot's theory. Therefore we used experimental values. For the experiments with the 2 kW horn, we used values available in literature (Kelder 1998) because our microphone did not function properly for such a strong signal. Kelder measured experimentally the damping coefficient for the fast wave for Berea Sandstone under different conditions. For the 700 W experiments, we measured the damping coefficient as described earlier. The values used are given in the Tab. 2.1.

With the parameter values from the table we can solve the heat balance equation. In this way the temperature is calculated as function of time for a certain experiment. The predictions compare reasonably well with the measured temperature as function of time. Two examples are given in Figs. 2.7 and 2.8. Now, assuming that the permeability is constant and taking into

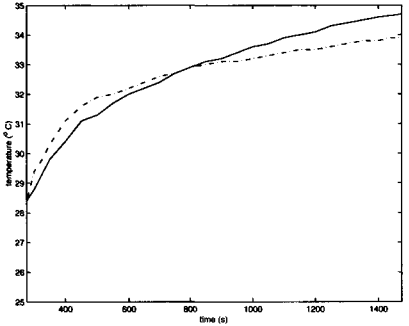

Figure 2.7: Comparison between the measured temperature (continuous line) and the calculated value (dash-point line), using the set-up in Fig. 2.2.2.

account the temperature dependence of the viscosity we can calculate the pressure drop over the middle part of the core using Darcy's law. The result of this calculation for the experiment with the temperature change shown in Fig. 2.8 is given in Fig. 2.9. As can be seen from this figure the experimental results and theoretical predictions are in reasonable agreement. This confirms again that the pressure drop decrease measured during the application of acoustic waves is due to the viscosity decrease caused by the heating of the liquid as a result of the acoustic energy dissipation.

Parameter	value
α_{fast}	8.3 m^{-1}
α_{slow}	182 m^{-1}
Intensity of incident wave	0.7 kW
ϕ	25%

Table 2.1: Parameters used for the calculation.

2.6 Conclusion

We investigated the influence of high-frequency acoustic waves on the flow in a porous material, in particular to find the main effect that is responsible for the decrease on pressure drop when acoustic waves are applied. In the literature many different explanations are suggested. They are all possible, but there are no careful experimental validations. To that purpose we performed experiments on Berea Sandstone and we measured the pressure gradient and temperature in the middle part of the core samples at constant superficial liquid velocity. From our experimental data we conclude that the permeability does not change when acoustic waves are applied. The decrease in the pressure gradient can completely be explained by the decrease in fluid viscosity due to the dissipation of the acoustic energy. This fact is also confirmed by theoretical calculations. So we have convincingly demonstrated, that beyond the effect of heating up the fluid, and thereby changing its viscosity, there is nothing unusual.

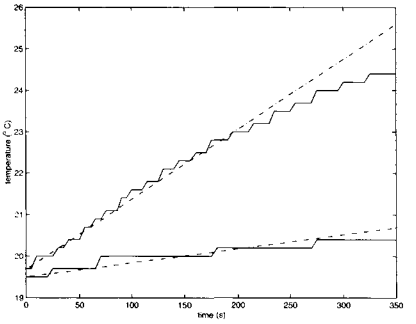

Figure 2.8: Comparison between the measured temperature (continuous line) and the calculated value (dash-point line), using the set-up in Fig. 2.2.

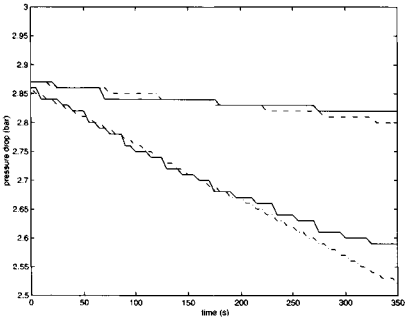

Figure 2.9: Comparison between the measured pressure gradient (continuous line) and the calculated value (dash-point line), using the set-up in Fig. 2.2.

In the previous chapter it was shown that ultrasonic waves cause a decrease in the pressure drop for the flow of a liquid through a porous material (at constant liquid flow rate). This effect was explained, both theoretically and experimentally, by the decrease of fluid viscosity as consequence of the strong damping of high-frequency waves in a porous material. Although the energy of the acoustic waves is transformed into heat as a result of the damping, the momentum of the acoustic waves cannot disappear. This momentum will be transferred to the liquid in the porous material. As a result the liquid will start to flow (when it was originally at rest), or it will change its velocity (when it was already flowing). The phenomenon is called acoustic streaming. In the coming chapter we will try to measure this streaming effect, although it is expected to be rather weak. Also a theoretical model is developed and compared with the experimental streaming data.

Chapter 3

Theoretical and experimental investigation of acoustic streaming in porous material*

Abstract

An experimental and theoretical investigation has been made of the influence of high-frequency acoustic waves on the flow of a liquid through a porous material. Particular attention was paid to the phenomenon of acoustic streaming of the liquid in the porous material due to the damping of the acoustic waves. The experiments were performed on Berea sandstone cores. Two acoustic horns were used with frequencies of 20 kHz and 40 kHz, and with maximum power output of 2 kW and 0.7 kW respectively. A high external pressure was applied in order to avoid cavitation. A microphone was used to measure the damping of the waves in the porous material and also temperature and pressure measurements in the flowing liquid inside the cores were carried out. To model the acoustic streaming effect Darcy's law was extended with a source term representing the momentum transfer from the acoustic waves to the liquid. The model predictions for the pressure distribution inside the core under acoustic streaming conditions are in reasonable agreement with the experimental data.

3.1 Introduction

In earlier publications (see Poesio, Ooms, Barake & v. Bas (2002) and Barake, v. Bas, Ooms & Poesio (2001)) we reported about an experimental and theoretical investigation of the influence of high-frequency acoustic waves on the flow of a liquid through a porous material. The experiments were performed on Berea sandstone cores. The reason for this type of sandstone is, that next to a fundamental study we are also interested in an application of high-frequency acoustic waves to clean the near well bore region of an oil reservoir, and Berea sandstones are representative for the type of porous material in an oil reservoir. Two acoustic horns were used with frequencies of 20 kHz and 40 kHz, and with maximum power output of 2 kW and 0.7 kW respectively. A high external pressure was applied in order to avoid cavitation. The acoustic waves were found to produce a significant effect on the pressure gradient at constant liquid flow rate through the core samples: during the application of acoustic waves the pressure gradient inside the core decreased. This effect turned out to be due to the decrease of the liquid viscosity caused by an increase in liquid temperature as a result of the acoustic energy dissipation inside the porous material. Also a theoretical model was developed to calculate the dissipation effect on the viscosity and on the pressure gradient. The model predictions were in reasonable agreement with the experimental data.

*P. Poesio, G. Ooms, A.P. Schraven, and F.v. Bas. "Theoretical and experimental investigation of acoustic streaming in porous material". *Phys. Rev. E* **66**:016309, 2002.

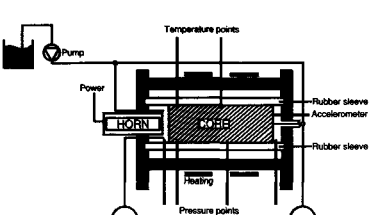

Figure 3.1: Experimental set-up.

In this paper, we will report about another effect of high-frequency acoustic waves on the flow of a liquid through a porous material; viz the streaming effect due to the damping of the acoustic waves. A traveling acoustic wave in a liquid induces a net steady flow in the direction of its propagation. This effect can only occur when the wave is being attenuated. The phenomenon is called acoustic streaming and is described in detail in the book by Lighthill (see Lighthill (1978)). From a physical point of view acoustic streaming is due to a transfer of momentum from the traveling acoustic wave to the liquid. A planar, traveling wave with intensity **I** has momentum:

$$M = \frac{\mathbf{I}}{c^2}, \tag{3.1}$$

where c is the sound velocity in the medium in which the wave propagates. There is a relation between energy and momentum. While energy is dissipated into heat in the liquid, momentum is passed on to the liquid. This generates a net steady flow away from the sound source. So even without a pressure drop over a core of porous material before the acoustic source is switched on, the liquid inside the core will start flowing after the source is switched on due to this momentum transfer. As the damping of high-frequency acoustic waves in a liquid inside a porous material is strong, also a strong and measurable acoustic streaming effect may be expected in such a material. To investigate this effect we have carried out streaming experiments in the experimental set-up mentioned above. During these experiments there was no pressure drop over the core before the acoustic horn was switched on. After the horn was put into action, the liquid started to flow. Because of the liquid flow and the momentum transfer from the acoustic wave a pressure profile developed inside the core as a function of time. This pressure profile development was measured. Also a theoretical model was developed to predict the streaming effect on the development of the pressure distribution inside the core. In this publication we report about this experimental and theoretical investigation.

3.2 Description of the experiments

The experiments were carried out in the set-up shown in Fig. 3.1.

The cores that were used for the experiments were cylindrically shaped Berea sandstone samples. The length of the cores was 20 cm and the diameter 7.62 cm. The porosity was about 0.25. The initial permeability was 100-300 mD for all samples. During an experiment a core was placed in a rubber sleeve to keep it fixed during the experiment. It was then placed in a steel vessel in which down-hole reservoir conditions were simulated (up to 150 bars and 100^oC). An acoustic

horn was placed at one end of the core (see Fig. 3.1). The high pressure in the vessel made it possible to avoid cavitation (for pressures lower than 100 bars the influence of cavitation becomes noticeable). The space between the vessel and sleeve, which was filled with water, was pressurized to 180 bars to make the rubber sleeve completely seal off.

There were four pressure measurements, two along the core (at 2.54 cm and 10.70 cm) and two at both ends of the core (see Fig. 3.1). dP_1 is the pressure drop over the first part of the core sample, dP_2 the pressure drop over the middle part and dP_c the total pressure drop over the core. The pressure drop over the third part dP_3 can be calculated in the following way $dP_3 = dP_c - (dP_1 + dP_2)$. To measure the temperature at two locations in the core (T1 and T2) we installed two thermocouples at the sidewall of the porous medium, through the rubber sleeve (see Fig. 3.1). Also the temperature in front and at the back (Tb) of the core could be measured. The data were sent to a digital data recorder and processed on a computer.

The ultrasonic equipment consisted of:

- A converter, which converts electricity into mechanical vibrations of a piezoelectric element.
- An amplifier, which is used to set the amplitude of the vibrations.
- An ultrasonic horn, which concentrates the mechanical vibrations onto the front side of the core sample. Two acoustic horns were applied: a Branson Module PGA 220 (a 20 kHz horn with maximum power output of 2 kW) and a Branson Module PGA 470 (a 40 kHz horn with maximum power output of 0.7 kW). The power output could be selected as a percentage of the maximum.

A microphone was placed at the end side of the core. It was used to measure the amplitude of the acoustic signal after passage through the core. In this way the damping of the signal was determined during the experiments.

A new core was used for each new series of experiments. Before performing experiments, the following steps were taken:

- The core was flushed with CO_2 to expel all the air in the porous material. The gas flow was kept on for several minutes.
- After the gas flow was stopped, a constant flow rate of the brine was started. The high pressure ensured that all the CO_2 dissolved into the brine. Brine instead of water was used in order to avoid the generation of fines clay particles inside the core sample by the swelling of clay, for more details see Khilar & Fogler (1998).
- The flow rate was increased up to the maximum value that the pump could deliver to detach and remove possible fines that were present in the core sample.

During a streaming experiment we set the initial temperature in the cell, the pore pressure (p_{pore}) and the confining pressure (p_{conf}). The two ends of the core were connected via a pipe (see Fig. 3.1), so no external pressure drop over the core was applied. This means that the pressure distribution inside the core was uniform before the acoustic horn was switched on. After the acoustic horn was switched on we measured the pressure profile inside the core as a function of time by measuring the pressure development at the front and back side of the core and at the two points inside the core. The development of this pressure profile is due to the acoustic streaming phenomenon: the transfer of momentum from the acoustic wave to the liquid. Also the temperatures at the two points inside the core (T1 and T2) and at the back (Tb) were measured as function of time. The temperature change is due to the dissipation of the acoustic wave. Some typical results that we got during these experiments are given in Fig. 3.2 (where the pressure drop evolution over the three parts of the core is shown) and in Fig. 3.3 (where the temperature evolution of T1, T2 and Tb is shown). Calculations show that the temperature profile in a cross-section of the core is almost uniform. In Fig. 3.2 two discontinuities are present in the pressure drop profile: one at 25 seconds which corresponds to the switching on of the horn, the second at 230 seconds which corresponds to the switching off. Further discussion of the results will be

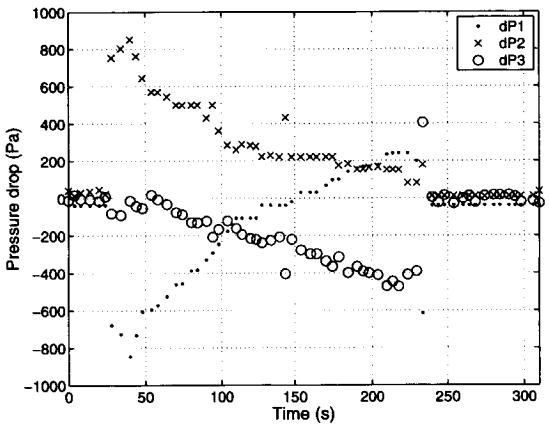

Figure 3.2: An example of the three pressure drops evolution during the sonification time.

given in the section on experimental results. During the experiments the temperature at the back side of the core sample remained nearly constant (see Fig. 3.3). The reason is that the fast wave has almost completely dissipated its energy inside the core before it reaches the end of the core sample.

3.3 Theoretical model

The influence of the acoustic wave on the liquid flow is modeled via a source term in the momentum equation and in the energy equation. The source term in the momentum equation represents the transfer of momentum from the wave to the liquid, and the source term in the energy equation represents the dissipation of acoustic energy into heat. The flow is assumed to be incompressible. Moreover the distribution of the pressure and velocity in a cross-section of the core is assumed to be uniform. So the model equations are one-dimensional with x as the axial coordinate.

The continuity equation can then be written as

$$\frac{\partial v}{\partial x} = 0, \tag{3.2}$$

where v is the superficial velocity of the liquid.

For the momentum equation we use the Darcy equation extended with a time-dependent term and with a source term representing the momentum transfer. For the source term we assume, that only a fraction (equal to the porosity) of the acoustic momentum is given to the liquid. The remaining part goes to the solid. In this way, the momentum equation is given by

$$\frac{\rho_f}{\phi}\frac{\partial v}{\partial t} = -\frac{\partial p}{\partial x} - \frac{\mu(T)}{K}v + S_{mom}, \tag{3.3}$$

in which ρ_f is the fluid density, p the pressure, ϕ the porosity and K the permeability. $\mu(T)$ is the viscosity, which is dependent on the temperature T. This temperature dependence has been taken from the book by Zaytsev & Aseyev (1992). S_{mom} is the rate of momentum transfer from the acoustic waves to the liquid. It can be written as

$$S_{mom} = c_{fast}\frac{\partial}{\partial x}\left(M^{fast}\right) + c_{slow}\frac{\partial}{\partial x}\left(M^{slow}\right), \tag{3.4}$$

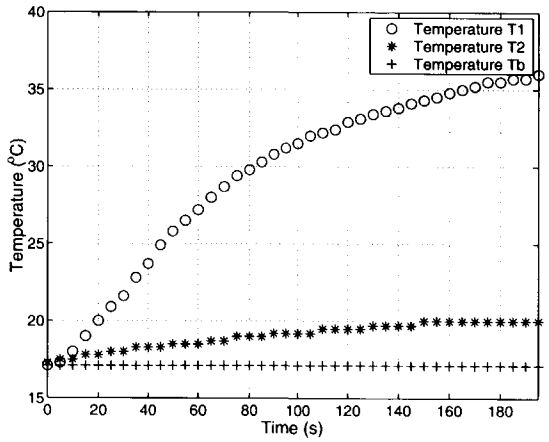

Figure 3.3: An example of the temperature evolution during the sonification time.

where M^{fast} and M^{slow} are the momentum of the fast and slow wave respectively. c_{fast} and c_{slow} are the velocities of the fast and slow wave. For the sake of completeness, more details on sound wave propagation through porous media can be found in Appendix A, where we present a brief review of the Biot's theory (see also the original paper by Biot (1956) for more details).

The momentum of the fast wave and slow wave M^{fast} and M^{slow} (and therefore also S_{mom}) are functions of the axial distance x due to the dissipation of the acoustic wave. For the calculation of M^{fast} and M^{slow} we used Eq. 3.18. This means that the acoustic intensity I as function of x has to be known. Due to the damping of the wave I can be written as

$$I = I_{fast,0}e^{-2\alpha_{fast}x} + I_{slow,0}e^{-2\alpha_{slow}x}, \tag{3.5}$$

where $I_{fast,0}$ and $I_{slow,0}$ are the initial values (at the front end of the core) of the intensities of the fast wave and slow wave, that are transmitted in the porous material as a result of the incident acoustic wave at the front end of the core caused by the acoustic horn. There is no transmitted shear wave as the incident acoustic wave is perpendicular to the porous material surface at the front end. The intensity of the incident acoustic wave has been measured. To calculate the initial values of the intensity of the fast and the slow waves from the incident wave we used a calculation procedure proposed by Wu et al. (1990). In Appendix B this calculation procedure is explained. As is well-known, there is a strong damping of the transmitted fast wave and a very strong damping of the transmitted slow wave. These damping coefficients are given by α_{fast} and α_{slow}. (α_{fast} is also dependent on the temperature T). The determination of the damping coefficients will be discussed later.

For the determination of $\mu(T)$ and $\alpha_{fast}(T)$ we need the temperature distribution inside the core. To that purpose we solve the temperature equation

$$(\phi\rho_f c_f + (1-\phi)\rho_p c_p)\frac{\partial T}{\partial t} + \rho_f c_f v\frac{\partial T}{\partial x} = \lambda\frac{\partial^2 T}{\partial x^2} + S_{therm}, \tag{3.6}$$

in which c_f is the specific heat for the liquid, c_p the specific heat for the solid, ρ_p the solid density, λ the thermal conductivity of saturated rock and S_{therm} the source term due to the acoustic energy dissipation. For the thermal conductivity of saturated sandstone we used the results published by Khan & Fatt (1965). They measured the thermal conductivity for a temperature up to $80°C$ and a pressure up to 125 bars. We took the heat conductivity into account, as we expected that at low velocities the heat transfer due to conduction can be important. In Eq. 3.6, we did not

include a term representing the heat transfer from the core sample via the side wall and the rubber sleeve to the water in the surrounding vessel. However, the heat conductivity of the rubber sleeve is very small and the heat losses to the water is (according to our calculation) therefore negligible compared to the convective heat transfer). The source term can be written as

$$S_{therm} = \frac{\partial}{\partial x}\left(I_0^{fast}(1 - e^{-2\alpha_{fast}(T)x}) + I_0^{slow}(1 - e^{-2\alpha_{slow}x})\right). \tag{3.7}$$

The following boundary conditions are applied: 1) the flow resistance of the connecting pipe between the front side and the back side of the core is very low and, therefore, the pressures at the two sides were chosen to be equal and 2) the temperature at the front and at back side are known functions of time: these temperatures were measured with the thermocouples placed in front and at the back of the core.

A finite difference code was written to solve the equations discussed in this section.

3.4 Measurement of damping coefficient

As mentioned, the incident acoustic wave is split in the porous material into a slow wave and a fast wave. The damping of the slow wave is very strong and is known according to Biot's theory. In Appendix A a brief review of Biot's theory and the calculation of damping coefficient are given. However, the damping of the fast wave is much more difficult to predict. Biot's theory (Biot 1956) predicts a damping coefficient for the fast wave which is too low for many materials. To the best of our knowledge, no models are available that can reliably predict the damping coefficient for the fast wave. This is the reason why we decided to determine this damping coefficient for our cores experimentally. In order to measure the attenuation we used cores of different lengths and measured the damping as function of the core length with the aid of the microphone. Each set of points could be interpolated by means of an exponential curve. In this way the damping coefficient was determined. Six different power outputs of the acoustic horn were used. For each power output, we measured as mentioned the damping coefficient of cores of three different lengths, viz. 5, 11 and 16 *cm*. As the microphone was fixed at a distance of 20 *cm* in the experimental set-up, we extended, for each core length, the core with an additional part made of a plastic material (Peek) in such a way that the total core was always 20 *cm*. The acoustic damping in the Peek is negligible. We measured the acoustic intensity at the end of the total core length. The results are presented in Fig. 3.4, where we have plotted, in a logarithmic scale, the ratio between the intensity of the attenuated wave and the input intensity as function of the position inside the core. For cores with a length of 16 *cm* the damping of the acoustic wave is almost complete at the back side of the core. So the intensity of the wave reflected at the back is very small and can be therefore neglected. According to our measurements this is still true for shorter core samples with a length of 11 *cm*. However for the shortest core samples with a length of 5 *cm* the damping of the acoustic wave is not complete and therefore the intensity of the reflected wave is significant. We have not compensated for this effect by including the reflection of the wave at the back side. In our opinion this is the cause for the (rather small) scatter of our measured points a x=5 *cm* in Fig. 3.4. As can be seen from Fig. 3.4 this scatter is no longer present at x=11 *cm* and at x=16 *cm*, as explained above.

The damping coefficient depends, for instance, on the viscosity of the liquid. As the viscosity is temperature dependent, also the damping coefficient is dependent on the temperature. Therefore the measurement of the damping coefficient was carried out at different temperatures. In Fig. 3.5 we show the result. The damping coefficient decreases quickly with increasing temperature.

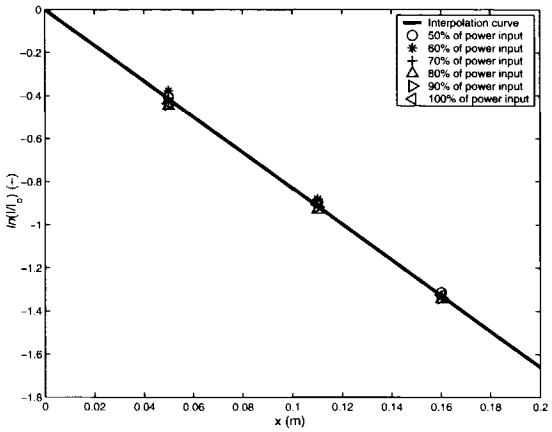

Figure 3.4: Output signal as a function of core length. Symbols refer to the percentage of the power input. The Berea sandstone core is saturated with 2% KCl brine. Frequency 40 kHz, permeability 140 mD, T=20°C, p_{pore}=120 bars, p_{conf}=185 bars.

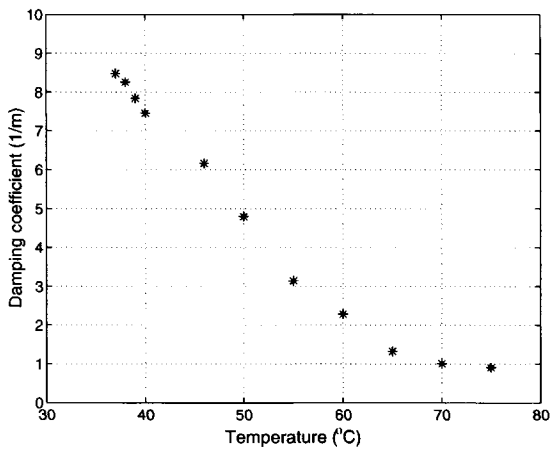

Figure 3.5: Damping coefficient as function of temperature. The Berea sandstone core is saturated with 2% KCl brine. Frequency 40 kHz, permeability 140 mD, p_{pore}=120 bars, p_{conf}=185 bars.

3.5 Comparison between experimental data and theoretical predictions

Two series of experiments have been carried out: one using the 20 kHz horn and one using 40 kHz horn. The results are summarized below.

3.5.1 Experiments with 40 kHz horn

It turned out that the 40 kHz horn had a too low power output (max. 0.7 kW) to cause measurable changes in the pressure distribution inside the core. However there was a measurable influence on the temperature distribution. A typical result is shown in Fig. 3.6. As can be seen the agreement between experimental data and model predictions is reasonably good.

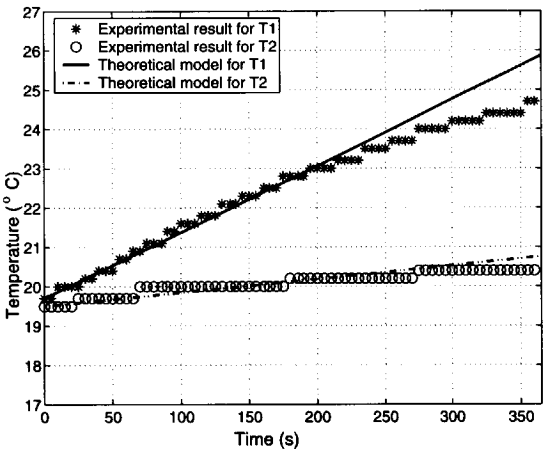

Figure 3.6: Temperature evolution according to theory and experimental data for T1 and T2. The Berea sandstone core is saturated with 2% KCl brine. Frequency 40 kHz, permeability 140 mD, p_{pore}=120 bars, p_{conf}=185 bars, power input 184 W.

3.5.2 Experiments with 20 kHz horn

The power output (max. 2 kW) of the 20 kHz horn is sufficiently large to cause a measurable effect on the pressure distribution inside the core due to acoustic streaming. An example of the comparison between model predictions and experimental data is given in Figs. 3.7-3.13. As can be seen the agreement is certainly not perfect. However the order of magnitude of the pressure distribution inside the core due to streaming and also its development as function of time is very reasonable. From a comparison of the results Figs. 3.7-3.13, the strong relation between the intensity of the sound wave and the induced pressure and temperature changes can be seen. For the cases of minimum and maximum power output we also show in Figs. 3.7(a) and 3.13(a) the measured and calculated temperature distribution inside the core. As can be seen, the agreement is rather good.

At the front part of the core there is a strong pressure build-up. This is due to the momentum transfer from the acoustic wave to the liquid. According to Eq. 3.3 this momentum transfer is used for the pressure build-up, but also for overcoming the viscous friction of the liquid flow and for the (negligible) inertia increase of the flowing liquid. The experiments show a pressure increase at the end side of the core. This is necessary for overcoming the viscous friction of the liquid flow in the connecting pipe between the end side and the front side of the core. This effect is not incorporated in the model, as we assumed the friction of the connecting pipe to be negligible. It is important to realize that at places with strong damping of the acoustic wave (the front part of the core) there is a large momentum transfer from the acoustic wave to the fluid. This causes a very significant initial pressure increase at the front end of the core (see Figs. 3.7-3.13). The relative decrease in pressure at the front end at later times is caused by the temperature increase with time, which

strongly influences the viscosity and the damping coefficient. These effects are well captured by our theoretical model.

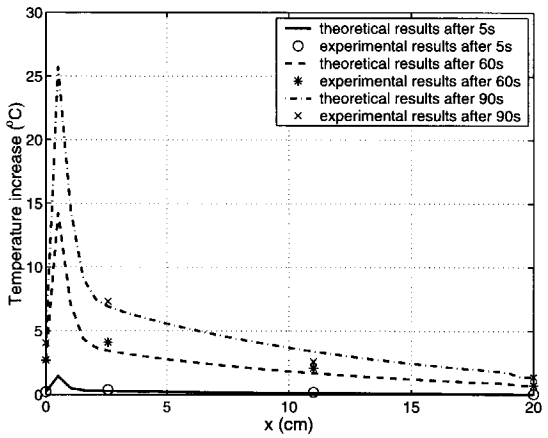

(a) Comparison between calculated and experimental temperature.

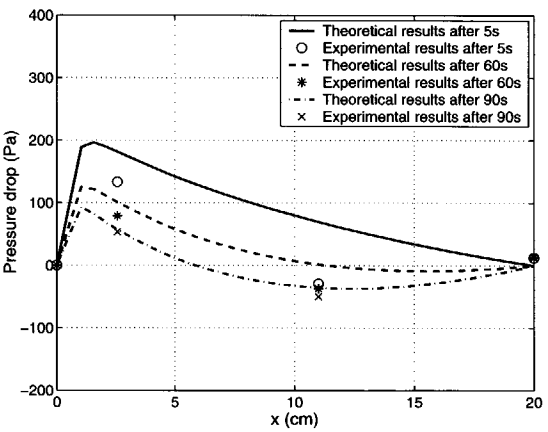

(b) Comparison between calculated and experimental pressure drop.

Figure 3.7: Pressure and temperature profiles inside the core as function of position plotted at three different times. Both experimental data and theoretical results are shown. The Berea sandstone core is saturated with 2% KCl brine. Frequency 20 kHz, permeability 270 mD, p_{pore}=120 bars, p_{conf}=185 bars, $I_0 = 0.55\ 10^5\ W/m^2$.

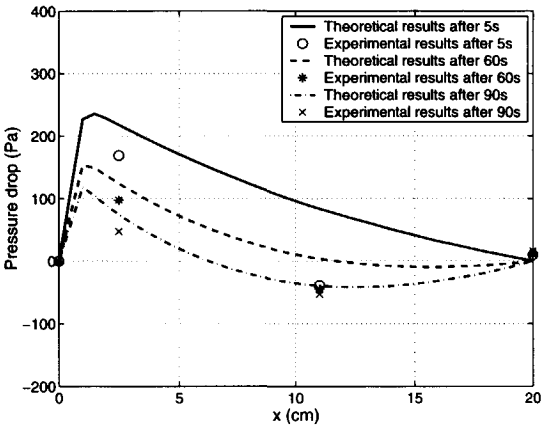

Figure 3.8: Pressure profile inside the core as function of position plotted at three different times. Both experimental data and theoretical results are shown. The Berea sandstone core is saturated with 2% KCl brine. Frequency 20 kHz, permeability 270 mD, p_{pore}=120 bars, p_{conf}=185 bars, I_0 = 0.67 10^5 W/m^2.

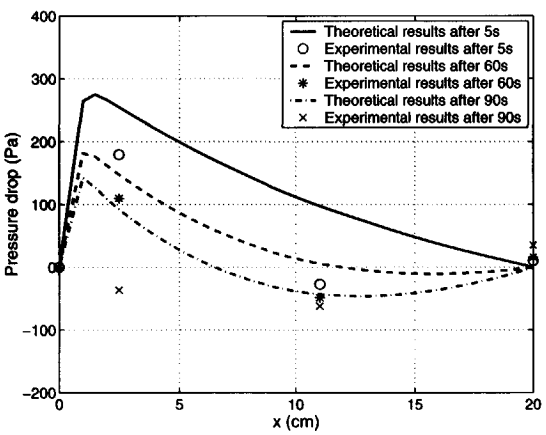

Figure 3.9: Pressure profile inside the core as function of position plotted at three different times. Both experimental data and theoretical results are shown. The Berea sandstone core is saturated with 2% KCl brine. Frequency 20 kHz, permeability 270 mD, p_{pore}=120 bars, p_{conf}=185 bars, I_0 = 0.78 10^5 W/m^2.

3.6 Conclusion

In this paper we have shown experimentally, that a measurable acoustic streaming effect due to the dissipation of (high energy and high frequency) acoustic waves can occur in a liquid inside a porous material. We measured the evolution of the pressure distribution in the liquid due to the momentum transfer from the acoustic waves to the liquid. Also the evolution of the temperature of the liquid due to the dissipation of acoustic energy was experimentally determined. The measurements were in reasonable agreement with model predictions based on an extension

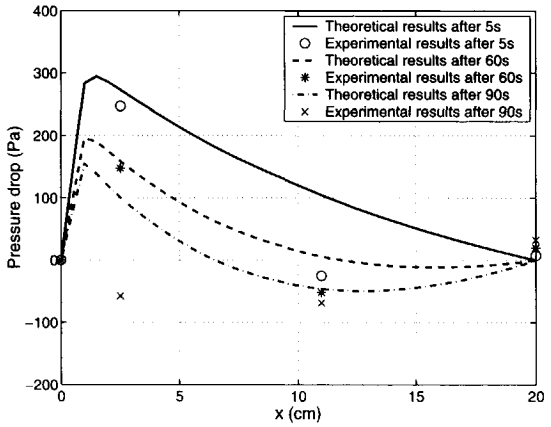

Figure 3.10: Pressure profile inside the core as function of position plotted at three different times. Both experimental data and theoretical results are shown. The Berea sandstone core is saturated with 2% KCl brine. Frequency 20 kHz, permeability 270 mD, p_{pore}=120 bars, p_{conf}=185 bars, I_0 = 0.83 10^5 W/m^2.

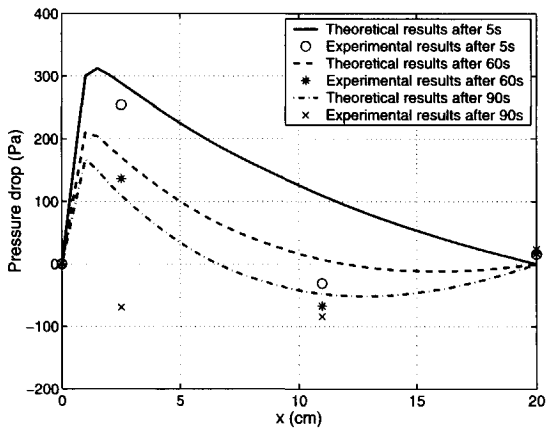

Figure 3.11: Pressure profile inside the core as function of position plotted at three different times. Both experimental data and theoretical results are shown. The Berea sandstone core is saturated with 2% KCl brine. Frequency 20 kHz, permeability 270 mD, p_{pore}=120 bars, p_{conf}=185 bars, I_0 = 0.89 10^5 W/m^2

of the Darcy equation. Although the pressure changes due to acoustic streaming are measurable, it has to be kept in mind that the effect is rather weak. The pressure change due to acoustic streaming is much smaller than the pressure drop over the core resulting from a flow through the core at a typical (oil reservoir) flow rate of 75 ml/min. So during a practical application of high-frequency acoustic waves to clean the near well bore region of an oil reservoir the streaming effect is likely not relevant. However from a scientific point of view the effect is very interesting.

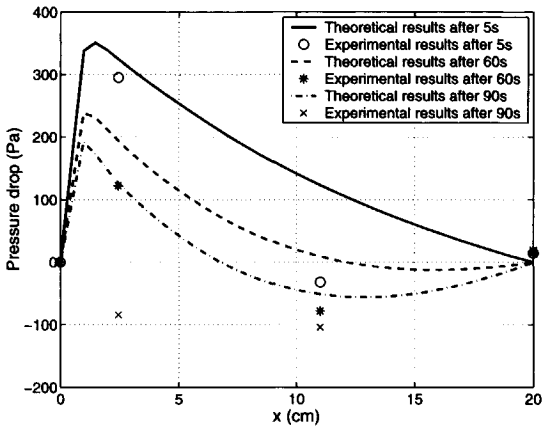

Figure 3.12: Pressure profile inside the core as function of position plotted at three different times. Both experimental data and theoretical results are shown. The Berea sandstone core is saturated with 2% KCl brine. Frequency 20 kHz, permeability 270 mD, p_{pore}=120 bars, p_{conf}=185 bars, I_0 = 1 10^5 W/m^2.

Appendix A: Brief review of Biot's theory and the calculation of damping coefficient

Biot's theory allows to calculate the velocity and the damping of acoustic elastic waves traveling through a porous material. In this appendix, we will give a brief review of this theory (simplified to the one-dimensional case). Introducing the averaged velocity of the solid, w_s, and the averaged velocity of the fluid, w_f (the relation between w_f and v introduced in section III is $v = \phi w_f$), the one-dimensional mass conservation laws for the solid and fluid phases in a porous medium can be written as

$$\frac{\partial}{\partial t}(1-\phi)\rho_s + \frac{\partial}{\partial x}(1-\phi)\rho_s w_s = 0 \tag{3.8}$$

$$\frac{\partial}{\partial t}\phi\rho_f + \frac{\partial}{\partial x}\phi\rho_f w_f = 0, \tag{3.9}$$

where ϕ is the porosity, and ρ_f and ρ_s are the densities of the fluid and solid respectively. Linearization of Eqs. 3.8 and 3.9 yields

$$(1-\phi)\frac{\partial \rho_s}{\partial t} - \rho_s\frac{\partial \phi}{\partial t} + (1-\phi)\rho_s\frac{\partial w_s}{\partial x} = 0 \tag{3.10}$$

$$\phi\frac{\partial \rho_f}{\partial t} + \rho_f\frac{\partial \phi}{\partial t} + \phi\rho_f\frac{\partial w_f}{\partial x} = 0. \tag{3.11}$$

Assuming that the grains are incompressible a combination of Eqs. 3.10 and 3.11 yields the so-called storage equation:

$$\frac{1}{K_f}\frac{\partial p}{\partial t} + \frac{1-\phi}{\phi}\frac{\partial w_s}{\partial x} + \frac{\partial w_f}{\partial x} = 0, \tag{3.12}$$

where we used the constitutive relation for the pore fluid

$$\frac{1}{\rho_f}\frac{\partial \rho_f}{\partial t} = \frac{1}{K_f}\frac{\partial p}{\partial t}. \tag{3.13}$$

K_f is the bulk modulus of the pore fluid.

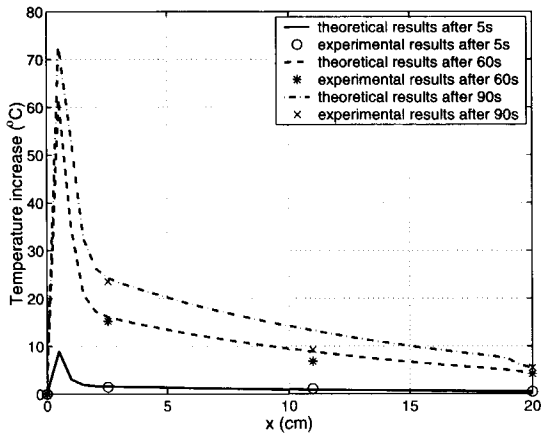

(a) Comparison between calculated and experimental temperature.

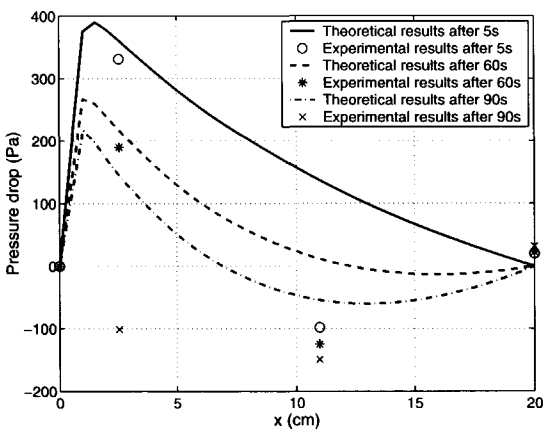

(b) Comparison between calculated and experimental pressure drop.

Figure 3.13: Pressure and temperature profiles inside the core as function of position plotted at three different times. Both experimental data and theoretical results are shown. The Berea sandstone core is saturated with 2% KCl brine. Frequency 20 kHz, permeability 270 mD, p_{pore}=120 bars, p_{conf}=185 bars, $I_0 = 1.11\ 10^5\ W/m^2$.

The linearized momentum equations for the solid and the fluid are given by

$$(1-\phi)\,\rho_s \frac{\partial w_s}{\partial t} = -\frac{\partial \sigma}{\partial x} - (1-\phi)\,\frac{\partial p}{\partial x} - f_x \tag{3.14}$$

$$\phi\rho_f \frac{\partial w_f}{\partial t} = -\phi \frac{\partial p}{\partial x} + f_x, \tag{3.15}$$

where we introduced the inter-granular stress σ (negative in tension), and the interaction force f_x between the solid and the fluid phases. A detailed expression for f_x will be given later. We finally close the system of equations by means of Hooke's law, relating the stress and the strain in the solid material

$$\frac{\partial \sigma}{\partial t} = -K_p \frac{\partial w_s}{\partial x}. \tag{3.16}$$

K_p is the constrained modulus (defined as $\lambda+2\mu$, with λ and μ the Lamé's coefficients). Taking the Fourier's transform of Eqs. 3.12-3.16 with respect to both time and space and eliminating p and σ, we obtain

$$-(1-\phi)\rho_s\omega^2\hat{w}_s = -\left[K_p + K_f\frac{(1-\phi)^2}{\phi}\right]\hat{w}_s k^2 - (1-\phi)K_f\hat{w}_f k^2 - i\omega\hat{f}_x \tag{3.17}$$

$$-\phi\rho_f\omega^2\hat{w}_f = -(1-\phi)K_f\hat{w}_s k^2 - \phi K_f k^2\hat{w}_f + i\omega\hat{f}_x. \tag{3.18}$$

At this stage it is necessary to provide an explicit formulation for $\hat{f}_x$. We have a precise definition due to the work of Johnson *et al.* (Johnson, Koplik & Dashen 1987)

$$\hat{f}_x = b(\omega)(\hat{w}_s - \hat{w}_f) + (\alpha_\infty - 1)\phi\rho_f i\omega(\hat{w}_s - \hat{w}_f) \tag{3.19}$$

where we have introduced the tortuosity α_∞. The frequency dependent friction force $b(\omega)$ is expressed as

$$\frac{b(\omega)}{b_0} = \sqrt{1 + \frac{1}{2}iM\frac{\omega}{\omega_c}}, \tag{3.20}$$

with $b_0 = \mu\phi^2/K_0$. K_0 is the stationary permeability, M is the so-called similarity parameter and ω_c is the critical frequency ($\omega_c = \mu\phi/K_0\rho_f\alpha_\infty$). Now solving Eqs. 3.18 and 3.19 we arrive at the dispersion relation

$$d_2\psi^2 + d_1\psi + d_0 = 0, \tag{3.21}$$

in which different quantities are defined by

$$\begin{aligned}
d_2 &= PR - Q^2 \\
d_1 &= -(P\rho_{22} + R\rho_{11} - 2Q\rho_{11} - 2Q\rho_{12}) + \tfrac{ib(\omega)}{\omega}(P + R + 2Q) \\
d_0 &= \rho_{11}\rho_{22} - \rho_{12}^2\tfrac{ib(\omega)}{\omega} \\
P &= K_p + K_f\tfrac{(1-\phi)^2}{\phi} \\
Q &= (1-\phi)K_f \\
R &= \phi K_f \\
\rho_{12} &= -(\alpha_\infty - 1)\phi\rho_f \\
\rho_{11} &= (1-\phi)\rho_s - \rho_{12} \\
\rho_{22} &= \phi\rho_f - \rho_{12} \\
\psi &= \left(\tfrac{k}{\omega}\right)^{1/2}.
\end{aligned} \tag{3.22}$$

Since the frequency is known, from Eq. 3.21 we can calculate the wave number (k) and then the velocity and the damping coefficient of the two waves. For instance, using the parameters given in Table 3.1 we derive the wave velocities and damping coefficients given in Table 3.2.

Appendix B: Reflection and transmission coefficients at the interface liquid/porous material

Wu *et al.* (Wu et al. 1990) developed a calculation procedure to deal with the problem of the transmission and reflection of acoustic waves at the interface between a fluid and a porous material.

The transmitted and reflected intensity are calculated by using the Poynting energy flux vector. We simplify the problem to the case of waves propagating perpendicular to the interface; in that case the shear wave is absent. If we introduce the potentials ϕ_+ and ϕ_- of the fast and slow wave (we will use the subscript + and − pointing respectively to fast and slow wave properties), we can write the displacements (for the free fluid, U', the fluid in the porous medium, U, and the solid material, u) as

$$U' = \frac{d\phi_f}{dx} \tag{3.23}$$

$$u = \frac{d\phi_+}{dx} + \frac{d\phi_-}{dx} \tag{3.24}$$

$$U = -G_+ \frac{d\phi_+}{dx} - G_- \frac{d\phi_-}{dx}, \tag{3.25}$$

where the coefficients $G_{+,-}$ are given by

$$G_{+,-} = \frac{c_{+,-}^2 \rho_{11} - P}{c_{+,-}^2 \rho_{12} - Q}. \tag{3.26}$$

$c_{+,-}$ are the velocities of the fast and slow waves. We can now impose the following three boundary conditions valid for the case of an open pore boundary condition

1. continuity of normal stress

$$(P+Q)\frac{du}{dx} + (Q+R)\frac{dU}{dx} - K_f \frac{dU'}{dz} = 0, \tag{3.27}$$

2. conservation of fluid volume

$$\phi U + (1-\phi)u = U', \tag{3.28}$$

3. proportionality between discontinuity in pressure and relative velocities in porous medium

$$(1/\phi)\left[Q\frac{du}{dx} + R\frac{dU}{dx}\right] - K_f \frac{dU'}{dx} = 0. \tag{3.29}$$

We define the Poynting vector as

$$\mathbf{P} = -\dot{\mathbf{u}} \cdot \mathbf{T} - \dot{\mathbf{U}} S, \tag{3.30}$$

where $\mathbf{T}$ is the stress tensor in the skeleton and S is the strain tensor. In one-dimensional case problem (assuming z the direction of propagation), the Poynting vector can be simplified as

$$\mathbf{P} = -i\omega \left[\mathbf{i}_z \left(uT + US\right)\right]. \tag{3.31}$$

The displacement potential can now be written as

$$\begin{aligned} \phi_f &= \left(e^{-i\gamma_f x} + Ae^{i\gamma_f x}\right) e^{-i\omega t} \\ \phi_+ &= B_+ e^{-i\gamma_+ x} e^{-i\omega t} \\ \phi_- &= B_- e^{-i\gamma_- x} e^{-i\omega t}, \end{aligned} \tag{3.32}$$

where the amplitude of the incident wave is taken equal to unity. A is the amplitude of the reflected wave and B_+ and B_- are the amplitude of the transmitted waves. In addition we have

$$\begin{aligned} \gamma_f^2 &= \omega^2 / V_f^2 \\ V_f &= (K_f/\rho_f)^{1/2} \\ \gamma_+ &= \omega / c_+ \\ \gamma_- &= \omega / c_-. \end{aligned} \tag{3.33}$$

If we now substitute the Eqs. 3.23-3.26 and 3.32 and 3.33 in Eqs. 3.27-3.29, we can determine A, B_+ and B_- and then the displacements. For fast and slow waves, we derive the following result

$$\begin{aligned} u &= -i\gamma_+\phi_+ - i\gamma_-\phi_-, \\ U &= -i\gamma_+ G_+\phi_+ - i\gamma_- G_-\phi_-, \\ T &= \left[(QG_+ - P + 2N)\,\omega^2/c_+^2 - 2N\gamma_+^2\right]\phi_+ \\ &\quad + \left[(QG_- - P + 2N)\,\omega^2/c_-^2 - 2N\gamma_-^2\right]\phi_-, \\ S &= (RG_+ - Q)\,\omega^2/c_+^2\phi_+ + (RG_- - Q)\,\omega^2/c_-^2\phi_-. \end{aligned} \tag{3.34}$$

If we substitute Eqs. 3.34 in Eq. 3.31 and take the absolute value of the Poynting vector, we obtain the sound intensity of the fast and slow wave in the fluid-saturated porous media

$$\begin{aligned} I_+ &= \left[(-2Q + RG_+)\,G_+ + P\right]\omega^4/c_+^3|\phi_+|^2 \\ I_- &= \left[(-2Q + RG_-)\,G_- + P\right]\omega^4/c_-^3|\phi_-|^2. \end{aligned} \tag{3.35}$$

Parameter	Value
Permeability	$0.1974{\cdot}10^{-12}$ (m^2)
porosity	25 (%)
K_p	36.1 (GPa)
K_f	2.06 (GPa)
μ	9.8 10^{-4} (Pa s)
ρ_f	1000 (kg/m^3)
ρ_s	2640 (kg/m^3)
ω	40 (kHz)
α_∞	2.8 (-)
M	1 (-)

Table 3.1: Parameters used for the calculation of the wave properties.

Parameter	Value
c_{fast}	4833.6 (m/s)
c_{slow}	658.4 (m/s)
α_{fast}	0.28 (m^{-1})
α_{slow}	182.3 (m^{-1})

Table 3.2: Wave velocities and damping coefficients.

In the previous chapters the influence of ultrasonic waves on the flow through a porous material was investigated in the absence of fouling particles in the material. However, as mentioned in the introduction an important aim of our research is to study the possibility of removing small fouling particles present in the pores (filled with a flowing liquid) of the porous material by means of ultrasonic waves. The particles can be generated inside the material itself (due to chemical or physical processes), or the particles can penetrate into the porous material from outside. In this chapter we consider only internally generated particles. These particles can cause two types of fouling: 1) fouling due to particles adhering to pore walls by colloidal forces and thus reducing the pore diameter, and 2) fouling due to particles bridge formation in the pore throats of the material thus reducing the flow rate. In this chapter we consider only fouling due to particles adhering to pore walls. A theoretical model is developed, in which the colloidal and hydrodynamic forces on a particle at a pore wall are described. Also the effect of acoustic waves on a particle is incorporated. A scale-up procedure is used to scale-up the (microscopic) pore level results to (macroscopic) permeability changes. The theoretical results are compared with experimental data.

Chapter 4

Removal of small particles from a porous material by ultrasonic irradiation*

Abstract

A study has been made of the removal of small particles from a porous material by means of ultrasonic irradiation. To that purpose a microscopic theoretical model has been developed to calculate the force of a traveling acoustic wave on a spherical particle attached to the wall of a smooth, cylindrical pore inside the porous material. This force was compared with the adhesion force between a small particle and a pore wall. From the comparison between the two forces the conditions were found, at which particles are detached from pore walls and removed from the porous material. The transformation of the results gained from the microscopic model to macroscopic property (permeability) of the porous material was made by means of the Kozeny relation. The aim is to be able to understand and predict qualitatively the influence of relevant parameters on the ultrasonic cleaning process. Predictions made with the theoretical model were compared with data from experiments carried out with ultrasound to remove particles from Berea sandstone. The agreement is reasonable.

4.1 Introduction

Reduction of the permeability of a porous material due to fouling by small particles has a negative effect on many industrial processes. For instance during the production of oil from an underground reservoir fouling by particles can decrease the permeability of the reservoir rock in the near well-bore region, reducing the well productivity considerably. Several techniques, such as acid treatment or hydraulic fracturing of the near well bore region, have been developed to overcome this problem, but several drawbacks make them unattractive. These techniques can be environmental unfriendly, dangerous or expensive. More details, both on the possible techniques and on their drawbacks, can be found in SPE reprint series *Formation Damage* (1990). Therefore a new technique has been proposed: irradiation of the near well-bore region with high-frequency acoustic waves. This promising technique seems to work only under certain conditions, but a method to predict these conditions is not available. So it is important to study the technique in more detail in order to be able to apply it with success. In previous publications, see Barake et al. (2001), Poesio, Ooms, Barake & v. Bas (2002) and Poesio, Ooms, Schraven & v. Bas (2002), we have already reported about the influence of high-frequency acoustic waves on the flow of a liquid without particles through a porous material. In this publication we go one step further and investigate

*P. Poesio, G. Ooms, M.E.H. v. Dongen, and D.M.J. Smeulders. "Removal of small particles from a porous material by ultrasonic irradiation". *Transport in Porous Media* 54(3):239-264, 2004.

how ultrasonic waves influence particles in a saturated porous material through which a liquid flows.

Before investigating the way in which ultrasound can remove particles from a porous material, it is important to discuss first the mechanisms that cause the permeability reduction by particles. Reduction in permeability can be due either to bridge formation of particles in the throats of pores inside the material, or due to the deposition of particles onto the pore walls leading to a reduction of the pore diameter. Of course a combination of the two mechanisms is also possible. Which mechanism occurs, depends on conditions like liquid flow velocity, particle properties and properties of the porous material. The cleaning (particle removing) efficiency of ultrasound is different for the two fouling mechanisms. In this publication we assume that the permeability reduction is due to the deposition of small particles onto the pore walls. The generation of such particles in an oil reservoir may be due to erosion of the reservoir rock by the liquid flow through the reservoir during the production. Also other causes are possible. The generation and migration of small particles in a porous material is well described in the book by Khilar & Fogler (1998).

The aim of this publication is to investigate the conditions at which particles attached to the pore walls can be removed by means of high-frequency acoustic waves. We start by developing a microscopic theoretical model to calculate the hydrodynamic force exerted by a traveling acoustic wave on a spherical particle attached to the wall of a smooth cylindrical pore. Also a model is applied to calculate the adhesion force between a particle and the pore wall. Next, we compare the hydrodynamic force and the adhesion force to find out at what conditions a particle will detach from a pore wall. The aim of this microscopic model is to understand and model qualitatively the physics of the detachment of small particles from a pore wall. In this idealized geometrical configuration of a smooth, cylindrical pore (where an analytical solution can be derived), we can change the values of the relevant parameters and check their influence on the cleaning mechanism. Therefore, a sensitivity study will be carried out in order to investigate the dependence of the particle removal on these parameters. The transformation of the results gained from the microscopic model to the permeability of the porous material is made by means of the Kozeny relation. This will be explained in detail. Next we will describe the experimental set-up that we used for our experiments to remove particles from Berea sandstone cores by ultrasound. Finally, we will compare theoretical and experimental results and draw some conclusions.

4.2 Microscopic model

4.2.1 Force on a particle attached to a pore wall by a traveling acoustic wave

Let us first assume, that there is no net pressure gradient over the porous material. Only a traveling acoustic wave generated by an acoustic source is present inside the pores of the material. The influence of friction on the oscillating flow in a solid-walled tube (a pore) has been described in detail in the literature. According to White (1991) we can calculate the oscillating flow in a cylindrical pore with radius R_p due to an acoustic wave with friction at the pore wall by using the following equation of motion (in cylindrical coordinates)

$$\frac{\partial u}{\partial t} = -\frac{1}{\rho}\frac{dp}{dx} + \nu\left(\frac{\partial^2 u}{\partial r^2} + \frac{1}{r}\frac{\partial u}{\partial r}\right), \tag{4.1}$$

in which u is the fluid velocity, t the time, ρ the density, p the pressure, x the axial coordinate, ν the kinematic viscosity, and r the radial coordinate. The oscillating pressure gradient is given by

$$\frac{dp}{dx} = \rho I e^{i\omega t}, \tag{4.2}$$

where I is determined by the intensity of the acoustic source and ω is the acoustic frequency. Based on ρI also a characteristic velocity $U_{max} = I R_p^2/4\nu$ can be defined. It can be interpreted as the velocity at the centerline of the pore, when a constant pressure gradient ρI is applied. Using

the continuity equation and the no-slip condition at $r = R_p$, the solution of the equation of motion can be written in terms of Bessel functions

$$u(r,t) = \frac{I}{i\omega} e^{i\omega t} \left[1 - \frac{J_0\left(r\sqrt{-i\omega/\nu}\right)}{J_0\left(R_p\sqrt{-i\omega/\nu}\right)} \right], \tag{4.3}$$

in which J_0 is the Bessel function of zeroth order.

U_{max} can, at a distance x from the entrance to the pore, be related to the acoustic power input P_0 of the acoustic source at the entrance of the pore in the following way

$$A\rho c U_{max}^2 = P_0 e^{-2\alpha x}, \tag{4.4}$$

where c is the propagation velocity of the acoustic wave, A is the surface area and α is the damping coefficient of the wave, Poesio, Ooms, Schraven & v. Bas (2002). So from Eqs. 4.3 and 4.4 (with the expression $I = 4\nu U_{max}/R_p^2$) the oscillating liquid velocity in a pore can be calculated as function of the axial coordinate x, the radial coordinate r and the time t when the acoustic power input P_0 at the entrance to the pore, the pore radius R_p, the acoustic frequency ω, the acoustic wave propagation c and the fluid viscosity ν, the density ρ, the surface area A and the damping coefficient α are known.

A spherical particle with radius R attached to a pore wall experiences a drag force due to the oscillating liquid flow calculated above. Higdon & Muldowney (1995) derived an expression for this drag force for the case of a particle in a steady Poiseuille flow through a cylindrical pore. Their result is still valid for the case of an oscillating velocity field at low frequencies, as at each moment the deviation from the parabolic profile is negligible. At higher frequencies this is only true for particles that are small compared to the pore radius, as only close to the pore wall (where the particles are located) the deviation from the parabolic profile remains rather small. So following Higdon and Muldowney we write the maximum of the drag force in the following way

$$F_D = C_d\, 6\pi\rho\nu R u(r=0,t)_{max}, \tag{4.5}$$

in which $u(r=0,t)_{max}$ is the maximum of the oscillating liquid velocity at the pore axis. $u(r = 0,t)_{max}$ is a function of the acoustic frequency. C_d depends on the ratio of the particle radius and pore radius. The value of C_d as function of R/R_p has been determined by Higdon and Muldowney; their result is given in Fig. 4.1.

We consider now the effect of a net (constant) liquid flow through the porous material due to a constant pressure gradient, since under practical conditions (and therefore also in our experiments) such a net flow is usually present. Due to the linearity of the Stokes equation it is allowed to add to the oscillating flow (due to the acoustic wave) a Poiseuille flow due to an applied constant pressure drop over the porous material. So in that case the drag force will be given by

$$F_D = C_d\, 6\pi\mu R[u(r=0,t)_{max} + v(r=0)], \tag{4.6}$$

in which $v(r=0)$ is the fluid velocity at the pore axis due to a constant pressure drop.

We will investigate the influence of some relevant parameters on the drag force keeping the other parameters constant. To that purpose, we have formulated the equations given above in a dimensionless way and we found the following relevant parameters:

$$F_D^* = \frac{F_D\sqrt{A\rho c}}{6\pi R\sqrt{P}e^{\alpha x}}. \tag{4.7}$$

$$\omega^* = \frac{\omega\rho R_p^2}{\mu}, \tag{4.8}$$

$$R^* = \frac{R}{R_p}, \tag{4.9}$$

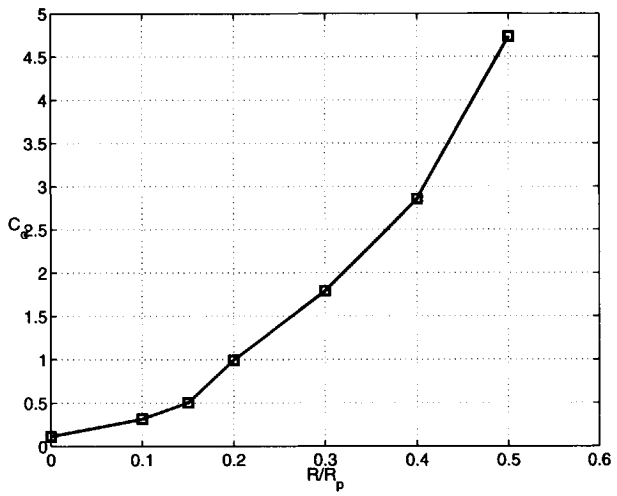

Figure 4.1: Value of C_d as function of R/R_p according to Higdon and Muldowney (1995).

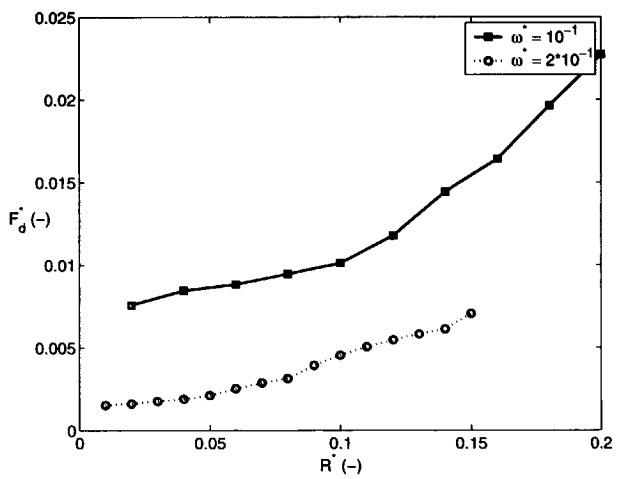

Figure 4.2: Dimensionless drag force as a function of the dimensionless particle radius for two values of the dimensionless frequency. The distance x is 10 cm.

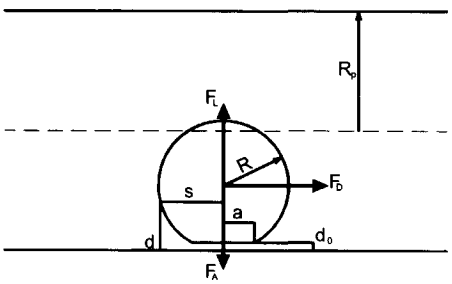

Figure 4.3: Particle attached to a pore wall by an adhesion force.

In Fig. 4.2, the dimensionless drag force (F_D^*) is plotted as function of the dimensionless particle radius (R^*) for two values of the dimensionless frequency (ω^*). As can be seen, the drag force increases with increasing dimensionless particle radius and with decreasing dimensionless frequency.

Now that we have a method to calculate the drag force on a particle as function of the relevant parameters, it is important to investigate at what conditions the drag force causes a detachment of the particle from the pore wall. A particle attached by an adhesion force to a pore wall can start moving due to the drag force according to three mechanisms: rolling, lifting or sliding. It has been proved, that the easiest way to start the movement process is by rolling the particle. Hubbe (1984) showed that at equilibrium between the drag force F_D and the adhesion force F_A and the lift force F_L the following relation between the forces holds

$$1.4RF_D = a(F_A - F_L), \tag{4.10}$$

where a is the radius of the flat particle part that exists between the particle and the pore wall due to the influence of the adhesion force (see Fig. 4.3). The adhesion force F_A and the radius a will be calculated in the next section. As mentioned, F_L is the lift force acting on the particle and it is in opposite direction to the adhesion force. For a spherical particle attached on a wall the lift force can be calculated in the following way (Leighton & Acrivos 1985):

$$F_L = 0.287RF_D; \tag{4.11}$$

in which the forces are expressed in Newton and R in meters. Applying this relation in our case shows that the lift force is always negligibly small compared to the drag force and the adhesion force.

From Eq. 4.10 follows, that the drag force that must be exerted by the oscillating fluid on a particle to get it rolling must be larger than

$$F_D = \frac{a(F_A - F_L)}{1.4R}. \tag{4.12}$$

where the negative sign indicates that lift force and adhesion force act in opposite direction.

4.2.2 Adhesion force between a particle and a pore wall

To calculate the adhesion force between a particle and a pore wall we use the method proposed by Tutuncu & Sharma (1992). As mentioned before there exists a circular-shaped flat part with

radius a in the particle surface between the particle and the pore wall (see Fig. 4.3). The distance between the flat part and the pore wall is d_0. The distance between each point of the remaining spherical part of the particle and the pore wall is described by

$$d(s,a,d_0) = d_0 + \frac{1}{\pi R}\left(a\sqrt{s^2-a^2} + (s^2-2a^2)\arctan\left(\frac{\sqrt{s^2-a^2}}{a}\right)\right). \tag{4.13}$$

The variables d and s are shown in Fig. 4.3.

The total force acting on the particle can be written as

$$F_{total} = F_{vdw} + F_{st} + F_{born} + F_{dl} + F_g, \tag{4.14}$$

where F_{vdw} is the (attractive) van der Waals force, F_{st} is the (repulsive) structural force, F_{born} is the (repulsive) Born force, F_{dl} is the (repulsive) electrical double-layer force and F_g is the gravitational force.

The van der Waals force per unit surface area between a flat plate and a spherical particle is, according to Russel, Saville & Schowalter (1989), given by

$$F''_{vdw} = -\frac{A}{6\pi d^3} f(p). \tag{4.15}$$

A is the Hamaker constant. It depends on the material properties of the particle, the wall and the liquid. If we assume the Hamaker constant for the particle to be A_{11}, for the liquid A_{22} and for the wall A_{33}, the Hamaker constant A for the interaction can according to Khilar & Fogler (1998) be written as

$$A = (A_{11} - A_{22})^{1/2}(A_{33} - A_{22})^{1/2}. \tag{4.16}$$

The function $f(p)$ is a correction factor equal to

$$f(p) = \frac{1+3.54p}{1+1.77p} \qquad p<1; f(p) = \frac{0.98}{p} - \frac{0.434}{p^2} + \frac{0.067}{p^3} \qquad p>1, \tag{4.17}$$

where $p = 2\pi h/\lambda_L$. λ_L is the London retardation length, taken of the order 100 nm as suggested by Khilar and Fogler. h is Planck's constant.

The structural force per unit area has been determined by Derjaguin, Churaev & Muller (1987) and is equal to

$$F''_{str} = K_l/sinh^2(d/2l), \tag{4.18}$$

where l and K_l are structural parameters.

The Born repulsion per unit area is according to Tutuncu and Sharma (1992) given by

$$F''_{born} = \frac{A\sigma}{45d^9}, \tag{4.19}$$

in which σ is called the collision diameter.

The electrical double-layer force per unit area has been calculated by Ven (1989) and is equal to

$$F''_{dl} = 64NkT\gamma^2 e^{-\kappa d}, \tag{4.20}$$

where

$$\gamma = \tanh\frac{e\psi}{4kT} \quad \kappa = \sqrt{\frac{8\pi Ne^2}{\epsilon kT}}. \tag{4.21}$$

e is the unit of electrical charge, k the Boltzmann constant, ψ the potential of the interacting surfaces, T the temperature, κ the inverse of the Debye length, N the number of ions per unit volume and ϵ the permettivity of the water.

The gravitational force is equal to

$$F_g = \rho_p g V, \tag{4.22}$$

in which ρ_p and V are the density and the volume of the particle, respectively. As is well known, for small particles F_g is negligible.

The total force acting on the particle is

$$F_{total} = \sum \left(\pi a^2 F_i'' + 2\pi \int_a^R F_i''(d(s, R, d_0)) s ds \right). \tag{4.23}$$

The summation includes all the contributions listed above. The first term in the equation represents the force acting on the deformed flat part of the particle, while the second term represents the interaction between the wall and the un-deformed spherical part of the particle. The second term is calculated using the so-called ring approximation. In the ring approximation the particle is considered as consisting of a number of circular rings centered on the line perpendicular to the wall and passing through the center of the sphere. The integration of the force exerted on each ring yields the total force acting on the spherical part of the particle.

Under equilibrium conditions the total force acting on the particle vanishes

$$F_{total} = 0. \tag{4.24}$$

When we assume the radius a of the flat particle part to be known, Eqs. 4.23 and 4.24 can be used to calculate the distance d_0 between the particle and the pore wall. However, for real particles the radius a is unknown. It depends on the (particle deforming) attractive van der Waals force and on the elastic properties of the particle and wall. The deforming force is assumed to be equal to the van der Waals force. Hertz's theory, see Timoshenko & Goodier (1951), can then relate the van der Waals force to the elastic properties in the following way

$$F_{vdw}(d, R, R_p) = \frac{4a^3(R + R_p)}{3\pi(k_1 + k_2)RR_p}. \tag{4.25}$$

k_1 and k_2 are elastic parameters given by

$$k_i = \frac{1 - \delta_i^2}{\pi E_i}. \tag{4.26}$$

δ is the Poisson's ratio and E is the Young modulus. The index i indicates the particle or the pore wall. We assume that the pore wall and the particle have the same structural properties, so $k_1 = k_2$ and $E_1 = E_2$.

As mentioned the purpose of this section is to determine the adhesion force F_A. The adhesion force (the van der Waals force) can be calculated in the following manner. We start by assuming a certain value for a. We use that value in Eq. 4.25 to make a first estimate of the van der Waals force. Then we calculate the equilibrium distance d_0 from Eq. 4.15. Next we compute the integral in Eq. 4.23 and check if its value is zero. If the value is not zero we choose another value for a and repeat the calculation. If the value is zero we have found a possible solution. There might be more than one solution. However it is possible to show that, for stability, it is necessary that $\partial F_{tot}/\partial d < 0$. If more than one solution fulfills this condition the smallest (more stable) distance is chosen.

To be able to make quantitative calculations, the values of the parameters, occurring in the different forces discussed above, need to be known. The values we used are the ones applied by Khilar & Fogler (1998). They are listed in Tab. 4.1. Using these values, we have calculated the adhesion force and the radius a of the flat part as functions of the particle radius and the Young modulus of the particles. The results are given in Figs. 4.4 and 4.5. From Fig. 4.4 can be seen that the radius of the flat part of the particle is usually much smaller than the particle radius. Figure 4.5 shows that the adhesion force increases with increasing particle radius and decreases with increasing Young modulus.

Parameter	Value	Units
A_{11}	$6\,10^{-20}$	J
A_{22}	$6\,10^{-20}$	J
A_{33}	$1\,10^{-20}$	J
ψ	20	mV
ϵ	80	-
N	$6.022\,10^{25}$	-
δ	.15	-
E	$1.6\,10^{10}$	Pa
l	10^{-9}	m^{-1}
K_l	10^{6}	N/m^2

Table 4.1: Parameters used for the theoretical calculation.

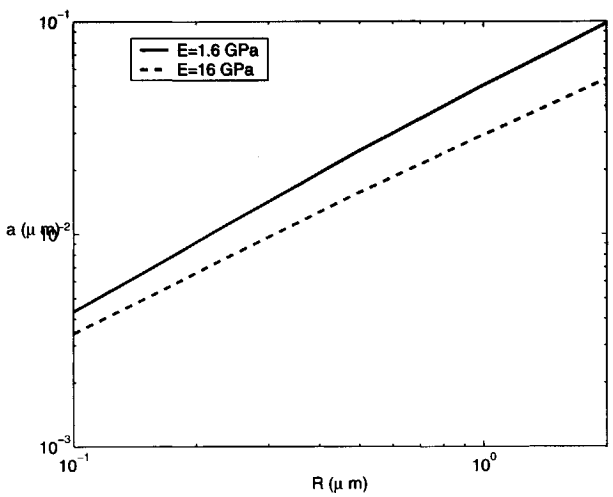

Figure 4.4: Radius a of flat particle area as function of particle radius R for two values of Young modulus.

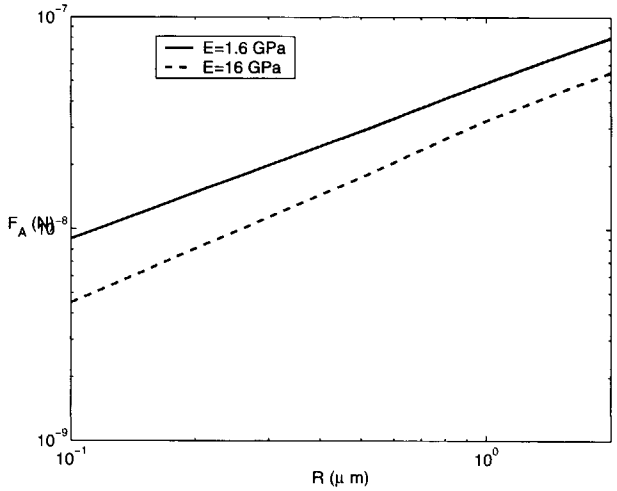

Figure 4.5: Adhesion force F_A as function of particle radius R for two values of Young modulus.

4.2.3 Sensitivity study

Using the detachment criterion given in Eq. 4.12 and the derived expressions for the drag force, the lift force and the adhesion force, we are now in a position to calculate the acoustic power needed for the detachment of particles as function of the relevant parameters. To that purpose we selected realistic values for the fluid and rock properties and also for the frequency and calculated the adhesion force and the drag force as a function of the power input. By equating these two forces, we find the required power and we could also check whether this power was available during our experiments. Some results are given in Figs. 4.6 to 4.9. In these figures the detachment power P is plotted as function of the particle radius R for several values of other parameters (Young modulus, fluid viscosity and pore radius respectively). It is clear that the acoustic power needed for detachment decreases with increasing particle radius. The reason is that although the adhesion force on a particle increases with particle radius, so does the drag force and this increase in drag force is significantly larger than the adhesion force. Fig. 4.6 shows that the detachment power decreases with increasing Young modulus. Particles with a large Young modulus do not deform easily and, therefore, the adhesion force is relatively small. From Fig. 4.7 can be seen that the detachment power decreases with increasing fluid viscosity. This is due to the fact that an increasing viscosity causes an increasing drag force, whereas the adhesion force remains nearly constant. Fig. 4.8 shows that the detachment power decreases with increasing pore radius. The pore radius is directly related to the permeability of the porous material: with increasing pore radius the permeability increases. So, Fig. 4.8 indicates that with increasing permeability of the porous material the acoustic power needed for the detachment of particles decreases. This result can be important for the understanding, why acoustic stimulation of the near well bore region in an oil reservoir only works under certain conditions. Finally, in Fig. 4.9, the dependence of the detachment power on the distance between the acoustic source and the particle location is shown. Due to damping the acoustic energy decreases with distance from the source. Hence more initial acoustic power is needed to remove far-away particles. The transformation of the results gained from the microscopic model to macroscopic properties of the porous material by means of the Kozeny relation will be discussed later.

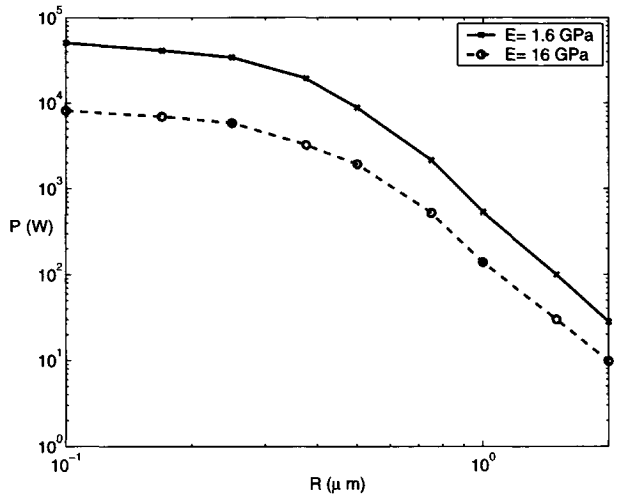

Figure 4.6: Power P required for detachment of particles as function of particle radius R for two values of Young modulus. $\nu = 10^{-6}\ m^2/s$, $R_P = 10\mu m$, $f = \omega/2\pi = 20\ kHz$, $x = 10\ cm$.

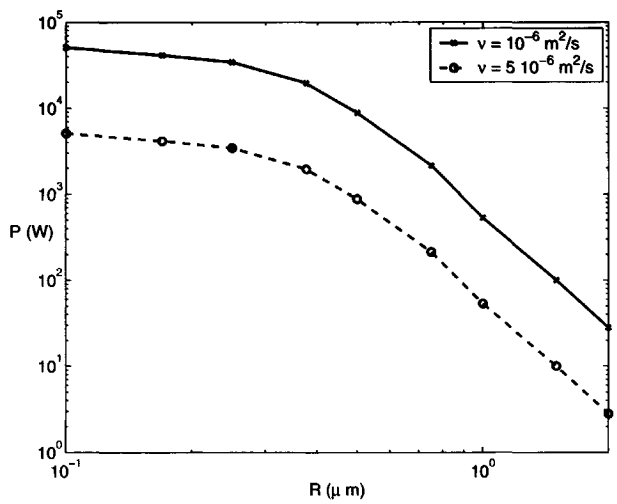

Figure 4.7: Power P required for detachment of particles as function of particle radius R for two values of fluid viscosity. $E = 1.6\ GPa$, $R_P = 10\mu m$, $f = \omega/2\pi = 20\ kHz$, $x = 10\ cm$.

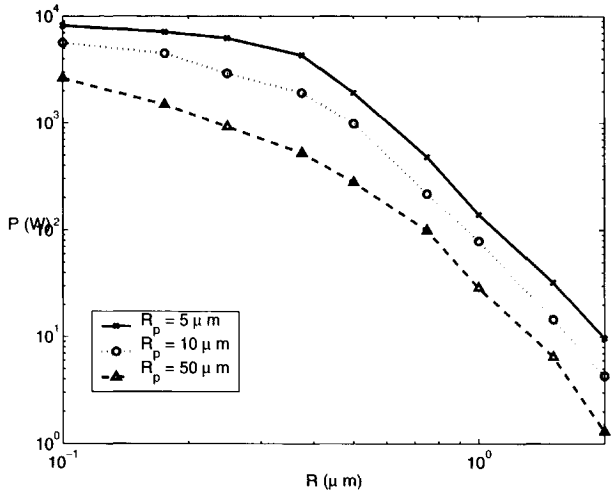

Figure 4.8: Power P required for detachment of particles as function of particle radius R for three values of pore radius. $\nu = 10^{-6}\ m^2/s$, $E = 1.6\ GPa$, $R_P = 10\mu m$, $f = \omega/2\pi = 20\ kHz$, $x = 10\ cm$.

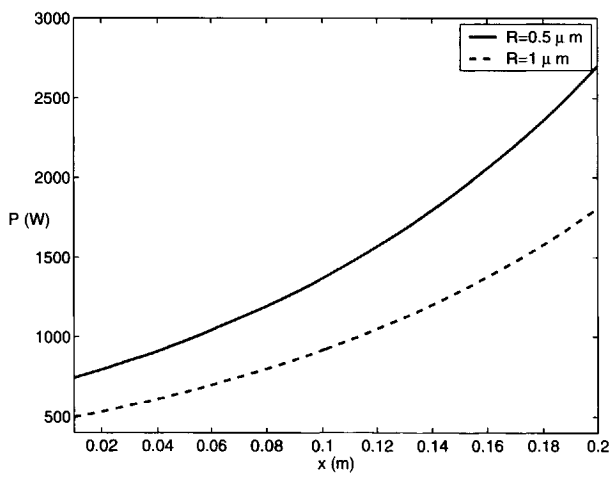

Figure 4.9: Power P needed to detach particles as a function of the distance x between acoustic source and particle location for two values of the pore radius. $\nu = 10^{-6}\ m^2/s$, $E = 1.6\ GPa$, $f = \omega/2\pi = 20\ kHz$.

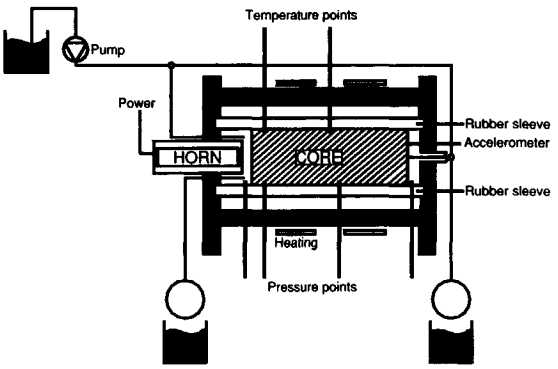

Figure 4.10: Experimental set-up.

4.3 Experiments

4.3.1 Experimental set-up

We have carried out experiments to investigate the particle removal from sandstone by ultrasound. The experiments were carried out in the set-up shown in Fig. 4.10.

The cores, used for the experiments, were cylindrically shaped Berea sandstone samples. The length of the cores was 20 *cm* and the diameter 7.62 *cm*. The porosity ranges from 19% to 25%. The initial permeability was 100-500 mD for all samples. During an experiment a core was placed in a rubber sleeve to keep it fixed during the experiment. It was then placed in a steel vessel in which down-hole reservoir conditions were simulated (up to 150 bars pore pressure and 180 bars confining pressure). An acoustic horn was placed at one end of the core (see Fig. 4.10). The high pressure in the vessel made it possible to avoid cavitation (for pressures lower than 100 bars the influence of cavitation becomes noticeable). The space between the vessel and sleeve, which was filled with water, was pressurized to 180 bars to make the rubber sleeve completely seal off.

There were four pressure measurements, two along the core (at 2.54 *cm* and 10.70 *cm*) and two at both ends of the core (see Fig. 4.10). dP_1 is the pressure drop over the first part of the core sample, dP_2 the pressure drop over the middle part and dP_c the total pressure drop over the core. The pressure drop over the third part dP_3 can be calculated in the following way: $dP_3 = dP_c - (dP_1 + dP_2)$. To measure the temperature at two locations in the core we installed two thermocouples at the sidewall of the porous medium, through the rubber sleeve (see Fig. 4.10). Also the temperature in front and at the back of the core could be measured. The data were sent to a digital data recorder and processed on a computer.

The ultrasonic equipment consisted of: 1) a converter, which converts electricity into mechanical vibrations of a piezoelectric element, 2) an amplifier, which is used to set the amplitude of the vibrations and 3) an ultrasonic horn, which concentrates the mechanical vibrations onto the front side of the core sample. An acoustic horn was applied: a Branson Module PGA 220 (a 20 kHz horn with maximum power output of 2 kW). The power output could be selected as a percentage of the maximum.

A microphone was placed at the back side of the core. It was used to measure the amplitude of the acoustic signal after passage through the core. In this way the damping of the signal was determined during the experiments.

By means of a system of valves the flow could be either in the same direction or in the opposite direction of the traveling acoustic waves. During the experiments discussed in this publication the flow was kept in the opposite direction of the acoustic waves.

4.3.2 Measurement of particle size distribution

To measure the particle size distribution the GALAI (*Ankersmit*) particle sizer was used. This instrument can measure the particle diameter down to 0.1 μm. Also the particle concentration can be measured. The upper limit for the concentration is $10^9 ml^{-1}$, while the lower limit is related to particle size. The particle sizer is based on a direct optical method. The result is not influenced by the refraction index, so results obtained with different fluids are comparable. In our experiments the particle are in the range 0.1-4 μm.

4.3.3 Experimental procedure

A new core (Berea sandstone) was used for each new series of experiments. Before performing experiments, the following steps were taken: 1) the core was flushed with CO_2 to expel all the air in the porous material, 2) after the gas flow was stopped, a constant flow rate of the brine was started (the high pressure ensured that all the CO_2 dissolved into the brine. Brine instead of water was used in order to avoid the generation of fine clay particles inside the core sample by the swelling of clay, for more details see Khilar and Fogler) and 3) the initial permeability of the core was measured.

During the sonification experiments (irradiation of high-frequency acoustic waves) a constant flow rate of 25 ml/min was imposed. The acoustic source was switched on for three minutes. Then we waited until the system cooled down to the initial temperature. We have reported earlier that due to the energy dissipation of the high-frequency acoustic waves the temperature of the fluid can increase significantly, see Poesio, Ooms, Barake & v. Bas (2002). Then the pressure distribution over the core was measured. Next a new burst of acoustic irradiation with the same intensity was applied and the system was cooled down again. Then the pressure distribution was measured and compared with the previous one. When the two distributions were the same we assumed that the second acoustic treatment had no further cleaning effect on the core and we measured its permeability. When the pressure distributions were different, another acoustic burst was applied. This procedure was repeated until the measured pressure distributions of the last two treatments were equal and the final permeability was measured. To measure the permeability we imposed a flow of up to 150 ml/min, starting from 25 ml/min with steps of 25 ml/min, and we measured the pressure distribution. The permeability was then calculated with the aid of Darcy's law. We also collected samples of the liquid with fouling particles coming out of the porous material and measured the particle size distribution.

4.4 Experimental results

During our experiments we measured the ratio of the final permeability (after acoustic treatment) and the initial permeability as function of the acoustic intensity, initial permeability (which is related to the pore diameter), fluid viscosity and distance to the acoustic source. The experimental results are summarized in Fig. 4.11. It is perhaps a somewhat complicated figure, but it shows very well the influence of the relevant parameters on the permeability increase due to ultrasonic irradiation. We will now discuss the details.

First we study the influence of the acoustic intensity. For some series of experiments (d, f and h, in Fig. 4.11) we recorded the permeability increase after treatments with different acoustic intensities. As can be seen from Fig. 4.11 the cleaning effect increases with increasing intensity. If, for instance, we focus our attention on experiments d and h, we can see that after an increase in permeability due to the application of acoustics irradiation with 50% power of the acoustic source, we can still further increase the permeability by applying an irradiation with 75% power and, even more, by applying a 100% power.

Another interesting parameter is the initial permeability. The initial permeability (K_0) as indicated along the horizontal axis in Fig. 4.11 is the averaged initial permeability for the total core length. The final permeability (after acoustic irradiation) indicated along the vertical axis (K) is given for the three parts of the core separately. The reason is that the cleaning effect

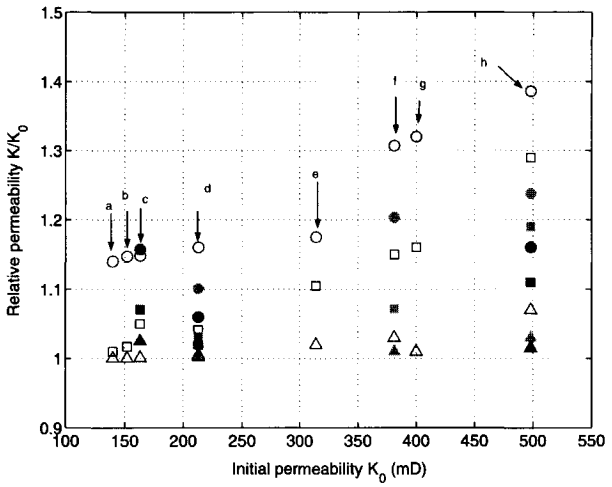

Figure 4.11: Ratio of final and initial permeability as function of relevant parameters. The circles represent the permeability of the first part, the squares of second part and the triangles of the third part of the core sample. The empty symbols always refer to the application of 100% input power. For experiments *d*, *f* and *h* the full symbols with the light color indicates 75% power input and the full symbols with the dark color 50% input power. For experiment *c* the full symbols refer to experiments with a higher viscosity.

decreases with distance from the source. So the final permeability of the three parts of the core will be different. From the data shown in Fig. 4.11, we can clearly see a trend in the cleaning efficiency as function of the initial permeability. With increasing initial permeability not only the final permeability increases, but also the ratio of the final and initial permeability. Focusing our attention in Fig. 4.11, for instance, on the first part of the core we see, that when we start with a permeability of about 140 mD (experiment a) the increase is about 13%, while if the initial permeability is around 500 mD (experiments h) the increase is 40% . Another interesting point arises from a comparison of the experiments *d* and *h*. The increase in permeability due to a power increase from 50% to 75% is always less than the permeability increase from 75% to 100%. This observation can be justified by arguing that, in the second case, the *initial* permeability is greater than in the first case. (However, a deviation from this behavior can be seen for the third part of the core used in experiment *g*.) In Fig. 4.12 we show the measured results for the particle size distribution and concentration in the out-flowing liquid stream as a function of initial permeability. It can be seen that the particle concentration is the highest for the most permeable medium, which was to be expected from the permeability measurements. It can be noticed that the particle size distribution is not much affected by the initial permeability, although for the more permeable material the number of small particles detached is larger than the number for the low permeable material.

The fluid viscosity is also an important parameter. Therefore, we performed one experiment using a mixture of brine-glycerol as saturating fluid (the mixture is made up with 50% brine and 50% glycerol). The result is reported in Fig. 4.11 (experiment *c*) and Fig. 4.13. From Fig. 4.11 we notice that an increase in permeability is found when the fluid viscosity increases. In Fig. 4.13 the particle size distribution in the out-flowing stream for the high-viscosity fluid is compared with the result for the low-viscosity fluid (brine). For the case of the high-viscosity the distribution is shifted to the left (towards smaller particles), while the concentration is comparable.

The final parameter that we want to discuss briefly is the distance from the acoustic source. As

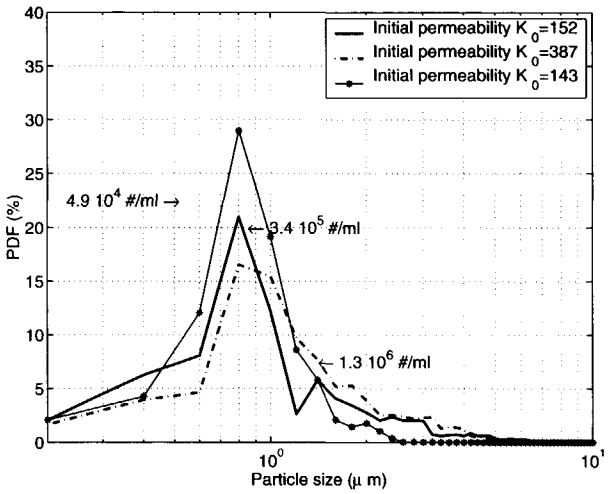

Figure 4.12: Comparison of the particle size distribution in the out-flowing stream for cores with different initial permeabilities.

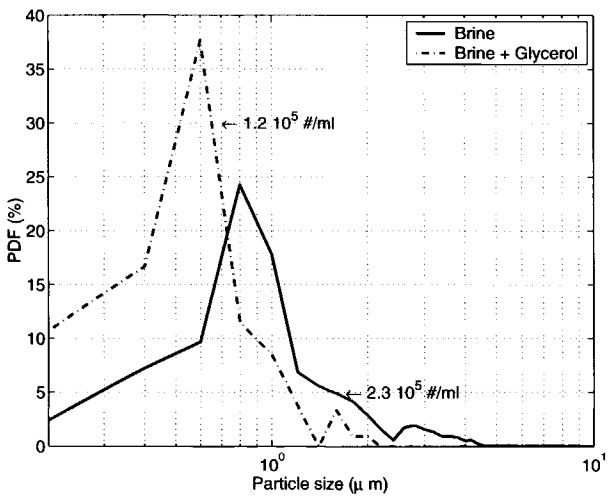

Figure 4.13: Particle size distribution measured after sonification with brine (solid line) and after sonification with water-glycerol mixture (dashed line).

can clearly be seen from Fig. 4.11, the cleaning efficiency decreases with increasing distance from the source. The reason is, of course, that due to the acoustic energy dissipation the intensity of the traveling acoustic wave decreases rather quickly with distance from the source. So the first part of the core (closest to the source) shows the strongest cleaning effect, then the second (middle) part and finally the third part (at the largest distance from the source).

4.5 Transformation of the results from the microscopic model to the permeability and comparison with experimental data

From the experimental results we can conclude, that the cleaning efficiency (the ratio of the final and initial permeability) increases with increasing acoustic power input and with increasing initial permeability. This is in qualitative agreement with the theoretical predictions made with the microscopic model as shown in Fig. 4.8. This figure shows that with increasing power input also the smaller particles are detached. Moreover, it shows that with increasing pore radius (increasing initial permeability) less input power is needed to detach particles of a certain size.

We have also tried to transform the microscopic model results to the macroscopic permeability of the porous material and compared this theoretical permeability with experimental data. For this transformation we have used the following Kozeny equation (see Bear (1972))*, which relates microscopic quantities with the macroscopic permeability

$$K = \frac{\phi D_{eff}^2}{8\tau}, \tag{4.27}$$

in which the effective diameter D_{eff} is equal to the pore radius minus the radius of the largest particle in the pore before acoustic irradiation; ϕ is the porosity and τ is the tortuosity. Kozeny equation may not be applied for the oscillating flow due to an acoustic wave, as in that case the inertia momentum dominates the drag momentum. We want to point that we indeed do not use the Kozeny equation during the period of ultrasonic irradiation. We only use this equation during the periods before (to evaluate what we call the initial permeability, noted as K_0) and after irradiation (to evaluate the permeability after acoustic treatment, indicated as K), when the drag momentum dominates the inertia momentum. By means of Eq. 4.27 we assume that D_{eff} is directly related to the initial permeability of the core sample. Moreover, for a certain power input we can calculate with the theoretical model $R_p - R_{min}$, where R_{min} is the smallest particle that remains attached to the pore wall after acoustic irradiation at a given power input. To calculate the size of the smallest particle that stays attached to the pore wall, we make use of Fig. 4.8 assuming we know the pore size and the power available at a certain distance from the acoustic source. The power available at distance x from the source can be calculated taking into account the reflection of the acoustic wave at the interface between the fluid and the porous material (by means, for instance, of the work by Wu et al. (1990)) and taking into consideration the damping of the fast wave (where the definition of the term "fast wave" is in the sense of Biot's theory). The difference between the pore radius and the radius of the smallest particle which stays attached is used to calculate the final permeability again by means of Kozeny relation, Eq. 4.27. We assume that the effect of acoustics is to remove the layer of particles larger than R_{min}. Some theoretical results are given in Fig. 4.14. The ordinate in Fig. 4.14 is the ratio of the final and initial permeability, as calculated according to the procedure described above. More details about this calculation can be found in Appendix A, where the procedure is explained in more detail together with a numerical example. It can be seen from Fig. 4.14 that the cleaning efficiency indeed increases with increasing

*In Bear (1972), relation 4.27 appears as (following our notation):

$$K = \frac{c_0 \phi D^2}{4\tau};$$

c_0 is a shape dependent function that is used to be equal to 1/2 for cylindrical pores.

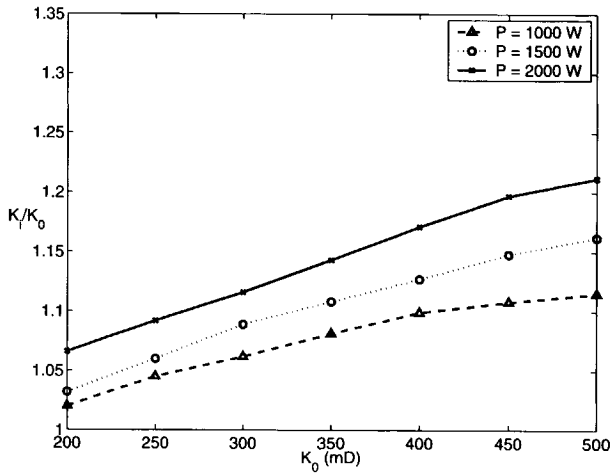

Figure 4.14: Ratio of final and initial permeability as function of initial permeability and for several values of the power input. Theoretical prediction for $x = 10\ cm$.

power input and with increasing initial permeability. From Fig. 4.11 the same information about the cleaning efficiency as function of the initial permeability can be derived for the experimental data. Some results derived from Fig. 4.11 are given in Figs. 4.15 and 4.16.

In Fig. 4.15 the result for the first part of the core is given; in Fig. 4.16 for the second part. As can be seen the experimental data in Fig. 4.16 agree reasonably well with the theoretical prediction shown in Fig. 4.14. Our model gives a smaller cleaning effect at high permeability than the measured one. This effect can be explained taking into account the dependence of damping coefficient on the permeability: as the permeability increases the damping reduces. In our model we used the damping coefficient measured in Poesio, Ooms, Schraven & v. Bas (2002) for permeability around 200-300 mD. As mentioned earlier it can also be observed, that the relative increase in permeability is larger when the initial permeability is larger. The influence of the initial permeability on the particle concentration and on the particle size distribution is given in Fig. 4.12 and has already been discussed.

From a comparison of Fig. 4.15 and Fig. 4.16 it can be concluded, that the cleaning effect in the first part of the core is stronger than in the second part. This is due to the dissipation of acoustic energy, which causes a weaker traveling acoustic wave in the second part compared to the first part. This is also in agreement with the theoretical prediction as shown in Fig. 4.9. In Appendix A a comparison between theoretical and experimental relative permeability is given as a function of the distance from the acoustic source.

The experimental finding for the influence of the fluid viscosity on the cleaning effect (see Fig. 4.11 and Tab. 4.2) agrees qualitatively well with the theoretical result shown in Fig. 4.7. With increasing viscosity the ratio of the final and initial permeability increases. As discussed this is due to the larger drag force on a fouling particle attached to a pore wall, when the viscosity is larger.

Finally we have studied theoretically the influence of the fluid temperature on the cleaning efficiency. To that purpose we have taken into account the temperature effect on the Hamaker constant (see Israelachvili (1985)) and on the viscosity (see Zaytsev & Aseyev (1992)). The results are shown in Fig. 4.17 where the detachment power is given as a function of the temperature for two values of the particle radius. As can be seen, the required power increases strongly with temperature.

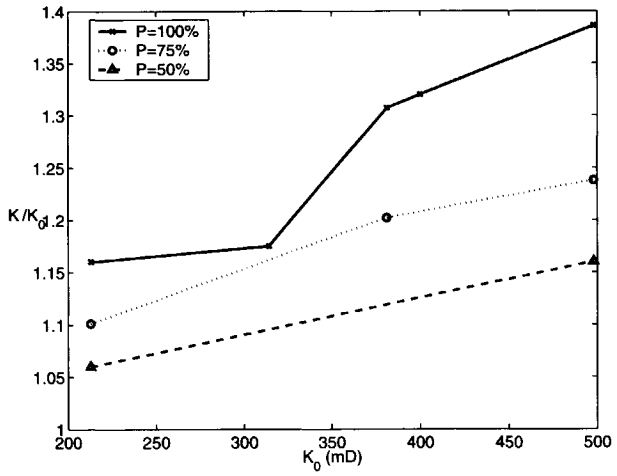

Figure 4.15: Ratio of final and initial permeability as function of initial permeability and for several values of the power input. Experimental data for the first part of the core sample.

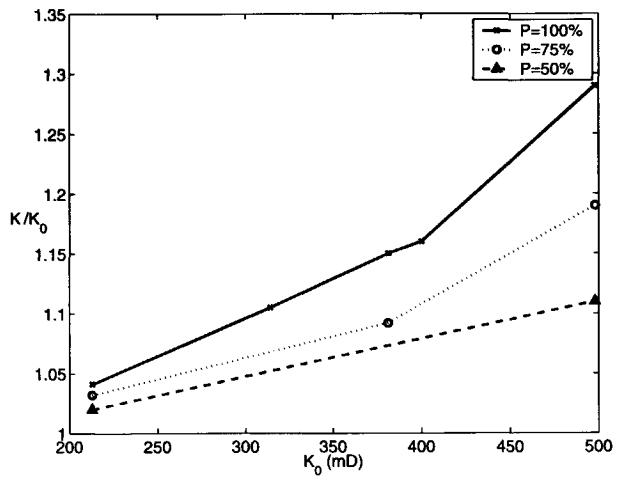

Figure 4.16: Ratio of final and initial permeability as function of initial permeability for several values of the power input. Experimental data for the second part of the core sample.

Part	Brine	50% Brine - 50% Glycerol
1	1.148	1.157
2	1.050	1.071
3	1.001	1.025

Table 4.2: Relative permeability of each part of the core after the ultrasonic irradiation with different saturating fluid.

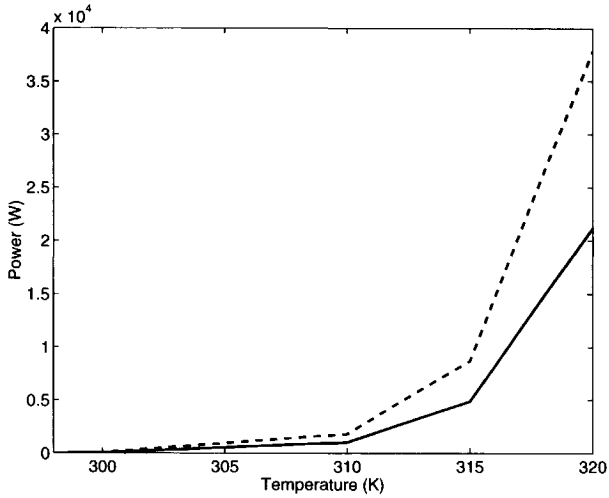

Figure 4.17: Power needed to detach particles with $R = 1\ \mu m$ (continuous line) and $R = 0.5\ \mu m$ (dashed line) as a function of the temperature.

4.6 Conclusions

We have investigated the removal by ultrasonic irradiation of small particles attached to the walls of pores inside a porous material. A theoretical model has been applied to predict this removal as function of the relevant parameters. Also experiments have been carried out to measure the removal efficiency and to check the theoretical model. It can be concluded that the agreement between predictions and experimental data is very reasonable. The influence of the initial permeability, the elasticity of the fouling particles, the input power, the distance from the acoustic source and the fluid viscosity on the removal efficiency can be predicted (at least) qualitatively. We think that this result is important, for instance, for the understanding and application of the cleaning of the near well-bore of an oil reservoir by means of high-frequency acoustic waves. It has to be kept in mind, however, that the fouling mechanism studied in this publication (particle attachment to pore walls) is one of several fouling mechanisms. Reduction in permeability due to bridge formation of particles in the throats of pores inside a porous material is another mechanism. We plan to study the influence of ultrasonic irradiation on fouling by bridge formation in the near future.

Appendix A: Numerical example

To calculate the initial and the relative permeability in Fig. 4.11, the following procedure is applied. First, assume that we have an initial permeability of 400 mD (measured as described in Section 3.3). By means of the Kozeny equation the initial effective pore diameter is calculated (assuming a tortuosity α of 3.1, which is reasonable for this kind of rock)

$$D_{eff} = \sqrt{\frac{8K\alpha}{\phi}}. \tag{4.28}$$

This yields a D_{eff} of 8.07 μm and, hence, $R_{eff} = 4.035\ \mu m$. Based on literature information about small clay particles in Berea sandstone and on our own measurements (shown in Fig. 4.12)

we can assume that the largest particles have a radius of 1 μm and, hence, calculate that the radius of the *clean* pore is $R_{pore} = 5.035\ \mu m$. Suppose we study the cleaning effect at 10 cm from the acoustic. To predict this effect we need to calculate the acoustic power available at that distance starting from the initial acoustic power (which is known). At the interface between a fluid and a saturated porous medium a part of the acoustic wave is reflected and a part is transmitted. According to Biot's theory (Biot 1956) the transmitted wave splits into three components: a fast wave (that has the highest propagation velocity), a slow wave (with the lowest velocity) and a shear wave. In our case the shear wave is not present since the angle of incidence is zero. The transmission coefficients for the fast and the slow wave can be found following the procedure proposed by Wu et al. The slow wave is damped very quickly (in the first few millimeters), so only the fast wave can provide the acoustic power necessary for the detachment of particles at distances larger than a few millimeters. The power of the fast wave available at distance x from the acoustic source can be calculated from

$$P(x) = t_{fast} P_0 e^{-2\alpha_{fast} x}, \tag{4.29}$$

where t_{fast} is the transmission coefficient of the fast wave. According to our calculation for this example only 45% of the input power goes into the fast wave. This wave is then damped with a damping coefficient of 3.21 m^{-1}, as measured by Poesio, Ooms, Schraven & v. Bas (2002). More information about the the damping coefficient can be found in Kelder (1998). So, if we have an input power of 2 kW, only 475 W will reach the particles located at 10 cm from the source. From the equation

$$P = A\rho c U_{max}^2, \tag{4.30}$$

we can calculate the velocity (U_{max}) at the centerline of the pore. Next we can compute the drag force acting on a particle of radius R in a pore of radius R_p as a function of the radius R itself. The lift force F_L can also be computed as a function of R

$$F_L = 0.278 R F_D. \tag{4.31}$$

At the same time, from the iterative solution of

$$d(s, a, d_0) = d_0 + \frac{1}{\pi R}\left(a\sqrt{s^2 - a^2} + (s^2 - 2a^2)\arctan\left(\frac{\sqrt{s^2 - a^2}}{a}\right)\right), \tag{4.32}$$

$$F_{total} = \sum\left(\pi a^2 F_i'' + 2\pi \int_a^R F_i''(d(s, R, d_0))sds\right), \tag{4.33}$$

$$F_{vdw}(d, R, R_p) = \frac{4a^3(R + R_p)}{3\pi(k_1 + k_2)RR_p}, \tag{4.34}$$

$$F_{total} = 0, \tag{4.35}$$

the adhesion force $F_A (= F_{vdw})$ and the deformation a can be calculated as a function of the radius of the particle, when the properties of the material are known. Finally, the size of the particles that can be detached are found by means of equation

$$F_D = \frac{a(F_A - F_{l,})}{1.4R}. \tag{4.36}$$

Those calculations have been carried out and are summarized in Fig. 4.8. If we assume in Fig. 4.8 a power of 475 W and a R_{pore} of 5 μm we find that particles down to $R = 0.7\ \mu m$ are detached from the pore walls. With this information we can calculate a new effective diameter of 8.6 μm. The new permeability is, then, found by using the Kozeny relation

$$K = \frac{D_{eff}^2 \phi}{8\alpha}, \tag{4.37}$$

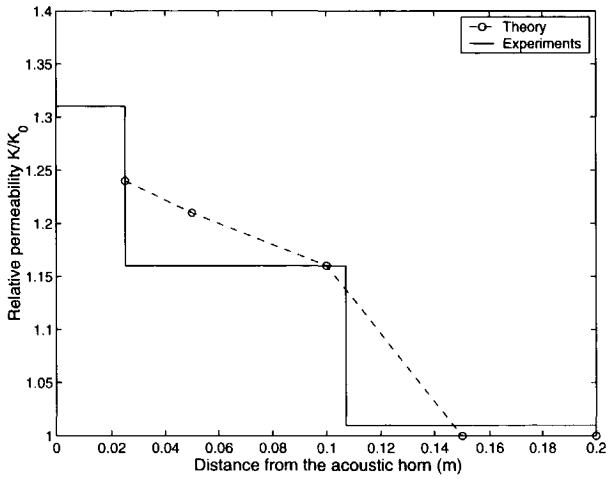

Figure 4.18: Comparison between experimental and theoretical relative permeability as a function of the distance from the acoustic source.

which yields a relative permeability of 1.16.

An example of the above described calculation procedure is given in Fig. 4.18. In this figure, we compare the relative permeability found from experiments with theoretical prediction from our theoretical model as a function of the distance from the source. The initial permeability is assumed to be 400 mD and the acoustic power 2 kW. As can be seen, there is a reasonable agreement between theory and experiments.

In the coming chapter we investigate the other form of fouling: particles-bridge formation in the throats of pores of the porous material. First an analysis is made of this fouling mechanism itself. Special attention is paid to the relevant parameters influencing the particles bridge formation. Thereafter, the possibility of removing such bridges by means of ultrasonic waves is studied.

Chapter 5

Particle bridge formation and removal from porous media by ultrasonic irradiation*

Abstract

Formation and ultrasonic removal of fouling particle structures in a porous material (caused by the flow of a liquid with small particles through the material) was studied with natural sandstone. Experiments were carried out during which fouling particles were generated inside the sandstone by changing the composition of the liquid from a 2% KCl brine solution to fresh water. It was found that the influence of liquid velocity, particle concentration and ratio of particle diameter to pore diameter on the permeability decrease due to the fouling particles is as anticipated from the formation of particle bridges inside the sandstone. The removal of fouling particles by high frequency acoustic waves was also investigated experimentally. The influence of fluid velocity, material permeability and acoustic power input on the cleaning efficiency indicates again that fouling is caused by particle bridges inside the sandstone. The understanding of the formation and ultrasonic removal of fouling particle structures in a porous material is of importance for the design of ultrasonic tools for the cleaning of the near wellbore region of oil reservoirs.

5.1 Introduction

Permeability reduction of porous materials due to fouling by small particles is a well-known phenomenon. This reduction of permeability can be either beneficial to the application (sealing of a waste disposal site) or adverse (fouling of an oil reservoir). A review of the subject was presented by McDowell, Hunt & Sitar (1986).

The objective of this work is the study of the formation and ultrasonic removal of fouling particle structures using Berea sandstone. During the production of oil from a reservoir the permeability decrease due to fouling particles in the near well-bore region leads to significant decline in productivity. Several techniques (acid treatment, fracturing the well-bore region) have been used to overcome this problem, but some drawbacks make them unattractive. These techniques are often expensive, environment unfriendly and dangerous. A new technique is the ultrasonic irradiation of the near well-bore region, which has been discussed by Venkitaraman et al. (1995), Roberts et al. (2000) and Wong et al. (2003); however, this technique is not always successful and can have

*P. Poesio and G. Ooms. "Particle bridge formation and removal from porous media by ultrasonic irradiation". *Accepted for publication in J.Petroleum Sci. & Eng.*, 2004.

a negative effect on the permeability, Beresnev & Johnson (1994). Therefore a more fundamental study was undertaken.

Barake et al. (2001) and Poesio, Ooms, Barake & v. Bas (2002) discussed the influence of high-frequency acoustic waves on flow of a liquid without particles through Berea sandstone and found that an increase in liquid flow rate occurred due to a decrease of the liquid viscosity caused by temperature rise from the dissipation of energy of the acoustic waves. Other phenomena, such as acoustic streaming (Poesio, Ooms, Schraven & v. Bas 2002) and peristaltic transport (Aarts & Ooms 1998), appeared to have negligible influence.

When colloidal suspensions flow through porous media different mechanisms of deposition and release of particles occur. When the particles are larger than the pore diameter they are captured at the entrance of the pores. When the particles are much smaller than the pore diameter they will flow through the porous material without causing significant fouling. When the particle diameter is smaller, but not much smaller, than the pore diameter (say not smaller than ten percent of the pore diameter) the permeability of the porous material may decrease due to several fouling mechanisms: inertial impact, sedimentation or particle-bridge formation. Inertial impact occurs when the particles (under influence of their inertia) deviate from the fluid streamlines and impact on the pore walls. This effect usually occurs for particles with a density much greater than the liquid density. When gravitational force is dominant, sedimentation takes place as the particles are deposited onto the pore walls.

Recently Ramachandran & Fogler (1999) discussed another fouling mechanism that is possible when the particle diameter is just slightly smaller than the pore diameter: formation of particle bridges at pore throats by particles due to simultaneous arrival of several colloidal particles. Colloidal particles exhibit electrical repulsion at short distances; nevertheless, when the hydrodynamic forces are strong enough, they overcome the electrical repulsion and a particle-bridge structure is formed. Ramachandran and Fogler studied the formation of bridges on the surface of a thin membrane through which a colloidal suspension was flowing into the pores of the membrane. An increase of pressure drop across the membrane registered the decrease of permeability as fouling occurred. The particle bridges at the entrances of pores were observed with electron microscopic photographs. They also analyzed the effect of some relevant parameters on the formation of particle bridges and the resulting permeability reduction.

Ramachandran and Fogler investigated fouling of the surface of a porous membrane by a liquid with particles penetrating from outside the membrane into its pores. In contrast, this work is the study of fouling due to flow of a liquid with small particles inside a sandstone. A natural sandstone contains a complicated network of pores with different shapes and sizes; in addition, the (clay) particles are released inside the sandstone as function of flow velocity and composition of the liquid. Therefore one cannot conclude, without further investigation, that for a natural sandstone the fouling must also be due to hydrodynamic bridging of particles.

The special interest for this fouling mechanism distinguishes the present work from earlier studies about the transport of particles through sandstones, see for instance Donaldson, Baker & Carroll (1977) and Jiao & Sharma (1992). The occurrence of particle bridges in the near wellbore region of oil reservoirs was already mentioned by Batli & Risnes (1979) and Risnes, Batli, Horsrud & Baker (1982); however, a physical interpretation was not provided.

5.2 Description of hydrodynamic bridging of particles inside a porous material

Particle-bridge formation is due to the blockage of a pore by the simultaneous arrival at a pore throat of two, or more, particles. Under the influence of hydrodynamic drag force particles approach each other near a pore throat and experience the drag force as well as mutual colloidal forces such as: the van der Waals force, the electrical force and the Born repulsion, Russel et al. (1989). As a consequence of the hydrodynamic and colloidal forces and due to the inertia of the particles (the particles will not follow the fluid streamlines exactly) for certain values of the

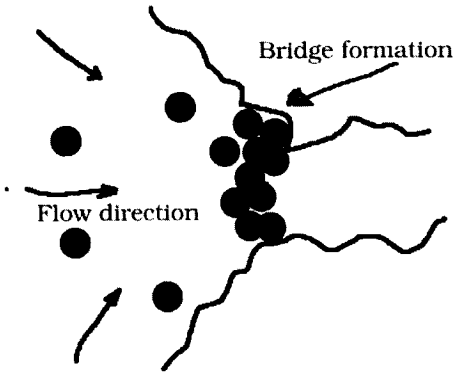

Figure 5.1: Sketch of hydrodynamic bridging of particles.

Figure 5.2: Example of particle bridge formation in a pore throat, scanning electron microscope photograph. The horizontal length of the picture is $20\mu m$.

relevant parameters (flow velocity, particle diameter, strength of the colloidal forces) the particles touch, stick together and form a bridge over the pore throat. Figure 5.1 is a sketch of the formation of a particle bridge. SEM-pictures of particle bridge formation that were taken after a fouling experiment are shown in Figs. 5.2 and 5.3 (see Appendix A for preparation of SEM samples).

Particle-bridge formation depends on the size distribution of particles and pores and on the properties of the particles and fluid. The particle size distribution was measured by means of an optical method (GALAI, *Ankersmit*). In Fig. 5.4 the size distribution of particles flowing out of a core of 190 mD is shown and compared to the pore size distribution for Berea sandstone. It is evident that the particles are considerably smaller than the pores.

Ramachandran & Fogler (1999) found that with increasing fluid velocity, the rate of particle-bridge formation increases (for the same total number of particles arriving at the membrane). The influence of the fluid velocity is different from other fouling mechanisms because there exists a critical velocity for the particle-bridge formation. Below the critical velocity colloidal repulsion forces are dominant and bridge formation does not occur; above the critical velocity the hydrodynamic force is larger than colloidal repulsion forces and bridge formation takes place. The value of the critical velocity depends on parameters such as (1) the strength of the colloidal forces between the

Figure 5.3: Example of particle bridge formation and subsequent filling up of the pore, scanning electron microscope photograph. The horizontal length of the picture is $20\mu m$.

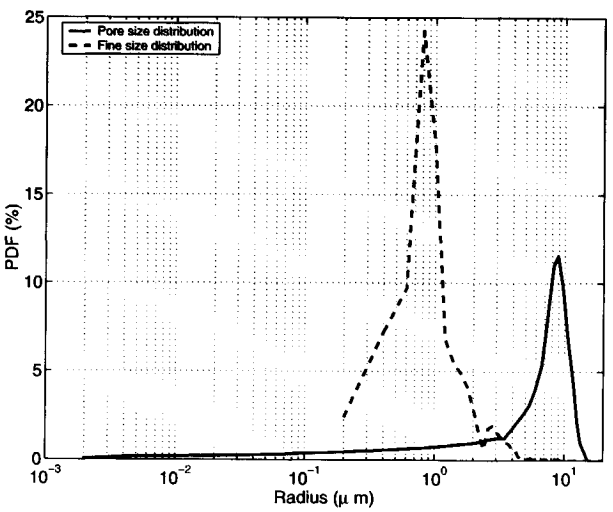

Figure 5.4: Comparison between pore size distribution and fine size distribution.

particles, (2) the ratio of the particle diameter to the pore diameter, and (3) particle concentration. At high particle concentration, the number of particles arriving at the pore throat increases and hence the probability of particles being at the right position to form a bridge increases. In addition, as the ratio of particle diameter to pore diameter (aspect ratio) increases the probability of particle-bridge formation also increases.

5.2.1 Fouling mechanism

Inertial impact of particles on pore walls with respect to viscous forces acting on the particle is defined by Stokes number (St):

$$St = \frac{2}{9}\left(\frac{d}{d_p}\right)^2 \frac{\rho_p}{\rho} Re. \tag{5.1}$$

In order to estimate the value of St the value of particle diameter and pore diameter are taken from Fig. 5.4. The fluid density ($\rho = 1020\ kg/m^3$) is taken from Zaytsev & Aseyev (1992) and the particle density ($\rho_p = 2650\ kg/m^3$) from Khilar & Fogler (1998). The value of Re is derived later on. This leads to an order of magnitude estimate for the value of St of 10^{-4}, showing that the possibility of inertial impact on the walls inside the sandstone is very small.

Dendrite formation begins when a particle deposits onto the pore wall and subsequently acts as a collector of other particles. Dendrite formation occurs when the particle inertia dominates the electrical repulsion forces between particles. An order of magnitude of the inertial forces (Russel et al. 1989) is:

$$\mathcal{O}\left(\frac{d_p^3 \rho_p U^2}{d}\right), \tag{5.2}$$

in which U is the typical liquid velocity in a pore determined from the experimental conditions. The averaged value is $U = 10^{-1}\ mm/s$; with a value of viscosity ($\mu = 1.12\ mPa\,s$) this leads to a value of $Re = 10^{-3}$. The electrical repulsion is estimated by:

$$\mathcal{O}\left(\epsilon_0 \epsilon \psi_p \psi\right), \tag{5.3}$$

where ψ_p is the zeta-potential of the particle ($\psi_p = -30\ mV$), ψ is the zeta-potential of the pore material ($\psi = -50\ mV$), ϵ is the fluid permettivity ($\epsilon = 80$) and ϵ_0 is the vacuum permettivity ($\epsilon_0 = 8.8542\,10^{-12}\ C^2 N^{-1} m^{-2}$). The values of these quantities were taken from Israelachvili (1985). An order-of-magnitude estimation shows that the electrical repulsion force is much larger (10^2 times larger) than the inertial force; therefore dendrite formation is also negligible.

Sedimentation is a fouling mechanism by which particles are deposited onto the pore walls under the influence of the gravity. The importance of this mechanism can be estimated by means of the sedimentation number, defined as

$$N_G = \frac{2}{9}\frac{d_p^2 \Delta\rho g}{\mu U} \tag{5.4}$$

in which $\Delta\rho$ is the density difference between the particle and the liquid, g is the acceleration due to gravity and μ is the dynamic liquid viscosity. From an order-of-magnitude estimate ($N_g = 10^{-3}$), it can be concluded that fouling due to sedimentation is also not a likely fouling mechanism.

A mathematical description of the fouling mechanisms described above has been given by several authors. For instance, Donaldson et al. (1977) proposed a statistical model to predict the decrease in permeability caused by particle deposition within a sandstone. Rege & Fogler (1987) proposed a network model to predict the permeability reduction due to particles. A comparison between their numerical results and the experimental results presented by Donaldson et al. (1977) showed a good agreement.

Length of the core	20 cm
Diameter of the core	7.62 cm
K_0	100-500 mD
ϕ	0.18-0.25

Table 5.1: Properties of the cores.

5.3 Fouling of Berea sandstone without acoustic stimulation

5.3.1 Experimental equipment and procedure

Figures 5.5(a) and 5.5(b) show a picture and a schematic diagram of the experimental equipment. It was described in detail by Poesio, Ooms, Barake & v. Bas (2002) and Poesio, Ooms, Schraven & v. Bas (2002).

A core (for core properties see Table 5.1) was placed in a rubber sleeve inside a steel vessel and the space between the vessel and sleeve, which was filled with water, was pressurized to 18 MPa to seal the sample. The core was positioned horizontally in order mimic as closely as possible the operating condition in the near wellbore region during the subsequent acoustic cleaning experiments. Moreover Eq. 5.4 shows that the effect of gravity is negligible with respect to the fouling mechanism with which this paper is concerned.

There were four pressure measurements, two along the core (at 2.54 *cm* and 10.70 *cm*) and two at both ends of the core, Fig. 5.5(b). The pressure drop across each section was monitored and recorded as dP_1, dP_2 and dP_c (the total pressure drop over the core). The pressure drop across the third part (dP_3) is calculated from $dP_3 = dP_c - (dP_1 + dP_2)$. Thermocouples were installed at the sidewall of the porous medium at two locations, through the rubber sleeve, Fig. 5.5(b). The temperature in front and at the back of the core also was measured and the data collected with a digital data recorder were sent to a computer for processing.

Before experiments were run:

- the core was flushed with CO_2 to expel all the air in the porous material,
- following the CO_2 flush, brine was injected at a constant flow rate at a pressure sufficiently high (18 MPa) to dissolve the residual CO_2.
- The flowing brine was used to calculate the initial permeability.

The flow of fouling particles in the core can be generated by two different procedures:

- colloidally induced generation of small particles (fines) by changing the electrical properties of the saturating fluid to release particles from the clay inside the porous material; this is achieved by changing the brine from a 2% KCl solution to fresh water.
- Hydrodynamically induced generation of fines occurs when the flow rate is increased to high values causing the hydrodynamic drag to remove small particles lodged within pores.

Mohan & Fogler (1997) studied the phenomena that occur in Berea sandstone when fresh water is introduced. They distinguish three possible mechanisms as a result of clay-water interaction: (1) swelling of clays, (2) breaking loose of clays, and (3) release of fines through the swelling of clay (micro-quakes). Smectites only swell, but do not break loose of the pore walls. Kaolinites and illites are non-swelling clays that tend to detach directly from the surface of the pore walls. The Berea sandstone was analyzed using X-ray diffraction, which revealed that it contained 45% illite, 50% kaolinite and 5% chlorite. This indicates that direct release and migration of fines will be the dominant mechanism. A detailed study of the detachment mechanisms was presented by Khilar & Fogler (1998).

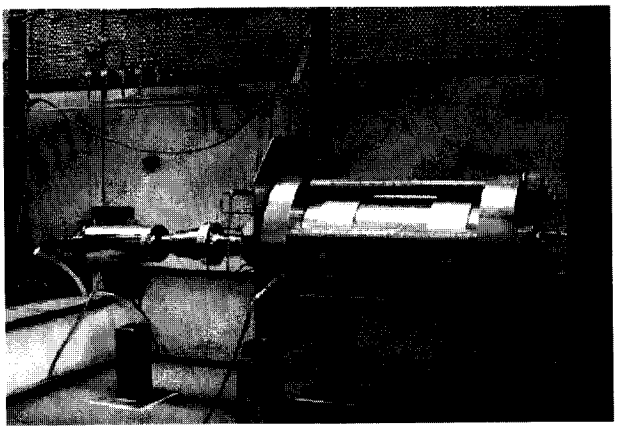

(a) Photograph of the experimental equipment.

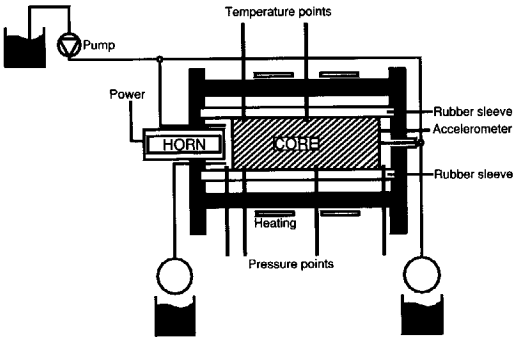

(b) Sketch of the experimental equipment.

Figure 5.5: Experimental equipment. The core is placed horizontally because in the near wellbore region ultrasonic cleaning will take place in horizontal direction. The gravity force is not important since the particles are very small and sedimentation plays a minor role.

Core No.	ϕ	K_0	K
1	0.21	290	98
2	0.20	320	130
3	0.22	465	195
4	0.20	96	27
5	0.22	540	90
6	0.20	310	242
7	0.20	300	118
8, x_A	0.22	210	206
8, x_B	0.23	215	187
8, x_C	0.22	210	135
8, x_D	0.21	205	36
12	0.21	220	157
13	0.22	270	190

Table 5.2: Properties of cores used in the experiments. K_0 and K are the permeability before and after fouling respectively.

5.3.2 Experimental results

The permeability in each part of the core was calculated from the pressure drops and fluid flow and labeled as K_1, K_2 and K_3; the averaged permeability was labeled K_{core}. The properties of the cores used for the experiments presented here are summarized in Table 5.2.

The first fouling experiment on core No. 1 began with a constant flow of 2% KCl brine at 5 ml/min. At this salinity and low flow rate particles were not generated within the core. The brine salinity was then changed abruptly to fresh water at t=500 s causing colloidal particles to be released inside the core. Different permeabilities occurred in the three parts of the core as shown in Fig. 5.6. During the period of low flow rate (5 ml/min), the permeabilities did not change; however, when the flow rate was increased to 10 ml/min at t=3500 s a significant reduction of the permeabilities occurred. The average permeability decreased from 280 mD to 110 mD, a reduction of about 60%. The change of salinity to fresh water at t = 500 s did not affect the permeability because the effect is confined to about 5% (swelling clays) of the total as mentioned previously. Small colloidal particles were detected in the liquid effluent from the core. The reduction of permeability occurred only after the flow rate was increased to 10 ml/min. This suggests that the fouling mechanism is particle bridging occurring at pore throats.

Several experiments were carried out to check the consistency of the results for core No. 1 shown in Fig. 5.6. The results of these additional experiments for core No. 2 are given in Fig. 5.7. The experiment for Fig. 5.7 is very similar to the one for Fig. 5.6. The concentration of the effluent particles from the experiments shown in Fig. 5.7 were found to be 7.6 10^6 ml^{-1} at 5 ml/min and 8.3 10^6 ml^{-1} at 10 ml/min. The dramatic decrease of permeability due to the step increase in flow rate cannot be attributed to the small increase of concentration of flowing particles, as expressed by Khilar (1981). Thus, hydrodynamic bridging must be the principal fouling mechanism.

The result of another fouling experiment with core No. 3 is shown in Fig. 5.8. The flow rate for core No. 3 had to be increased from 10 ml/min to 25 ml/min before the reduction in permeability occurred, probably because the averaged permeability of core No. 3 is greater than that of core No 2. whose results are shown in Fig. 5.7. The data for core No. 3 (Fig. 5.8) show that the permeability is reduced from 400 mD to 220 mD and the critical flow rate is between 10 ml/min and 25 ml/min. The greater critical velocity for the occurrence of permeability reduction is probably because the permeability of core No. 3 was larger than that of core No. 2, indicating that the pore throats are larger and particle bridging is less because more particles, at a higher velocity, are needed to form bridges.

The reduction in permeability for core No. 2 (Fig. 5.7) is larger (~60%) than for core No. 3 (~50%, Fig. 5.8). The average pore diameter is proportional to the square root of the permeability and assuming that the particle diameter remains the same, the level of fouling apparently increases

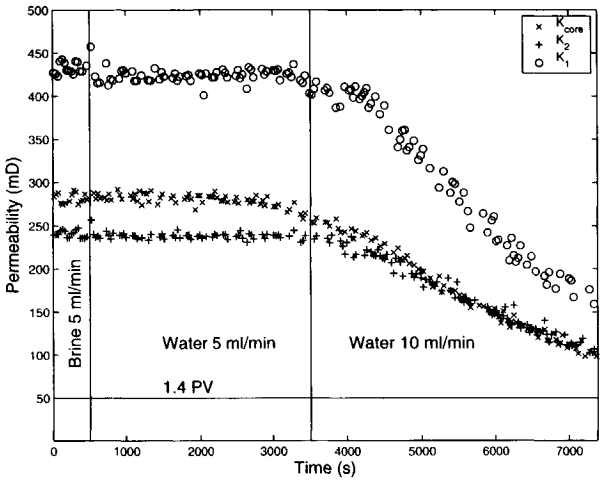

Figure 5.6: Permeability as a function of time; 1.4 pore volumes are passed through the core No. 1 during the 5 ml/min period.

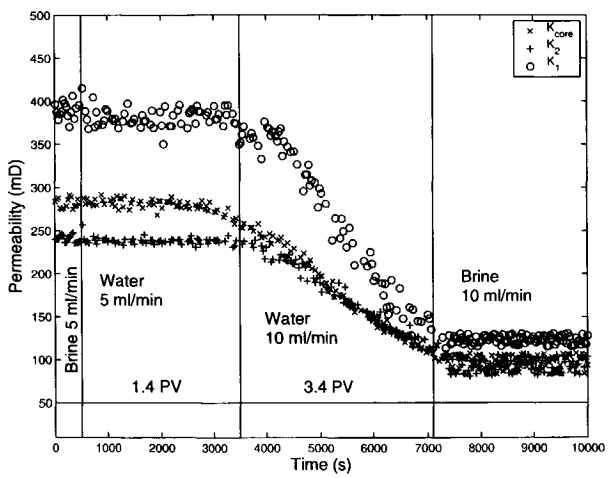

Figure 5.7: Permeability as a function of time. A total of 1.4 pore volumes (PV) was passed through the core No. 2 at 5 ml/min and 3.4 pore volumes during the 10 ml/min period.

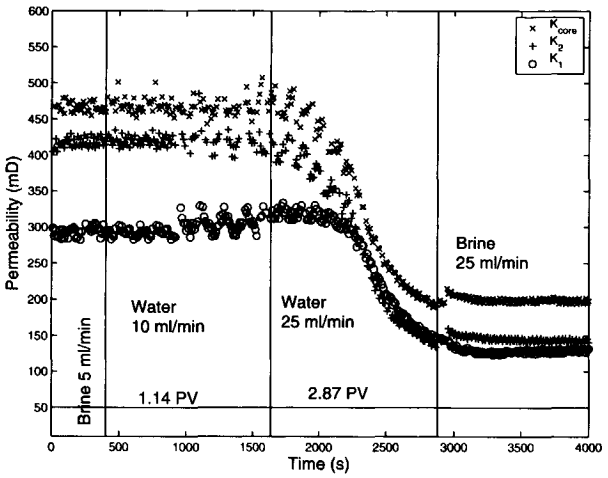

Figure 5.8: Permeability as a function of time, for core No. 3.

with increasing aspect ratio. The influence on the level of fouling for a core with a much lower initial core permeability (core No. 4) than in case of the first experiment, is shown in Fig. 5.9. A significantly smaller initial permeability leads to a much greater level of fouling, a 70% reduction of averaged permeability. A core whose initial permeability was 73 mD was impossible to flush completely, because the permeability decreased to such an extent (at a flow rate of 5 ml/min) that the pump could not function.

Another set of experiments was conducted using step increases of the fluid flow rate and the results were analyzed using a relative permeability defined as the ratio of the permeability of the fouled core (K) to the initial permeability (K_0). The effect of flow rate on the permeability reduction was investigated using step increases of flow rate as shown in Fig. 5.10. A decrease of the relative permeability occurs at each step increase of flow rate.

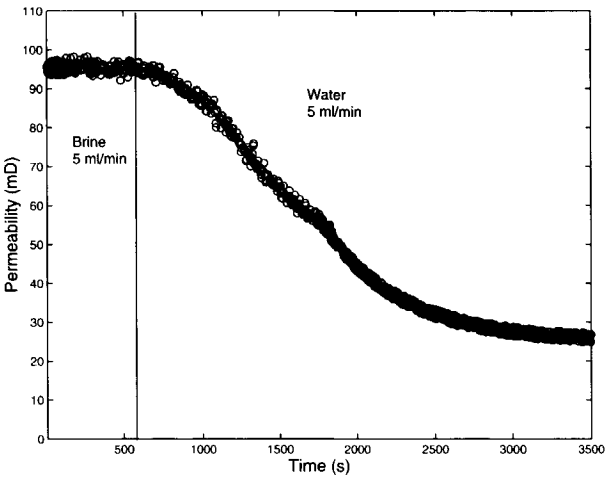

Figure 5.9: Reduction of average permeability caused by increase of flow rate above a critical value for core No. 4.

The existence of a critical velocity at which an immediate decrease of permeability occurs is illustrated in Fig. 5.11. Two similar cores (cores No. 6 and No. 7) were fouled with water (after a flushing with KCl brine at 25 ml/min). Fresh water at 10 ml/min was then introduced but fouling did not occur, therefore the flow rate was increased to 20 ml/min and fouling began. When three pore volumes have flowed through the cores, the flow rate through core No. 6 was switched to 5 ml/min, while it is left unchanged for core No. 7. The fouling stops almost immediately for core No. 6 when the flow rate was changed to 5 ml/min while it continues for core No. 7. If the flowing particle concentration is the same at the beginning of the last period shown in Fig. 5.11, the continued reduction of permeability observed for core No. 7 must be due to the high flow rate.

The influence of the particle concentration on the level of fouling was measured. The concentration of particles released inside the sandstone can be changed by changing the liquid temperature which changes electrical repulsion. This increase of particle concentration only occurs when fresh water flows through the core; it does not occur with brine. The effects of temperature were examined by cutting core No. 8 into four pieces to ensure almost identical initial condition with respect to particle concentration. Each sub-core (x_A, x_B, x_C and x_D) was subjected to a separate temperature ($15°C$, $30°C$, $60°C$ and $80°C$, respectively) and a constant flow rate of fresh water at 5 ml/min, Fig. 5.12. The relative permeability was then monitored; it decreased in a direct relationship to each temperature that was used, Fig. 5.12. The effluent from x_A ($15°C$) had a particle concentration of 6.2 10^5 ml^{-1}, while the effluent of core x_D ($80°C$) was significantly higher, 3.1 10^7 ml^{-1}.

Conway, Himes & Gray (2000) reported that K-ions increase the sensitivity of clays to fresh water in Berea sandstone while Ca-ions decrease it. $CaCl_2$ has a tendency to stabilize the clay inside the sandstone and hence to suppress the generation of small particles. To test this, three almost identical cores with the same initial permeability of about 300 mD were saturated with brines of different compositions. Core No. 5 was saturated with KCl, No. 12 with a mixture of KCl and $CaCl_2$ and No. 13 with $CaCl_2$. The cores were then flushed with different flow rates of fresh water. The relative permeability of each core decreased in step with the type of electrolyte that was used, from core No. 5 to core No. 13, Fig. 5.13. The tests show that the fouling is a function of the type of electrolyte and rate of fluid flow.

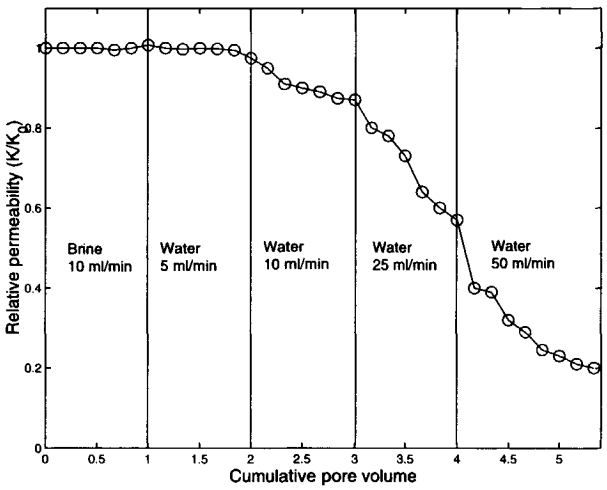

Figure 5.10: Reduction of relative permeability caused by increase of flow rate for core No. 5.

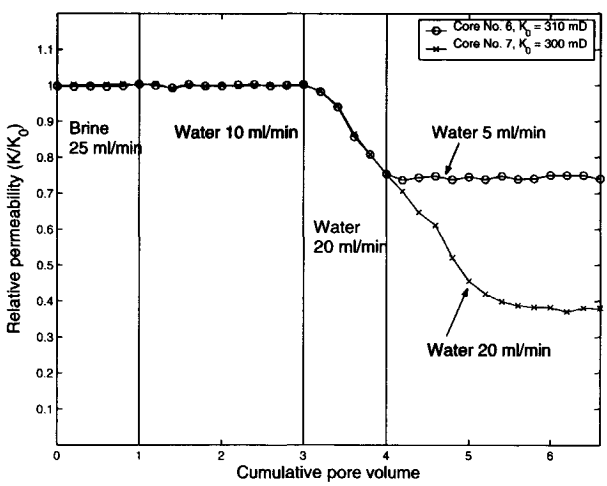

Figure 5.11: Reduction of relative permeability caused by increasing the fluid flow rate.

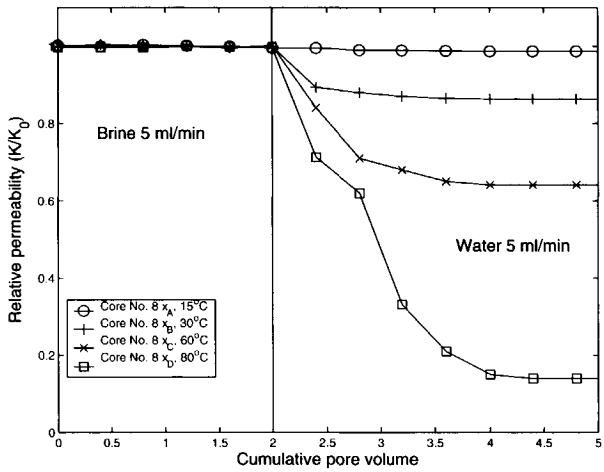

Figure 5.12: Relative core permeability for different particle concentrations. An increase of temperature increases the amount of particles released from the rock and hence flowing in the water stream.

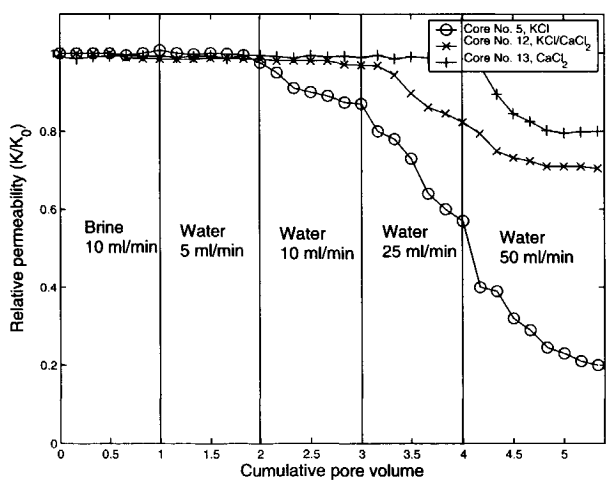

Figure 5.13: Relative permeability as function of type of electrolyte used. The sensitivity to fouling for K-ions is significantly larger than for Ca-ions.

5.4 Acoustic removal of fouling particles in Berea sandstone

5.4.1 Equipment and procedure

The ultrasonic equipment consisted of:

- an electrical converter to produce mechanical vibrations of a piezo-electric element;
- an amplifier for adjustment of the amplitude of the vibrations;
- an ultrasonic horn to concentrate the mechanical vibrations onto the front side of the core. Two acoustic horns were used: a Branson Module PGA 220 (a 20 kHz horn with maximum power output of 2000 W) and a Branson Module PGA 470 (a 40 kHz horn with maximum power output of 700 W). The power output can be selected as a percentage of the maximum.

Typically the acoustic stimulation experiments were conducted as follows:

- The initial permeability of the core was measured using a brine (2% KCl).
- The core was fouled using the procedure discussed previously.
- The core was saturated with KCl brine and back-flow at 5 ml/min was applied. The permeability was measured when the pressure drop remained constant. Back-flow was used to remove the less stable particles and loose particles (without affecting the fouling particle structures created during the preceding step).
- Acoustic treatment was applied for 30 s while brine was pumped through the core. The acoustic wave could be co-current or counter-current with respect to the flow of fluid in the rock.
- After the core cooled to the ambient temperature, the new permeability was measured.
- A second acoustic treatment was then applied, and the permeability was measured until the permeability was equal to the previously measured value. Otherwise another acoustic treatment was applied; two acoustic treatments were sufficient.

When an acoustic wave encounters an interface between a liquid and a porous material, three waves are transmitted: a shear wave (absent in this case because the wave propagation is perpendicular to the core surface), a slow wave and a fast wave, Biot (1956). The slow wave is dissipated quickly in the first few millimeters, therefore its importance is marginal with respect to the cleaning effect. The most important contribution comes from the fast wave that propagates 20-30 cm into the core (dependent on the acoustic frequency) before being attenuated almost completely. Therefore, in the following we will always refer to the fast wave.

Acoustic cleaning experiments were conducted using 40 different cores of Berea sandstone. Quantitative comparisons between the results obtained with all of the cores are difficult because the initial conditions of each core are different. Therefore, the detailed results of only four individual experiments are discussed together with the influence of some relevant parameters on the acoustic cleaning efficiency of all the experiments. The properties of the cores are reported in Table 5.3.

5.4.2 Discussion of four of the experiments

The conditions used for the different steps of the first experiment (core A1) are shown in Table 5.4. The value of the relative permeability after each step is shown in Fig. 5.14. The flow rate during the fouling phase was 25 ml/min, but during the acoustic treatment it was kept at 75 ml/min. The cleaning (removal of particles by acoustic treatment) was effective in the first part of the core, but was almost negligible in the second and third part. Most of the acoustic power was attenuated in the first part. The acoustic power, pressure and temperature were varied independently from each other. The cleaning effect, as shown by the increase of relative permeability in Fig. 5.14(a),

Core No.	ϕ	K_0	K
A1	0.21	290	98
A2	0.20	320	130
A3	0.22	465	195
A4	0.20	614	320
A5	0.19	147	46
A10	0.21	215	78
A11	0.21	195	72

Table 5.3: Properties of cores used in the cleaning experiments. K_0 and K are the permeability before and after fouling respectively.

increases significantly with respect to the increase of power (steps 4 and 5). For steps 6 and 7, the pressure was reduced from 10 MPa to 5 MPa. The relative permeability increased slightly probably due to cavitation. For steps 8-10, the temperature was increased from 20 to 80°C. The relative permeability of the first part increased once more along with the relative permeability in the second and third part (Fig. 5.14(b) and (c)). The growth in relative permeability in the first part of the core is probably due to collapse of the particle bridge structures as the electrical double layer repulsion between particles increases at a higher temperature. The increase in relative permeability in the second and third part (Fig. 5.14(b) and (c), steps 9 and 10) probably occurs because the damping coefficient of the fast wave reduces with increasing temperature (Poesio, Ooms, Schraven & v. Bas 2002), allowing the fast wave to penetrate deeper into the core.

The results obtained with the second example (core A2) are shown in Table 5.5 and Fig. 5.15. The pressure and temperature were kept constant for this case. The flow rate was varied during the various steps, as listed in Table 5.5. The acoustic power was doubled for the final step. The cleaning effect is most pronounced in the first part of the core because of the attenuation of the fast wave. The relative permeability in the first part increases significantly with decreasing flow rate (steps 4, 5 and 6 in Fig. 5.15(a)). A probable mechanism is that at high fluid velocity the particle bridge structures in the pore throats are stabilized by hydrodynamic drag force on the particles. Apparently the particle bridges become weak enough for the acoustic waves to break them only below a certain flow rate. The influence of the flow is also evident in the second and third part of the core.

The results for core A3 are presented in Table 5.6 and Fig. 5.16. The pressure and temperature were kept constant. The flow rate during fouling was 25 ml/min. The acoustic power, fluid velocity and the fluid flow direction were varied independently of each other during acoustic treatment. The principal effect of the acoustic treatment is evident in the first part of the core. The influence of the acoustic power for this case (step 4, 5 and 6, Fig. 5.16(a)) is small, probably because the level of acoustic power used is much lower than for the first and second examples. The relative permeability increases with decreasing flow rate. A small additional increase occurred when the flow direction of fluid flow was changed.

The results of the fourth and last test (cores A4 and A5) are presented in Table 5.7 and Fig. 5.17. The flow rate during fouling was maintained at 25 ml/min and the pressure and temperature were kept constant. The flow rate during the acoustic treatment was changed from 25 ml/min to 5 ml/min. The initial absolute permeability of the first core was 614 mD and of the second core 147 mD. The effect of the acoustic treatment after fouling is more effective in the case with larger initial absolute permeability than for the lower initial absolute permeability. The difference is probably because the pores are smaller in the low permeability material; hence, the particle bridge structures are more stable. The final permeability of the first core is much larger than the initial permeability perhaps because in a core with high permeability particles adhered on the pore walls are more easily removed than for cores with a low permeability (with smaller pore size distribution), Poesio, Ooms, van Dongen & Smeulders (2004).

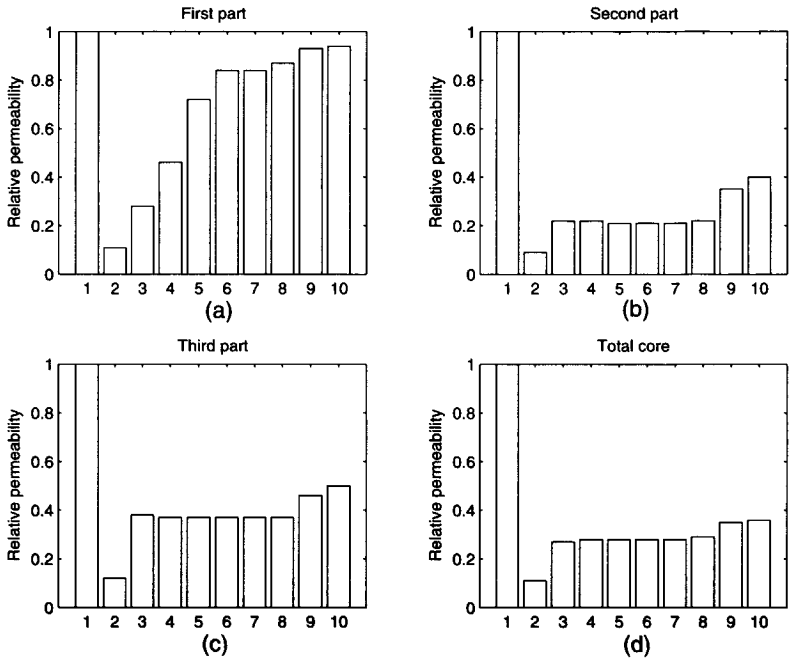

Figure 5.14: Relative permeability of the three parts of core A1 (and the overall permeability) after each treatment step, Table 5.4. The 20 kHz horn was used.

Treatment step	Description	Power (W)	Pressure (MPa)	Temperature ($°C$)	Flow rate (ml/min)
1	Start	-	12	20	-
2	Fouling	-	12	20	25
3	Back flow	-	12	20	5
4	Acoustic treatment	1000	12	20	75
5	Acoustic treatment	2000	12	20	75
6	Acoustic treatment	1000	5	20	75
7	Acoustic treatment	2000	5	20	75
8	Acoustic treatment	1000	12	80	75
9	Acoustic treatment	1500	12	80	75
10	Acoustic treatment	2000	12	80	75

Table 5.4: Experimental conditions used at each stage of the test on the core A1. The relative permeabilities (K/K_0) measured at the end of each step for core A1 are shown in Fig. 5.14.

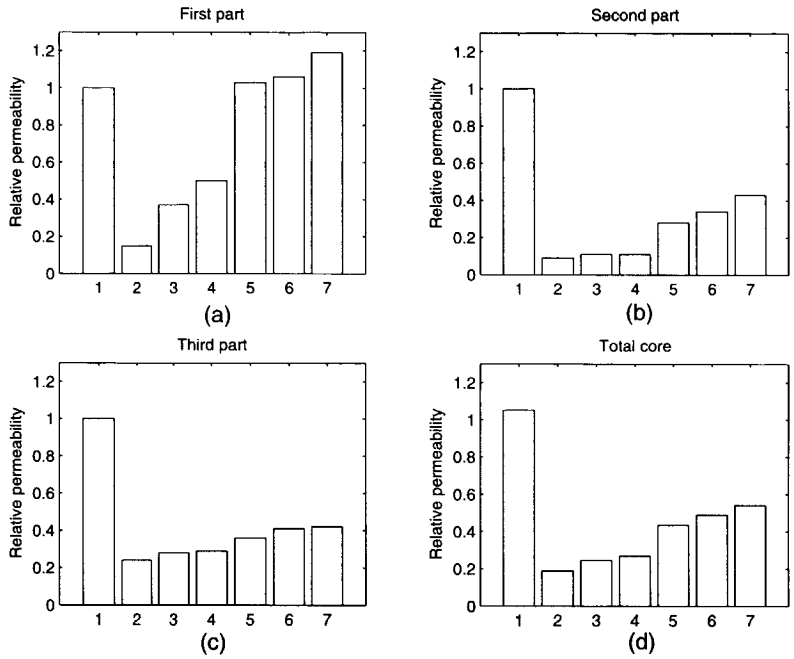

Figure 5.15: Relative permeability of the three parts of core A2 (and the overall permeability) after each treatment step, Table 5.5. The 20 kHz horn was used.

Treatment step	Description	Power (W)	Pressure (MPa)	Temperature (^oC)	Flow rate (ml/min)
1	Start	-	12	20	-
2	Fouling	-	12	20	25
3	Back flow	-	12	20	5
4	Acoustic treatment	1000	12	20	75
5	Acoustic treatment	1000	12	20	10
6	Acoustic treatment	1000	12	20	5
7	Acoustic treatment	2000	12	20	5

Table 5.5: Experimental conditions used at each stage of the test on core A2. The relative permeabilities (K/K_0) measured at the end of each step for core A2 are shown in Fig. 5.15.

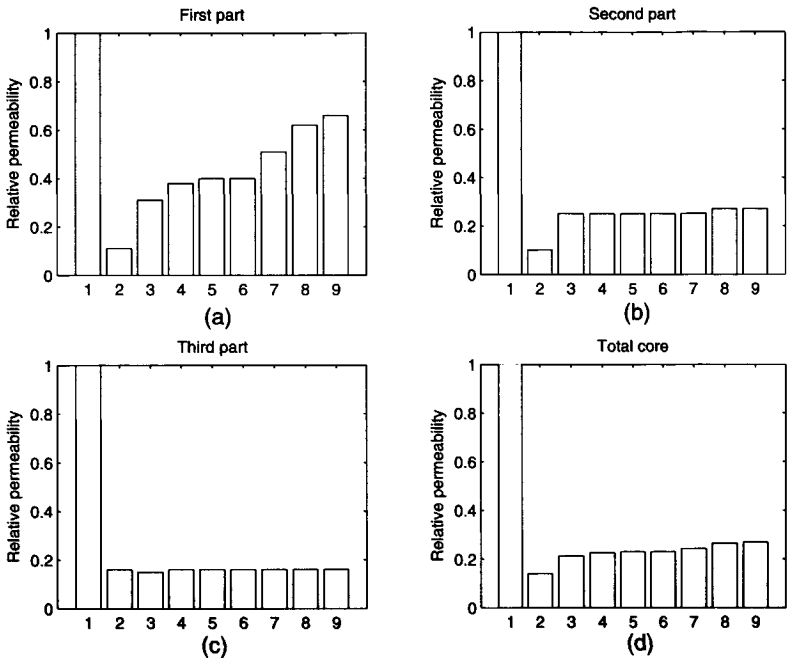

Figure 5.16: Relative permeability of the three parts of core A3 (and the overall permeability) after each treatment step, Table 5.6. The 40 kHz horn was used.

Treatment step	Description	Power (W)	Pressure (MPa)	Temperature (^{o}C)	Flow rate (ml/min)
1	Start	-	12	20	-
2	Fouling	-	12	20	25
3	Back flow	-	12	20	5
4	Acoustic treatment	350	12	20	75
5	Acoustic treatment	500	12	20	75
6	Acoustic treatment	700	12	20	75
7	Acoustic treatment	700	12	20	5
8	Acoustic treatment	700	12	20	0
9	Acoustic treatment	700	12	20	-5

Table 5.6: Experimental conditions used at each stage of the test on core A3. The relative permeabilities (K/K_0) measured at the end of each step for core A3 are shown in Fig. 5.16.

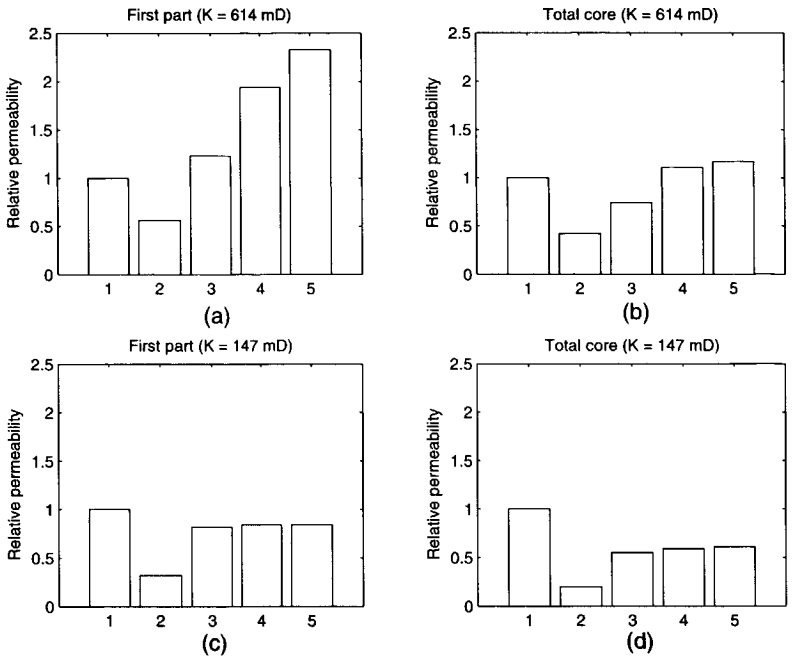

Figure 5.17: Effect of the initial permeability. Comparison of the relative permeability for two cores (A4 and A5) with different initial absolute permeability. The relative permeability is shown for the first part of the cores (and the overall permeability) after each treatment step as described in Table 5.7. The 20 kHz horn was used.

Treatment step	Description	Power (W)	Pressure (MPa)	Temperature (^oC)	Flow rate (ml/min)
1	Start	-	12	20	-
2	Fouling				
	Back flow	-	12	20	25
3	Acoustic treatment	1000	12	20	5
4	Acoustic treatment	1500	12	20	5
5	Acoustic treatment	2000	12	20	5

Table 5.7: Experimental conditions used at each stage of the test on cores A4 and A5. The relative permeabilities (K/K_0) measured at the end of each step for cores A4 and A5 are shown in Fig. 5.17.

Core No.	ϕ	K_0
A6	0.20	240
A7	0.21	290
A8	0.20	215
A9	0.23	525

Table 5.8: Properties of cores used in the cleaning experiments shown in Fig. 5.18.

5.4.3 Influence of relevant parameters on the efficiency of the acoustic cleaning technique

Effect of temperature

The influence of temperature between $15°C$ to $80°C$ was investigated. The acoustic waves penetrated further into the sandstone as the temperature was increased, and the cleaning efficiency improved. The increase of acoustic wave penetration is due to lower liquid viscosity at higher temperatures, which causes a decrease in the dissipation of the acoustic waves, Poesio, Ooms, Schraven & v. Bas (2002). Assuming that fouling is due to hydrodynamic bridging of particles, the increase of cleaning efficiency may also be due to an increase of the electrical double layer repulsion between particles within particle bridge structures at higher temperature. The increase of temperature may induce extra-generation of fines, but this was only observed when fresh water was flowing through the core; it was not observed when brine was used.

Effect of pressure

The pressure was varied between 5 MPa and 18 MPa. At low pressures an increase in the cleaning efficiency occurred in the first part of the core; this was previously observed by Venkitaraman et al. (1995). The effect is probably due to cavitation. When the front part of the core was exposed to acoustic irradiation at low pressures, damage (formation of holes into the front face of the core) occurred in this part of the core. At high pressures (> 10 MPa) cavitation was suppressed and no effect on the cleaning efficiency was observed.

Effect of cleaning velocity

Liquid flow velocity plays a crucial role during the formation of fouling particle structures probably due to hydrodynamic bridging of particles and the formation of bridges is more likely to occur at higher velocities. This phenomenon was also observed by Ramachandran and Fogler for fouling of the surface of a membrane. A similar influence of the velocity was observed during acoustic cleaning experiments: the efficiency of the acoustic cleaning increases with decreasing liquid flow rate. This is probably caused by the lower hydrodynamic drag on the particles in the bridge structures at lower liquid velocities. Hence, the particle bridge structures become less stable and can more easily be broken by the additional fluctuating liquid velocity caused by the acoustic waves. This influence is important from an application point of view: cleaning of the near well-bore region of an oil reservoir can most efficiently be carried out at low velocities; this is additionally evident in Fig. 5.18 where the results of four experiments are given showing the relative permeability of cores after acoustic treatment at three different liquid flow rates. Figure 5.18 clearly shows that the relative permeability increases significantly with decreasing flow rate. The strength increase of particle bridge structures with increasing flow rate was also observed by Batli & Risnes (1979) for sand arches. They found that as the flow rate increases the arch permeability decreases (up to the collapse of the arch) meaning that the particles forming the structure get closer together. This reduces the particle-particle distance, increasing the short range colloidal attractive force.

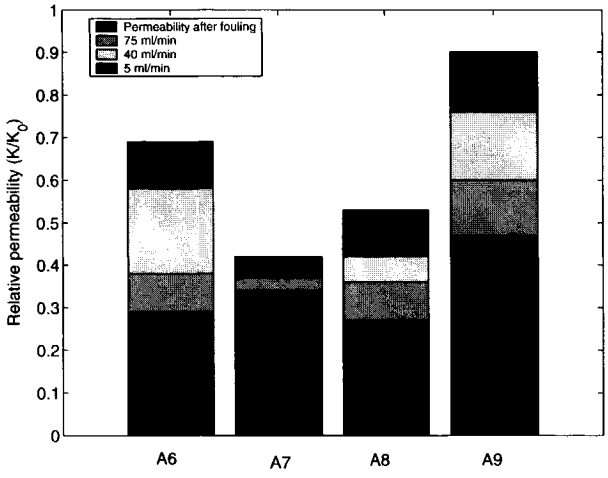

Figure 5.18: Effect of liquid flow rate on the relative permeability for four different experiments. The properties of the cores are shown in Table 5.8.

Effect of flow direction

The effect of liquid flow direction on the cleaning efficiency was also investigated. No differences in the relative permeability were found at low flow rate: once particles are removed from fouling particle structures they will be flushed out of the core. At high flow rates, however, more effective cleaning is observed when the acoustic wave propagates in the direction opposite to the liquid flow. As pointed out the cleaning effect is strongest in the first part of the core, because of the rapid damping of the fast acoustic wave. Therefore when particle bridge structures have been broken by the acoustic waves, the loose particles can (in case of acoustic waves propagation in the direction opposite to the liquid flow) relatively easily be removed from the core as the distance to the end of the core (where the acoustic source is located) is relatively short and the chance of being captured into a new particle bridge structure is small. When acoustic waves propagate in the same direction as the liquid flow, the loose particles must travel through almost the full length of the core and the chance of being captured into a new particle bridge structure is significantly greater.

Effect of initial level of fouling

The effect of the initial level of fouling on the cleaning efficiency was investigated using the fouled cores as shown in Fig. 5.13. The values of the relative permeability for the three cores (before acoustic treatment) were 21 % (core No. 5), 71 % (core No. 12) and 82.5 % (core No. 13). During acoustic treatment the flow rate was 5 ml/min and the duration of the acoustic treatment was 30 s. The results are shown in Table 5.9. The efficiency of acoustic cleaning decreases with increasing level of fouling; therefore when the level of fouling is high, it is hard to remove the fouling particle structures. This means that at high fouling levels multi-layer particle bridge structures are formed (Figs. 5.2 and 5.3) that cannot be easily broken. In addition the pores tend to fill up at high fouling levels.

Experiment	Relative permeability after fouling	Relative permeability after treatment
Core No. 5	21%	39%
Core No. 12	71%	98%
Core No. 13	82.5%	103%

Table 5.9: Effect of the initial level of fouling on the acoustic cleaning efficiency.

Core	Treatment	Init. rel. perm.	Rel. perm. after fouling	Rel. perm. after treatment
A10	Continuous	100%	36%	48%
A11	Pulses	100%	37%	54%

Table 5.10: Comparison of the acoustic treatment (pulses versus continuous irradiation) on two almost identical cores.

Effect of acoustic pulses versus continuous acoustic irradiation

The acoustic cleaning efficiency of acoustic pulses were compared to continuous acoustic irradiation at the same total acoustic energy. Continuous irradiation of 30 s was compared to six pulses of 5 s each (interrupted for 5 s intervals) for two almost identical cores with almost identical fouling. The total acoustic energy delivered was 60 kJ. The results are given in Table 5.10, as can be seen pulses are more effective.

A slightly different procedure was used with a single core which was first continuously treated acoustically and when no further increase of permeability occurred, pulses were applied. The results are given in Table 5.11. The pulses increased the relative permeability another 4%. Using the same procedure with six other cores a small increase (on average 6%) of cleaning efficiency was always observed.

5.5 Conclusions

Fouling of Berea sandstone cores by particle movement within the core was apparently caused by particles bridging at the pore throats. A precise interpretation of the results obtained from observation of particle transport in cores is difficult because of the variability and complexity of the porous system within sandstone. From the experimental results the following conclusion are drawn:

- Fouling takes place only after a critical flow rate (different for each rock) is exceeded.
- The reduction of permeability (hence fouling by particles) increases as:
  1. the aspect ratio (particle diameter to pore diameter) is increased,
  2. the concentration of particles moving with the liquid flow in the rock increases,
  3. the composition of the brine changes from Ca-ions to K-ions,
  4. the fluid temperature in the sandstone increases.

Initial rel. perm.	100%
Rel. perm. after fouling	39%
After continuous treatment	74%
After pulsed treatment	78%

Table 5.11: Relative permeability of a core with initial permeability of 364 mD first acoustically treated in a continuous manner with a 2 kW source and with a flow rate of 5 ml/min and then, for the same conditions, treated with 6 acoustic pulses of 5 s each.

Removal of the fouling particles by means of high-frequency acoustic waves is possible. The acoustic cleaning efficiency increases as:

- the liquid flow velocity decreases;
- the temperature increases;
- permeability increases;
- a pulsed stimulation is used instead of a continuous one.

Appendix A: Preparation of the SEM samples

A SEM-sample is prepared in the following way. The dry core is mechanically cut in the direction of the flow so that a sample can be removed. Dry conditions are used to avoid contact between water and clays. The sample is then impregnated by epoxy resin using 3 MPa pressure; the process is very slow requiring several hours to complete in order to ensure that the small pores are filled (the slow impregnation is also beneficial because it avoids the removal of particle structures). A small piece of the sample is cut. The sample is then polished. This procedure produces a flat surface for SEM analysis and allows analysis of a region that was not influenced by cutting. The sample is finally sprayed with carbon to enhance the contrast and electrical conductivity.

The coming chapter is again devoted to fouling due to particles bridge formation and its ultrasonic removal. We will study in detail the influence of acoustic waves on a particle in a two-particles bridge (blocking a pore throat). To that purpose we apply a numerical code based on the lattice-Boltzmann technique to determine the hydrodynamic forces on the particle due to the liquid flow and due to the acoustic waves. Also the colloidal forces are considered. Again an up-scaling procedure is used to translate the pore level results to (macroscopic) information about permeability changes.

Chapter 6

Removal of particle bridge formation by ultrasonic stimulation*

Abstract

Particle-bridge formation during the flow of a liquid with particles through a porous material is a fouling mechanism that can block the pores and, hence, decrease the permeability of the material. Ultrasonic irradiation of the material is a cleaning method that can restore the permeability. We make a numerical study of this cleaning method using the lattice-Boltzmann technique. We start from a pore blocked by two spherical particles attached to the pore wall by colloidal adhesion forces. Next we calculate the hydrodynamic force exerted by a high-frequency acoustic wave on bridges of two-particles. By comparing the hydrodynamic force and the adhesion force we investigate, whether the fouling particle bridges will be removed by the ultrasonic irradiation. A sensitivity study is carried out to investigate the influence of some relevant parameters, such as the acoustic wave amplitude, the acoustic frequency, the fluid flow velocity and the ratio of particle diameter and pore diameter. An up-scaling procedure is applied to translate the microscopic results for the fouling removal at the pore level to the permeability improvement of the material at the macroscopic level. A comparison is made between the numerical results and experimental data. The agreement is reasonable.

6.1 Introduction

During the production of oil from an underground reservoir the permeability of the sandstone in the near wellbore region can decrease dramatically due to fouling of the sandstone by small particles. This attenuation in permeability causes also a decrease in the oil production rate. An environmental friendly and cheap cleaning method is the irradiation of the near wellbore region by high-frequency acoustic waves. However, during field tests it was found that the technique gave positive results in only 50% of the cases, while it failed in other cases. Therefore we decided to make a detailed experimental and numerical study of the phenomenon.

It is important to discuss first the mechanisms that cause the permeability reduction by particles. Reduction in permeability can be due either to bridge formation of particles in the throats of pores inside the sandstone, or due to the deposition of particles onto the pore walls leading to a reduction of the pore diameter. Of course a combination of the two mechanisms is also possible. Which mechanism occurs, depends on production conditions like oil flow rate, particle properties and properties of the sandstone. The cleaning (particle removing) efficiency of ultrasound is different for the two fouling mechanisms. In this publication we assume that the permeability reduction

*P. Poesio and G. Ooms. "Removal of particle bridges from a porous material by ultrasonic irradiation". *Submitted for publication to AIChE J.*

is due to particle bridge formation. The generation of such particles in an oil reservoir may be due to erosion of the reservoir rock by the oil flow through the reservoir during production. Also other causes are possible such as colloidally induced migration of fines. The generation and migration of small particles in a porous material are well described in the book by Khilar & Fogler (1998).

The aim of this publication is to investigate the conditions at which particle bridges can be removed inside a porous material by means of high-frequency acoustic waves. We start by developing a microscopic numerical model to calculate the hydrodynamic force exerted by a traveling acoustic wave on the particles in a bridge consisting of two particles. Due to computer limitations it is not (yet) possible to make calculations for particle bridges with more than two particles. A future parallelization of the code will make possible to take into account more than two particles. These calculations are carried out by means of the lattice-Boltzmann technique (that will be described). Also a model is developed to calculate the adhesion force between the particles in the particle bridge and the porous material at the pore throat. Next, we compare the hydrodynamic force and the adhesion force to find out at what conditions a particle from the particle bridge will detach from the pore throat. Thereafter we change the values of some relevant parameters and study their influence on the cleaning effect. Also an attempt is made to up-scale the results found at the microscopic level to macroscopic quantities such as the permeability of the porous material. Finally a comparison is made between numerical predictions and some experimental data.

6.2 Lattice-Boltzmann method

6.2.1 Numerical technique

For our numerical simulations the lattice-Boltzmann method is used. The lattice-Boltzmann method uses a mesoscopic model for the fluid behavior, which is based on collision rules for the movement of hypothetical particles (not to be confused with the physical particles) on a grid. The grid is a uniform simple cubic lattice. It can be shown that, after averaging, the continuity equation and Navier-Stokes equations are satisfied. The lattice-Boltzmann method has been applied earlier to calculate the laminar or turbulent flow in a complex geometry, see for instance Succi (2001). Our method is based on the work of Eggels & Somers (1995); it is described in detail by Cate (2002). The boundary condition at the surface of a particle is taken into account by means of an induced force-field method, similar to the one used by Derksen & van den Akker (1999). In this method a particle is represented by a number of points located in its surface. The surface points are evenly distributed with a mutual distance smaller than the grid spacing. The no-slip condition at the particle surface is satisfied in two steps. First, the fluid velocity at each surface point is determined via a first-order interpolation of the fluid velocities in the surrounding grid points. Then, (induced) forces are assumed to be present at the surface points of the particle of such a magnitude, that the fluid velocity in the surrounding grid points is changed in such a way that the no-slip condition at the surface points is satisfied. Thereafter, the hydrodynamic drag force ($\mathbf{F_d}$) and also the torque ($\mathbf{M_d}$) acting on a particle by the fluid are computed.

The method of induced forces used to satisfy the no-slip condition at the particle surface causes a problem in the calculation of the drag force. According to this method the fluid is assumed to be present at all lattice grid points, so also at the locations where the particles are present. The particle presence is only taken into account via the no-slip condition at the surface points of the particles. The (imaginary) fluid inside the particles causes an (unreal) contribution to the drag force on the particles. This problem is well-known and techniques have been developed to correct for the artificial drag force. We do not discuss these techniques here, but refer to the specialized literature mentioned before, see Cate (2002) and references therein

6.2.2 Calibration procedure for the particle radius

As discussed, a particle surface is approximated in the lattice grid by means of particle surface points. It is known that this approximation causes the particle to experience a drag force that

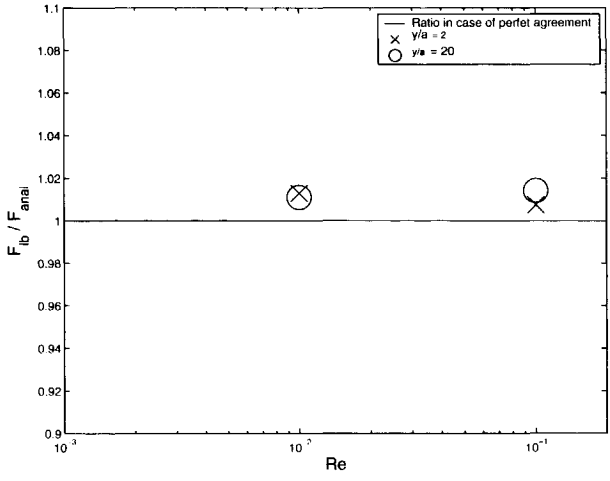

Figure 6.1: Comparison between the lift force calculated by our lattice-Boltzmann code F_{lb} and the analytically calculated lift force on a particle F_{anal} for two dimensionless distances from the wall ($y/a = 2$ and $y/a = 20$).

corresponds to a particle with a diameter larger than the real one (see the specialized literature for more details). This effect can be compensated by ascribing to the particle a hydrodynamic radius that is smaller than the real radius. For the determination of this hydrodynamic radius a calibration procedure is applied. A well known procedure was proposed by Ladd (1994*a*). He calculated the drag force acting on a particle located in an array of particles with a periodic arrangement in two ways. He applied his lattice-Boltzmann method and used also the analytical solution for this particular problem. From the comparison between the two results he found the hydrodynamic radius. The calibration procedure is based on the following analytical expression of Hasimoto (1959) for the drag force F_D on a fixed spherical particle in a periodic array of spherical particles by a fluid flow through the array of particles under creeping flow condition

$$\frac{6\pi\mu a U_u}{F_D} = 1 - 1.7601 C_\tau^{1/3} + C_\tau - 1.5593 C_\tau^2 \tag{6.1}$$

where μ represents the dynamic viscosity of the fluid, a the particle radius. $C_\tau = \frac{4\pi a^3}{3L^3}$ in which L indicates the size of unit cell of the periodic array and U_u is the volumetric averaged fluid velocity across the periodic cell. We use the results of this procedure for our calculations.

As mentioned above, the hydrodynamic radius was determined for creeping flow conditions. One may wonder whether this result holds also at finite Re-number when inertial effect comes into play. In order to investigate this point we also compute with our lattice-Boltzmann code the lift force on a sphere held stationary in a linear shear flow in presence of a wall at low, but finite, Re-number using the hydrodynamic radius as explained above. The numerical calculations are compared with the analytical solution of Cherukat & McLaughlin (1994) in Fig. 6.1. As can be seen the agreement is reasonable.

As the numerical code will be applied to oscillating flow conditions, we check its reliability also for such flow conditions by comparing numerical and analytical results for the drag force on an oscillating spherical particle in an infinite unbounded fluid. The analytical solution for this problem can be found in the book by Lifshitz & Landau (1987). The drag force as function of

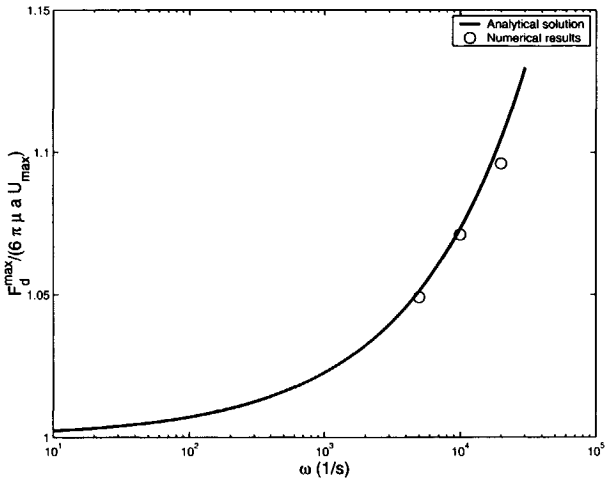

Figure 6.2: Comparison between the analytical and numerical result for the drag force in an unbounded oscillating flow.

time reads as

$$\mathbf{F_D} = 6\pi\mu a\left(1+\frac{a}{\gamma}\right)\mathbf{u} + 3\pi a^2\sqrt{\frac{2\mu\rho}{\omega}}\left(1+\frac{a}{\gamma}\right)\frac{d\mathbf{u}}{dt}, \tag{6.2}$$

where $\gamma = \sqrt{2\nu/\omega}$ can be interpreted as the depth of penetration of the rotational flow around the particle. ν is the kinematic viscosity of the fluid and ω the frequency of the oscillation. We compute the maximum drag force during an oscillation cycle and compare it with the theoretical expression given by (Eq. 6.2). The results are shown in Fig. 6.2. As can be seen, the drag force is reliably predicted by the lattice-Boltzmann code.

6.2.3 Geometry of the flow domain

The computations are carried out on a three dimensional grid with a geometry as sketched in Fig. 6.3. As can be seen this geometry is used to simulate the blocking of a cylindrical pore by two particles. The particles are assumed to have their centers in a plane passing through the pore axis. Since the geometry is three dimensional, the fluid can go around the particles. So complete blocking is not possible in a three-dimensional flow. We choose the radius of the particles to be equal to 10 lattice units. The radius of the wide part of the pore channel is chosen in such a way that any further enlargement does not change the results. Also the lengths of the wide and narrow part of the pore are chosen in such a way that the results do not change with a further increase in length of those parts. The size of the narrow part of the pore is a parameter in our calculations. A parabolic inflow and outflow profile of the fluid is imposed. This condition is justified since we are looking at frequencies well-below the critical Biot's frequency (Biot 1956). All the walls are non-slip boundary conditions. For some cases, we double the mesh dimension in each direction to check that the numerical results are independent of the mesh size.

6.3 Modeling of the high-frequency acoustic wave

As discussed we are interested in the possibility of removal of a two-particles bridge structure from a pore throat (see Fig. 6.3) by a high-frequency acoustic wave. To that purpose we will

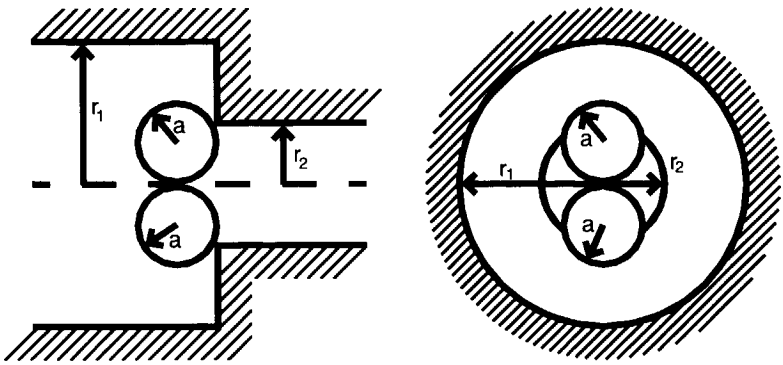

Figure 6.3: Geometry of the flow domain. Two particles are shown blocking the entrance to a pore.

calculate the drag force on the particles in the two-particles bridge structure due to the oscillating flow generated by the ultrasonic wave. The pore diameter is of the order of a few micrometers, while the acoustic wave length is of the order of a few centimeters. So the flow can be considered incompressible, as the pore diameter is much smaller than the wave length. The acoustic wave is modeled in the numerical simulation by adding an oscillating body force to the equation of motion of the following form

$$\mathbf{f} = \rho\omega A sin\omega t\ \mathbf{i}_x \tag{6.3}$$

where ρ is the fluid density and A the acoustic wave amplitude. $\mathbf{i}_x$ is the unit vector in the direction of wave propagation.

We will compare numerical predictions made with the lattice-Boltzmann code for acoustic cleaning at the pore level with results from acoustic cleaning experiments carried out on sandstone cores in the laboratory. In order to be able to make such a comparison it is necessary to know the amplitude A of the oscillating body force as applied during the experiments with a core and use it in the numerical simulations at the pore level. This amplitude is calculated by means of the following relation for the oscillating pressure

$$\frac{dp}{dl} = G\rho e^{i\omega t}, \tag{6.4}$$

in which p is the hydrodynamic pressure generated by the acoustic source in the pore liquid during the ultrasonic cleaning experiments with sandstone cores, l the coordinate in the direction of the centerline of the core; G is determined by the acoustic intensity ($I = P/S$) and by the frequency such as $G = \omega\sqrt{I/\rho c}$; P the acoustic power input during the experiments, S the irradiated surface area, ρ the fluid density, c the sound velocity and t the time. So when P and S are known, it is possible to determine the amplitude of the oscillating pressure in the fluid and also the amplitude A of the body force as used in Eq. 6.3. Equation 6.4 is only valid in the very first part of the core close to the acoustic source, where damping of the oscillating wave is still negligible. At larger distances from the source damping has to be taken into account. This is done in the following way

$$\left(\frac{dp}{dl}\right)_{x_0} = G\rho e^{i\omega t - \beta x_0}, \tag{6.5}$$

where β is the damping coefficient of the fast Biot wave, see Biot (1956) and x_0 is the distance from the point of interest inside the porous material to the acoustic source. (The slow wave is

damped very quickly and is not relevant for cleaning at distances larger than a few millimeters.) The damping coefficient of the fast wave was determined experimentally; the details can be found in Poesio, Ooms, Barake & v. Bas (2002), Poesio, Ooms, Schraven & v. Bas (2002) or Kelder (1998).

Next to the oscillating flow in the sandstone core due to the acoustic wave there is a steady flow through it during the experiments to simulate the oil flow rate during production. Therefore, this steady component is also taken into account during our numerical simulations. The Reynolds number for the steady flow component based on the pore radius is between 10^{-4} and 10^{-3}. This value is realistic for an oil reservoir.

In our simulations the aspect ratio (ratio of pore diameter and particle diameter) is between 1 and 2. In real conditions the aspect ratio can be of the order of 20 and particle bridges can be formed by many particles. Because of computer limitations we will only investigate two-particles bridges.

6.4 Modeling of the adhesion force between a particle and the pore throat material

As discussed by Poesio et al. (2004) the adhesion force acting on a particle in the two-particles bridge is due to the attractive van der Waals force between the particle and the pore throat material. For symmetry reason this force lies in the plane through the centerline of the pore and the particle centers. To compute the adhesion force we use the following method: we assume the material of the pore throat walls to be composed of fictitious small particles of radius δ_i and we compute the force acting between the (real) particle in the particle bridge and each fictitious particle and sum all the contributions. The force between the real particle and a fictitious particle is given by

$$F_{vdW}(a, \delta_i, x_i) = -\frac{H}{6}\left(\frac{2a\delta_i}{x_i^2 - (a+\delta_i)^2} + \frac{2a\delta_i}{x_i^2 - (a-\delta_i)^2} + ln\frac{x_i^2 - (a+\delta_i)^2}{x_i^2 - (a-\delta_i)^2}\right), \qquad (6.6)$$

where H is the Hamaker constant, x_i is the distance between the center of the fictitious particle i and the real particle and δ_i is the radius of the fictitious particles. The Hamaker constant is dependent upon the material properties only.

To verify the validity of this calculation method, we compare its predicted adhesion force with the known analytical expression for a spherical particle interacting with a plane wall at a distance b of the wall (see Fig. 6.4). When the fictitious particles become small enough we expect that the calculated adhesion force becomes independent of the radius δ_i of the fictitious particles and equal to the analytical expression. The result is given in Fig. 6.5. Indeed for small enough fictitious particles the numerical adhesion force becomes independent of δ_i and approximates the analytical solution (although the difference remains about 7%).

In the same way we calculate the adhesion force for the geometry as given in Fig. 6.6: a particle at the entrance of a pore throat. The calculated (horizontal and vertical) components of the force are given in Fig. 6.7. Again when the radius of the fictitious particles is small enough the calculated result is independent of δ_i. During these calculations we also find, that the adhesion force is independent of the lengths of the wide and narrow part of the pore when these lengths are larger than twice the particle radius. This effect can be easily understood since the adhesion force is decaying very rapidly with the distance x_i ($\sim 1/x_i^2$). Also the influence of the width of the narrow part of the pore on the adhesion force is limited to the very first part of the narrow part. For the geometry of Fig. 6.6, we find that the adhesion force is of the order of 10^{-8} N, two orders of magnitude smaller than the adhesion force for the geometry of Fig. 6.4. This result can explain why, for a given acoustic power, it is much easier to remove a particle bridge structure from a pore throat than a particle adhering to a pore wall (Poesio et al. 2004).

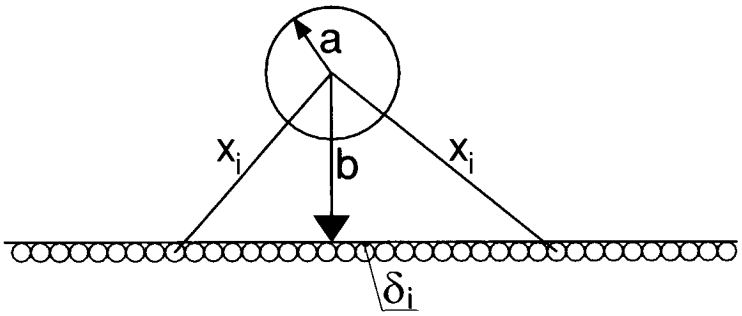

Figure 6.4: Sketch of the model used for the calculation of the adhesion force. The material of the wall is assumed to be composed of many fictitious particles and their interaction with the real particle is calculated and summed.

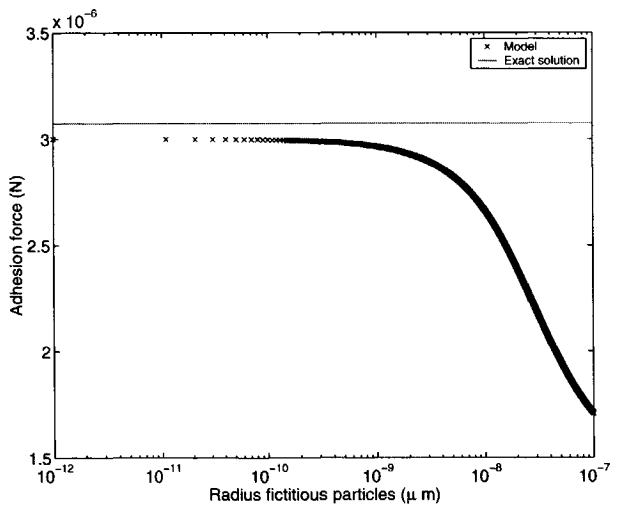

Figure 6.5: Comparison between numerical result and analytical solution for the particle-wall adhesion force as function of the fictitious particle radius δ_i for the geometry shown in Fig. 6.4.

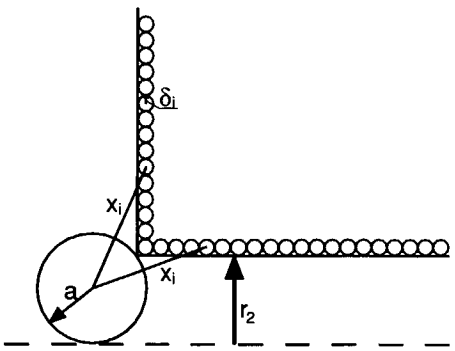

Figure 6.6: Sketch of the model used for the calculation of the adhesion force between a particle and the pore throat material.

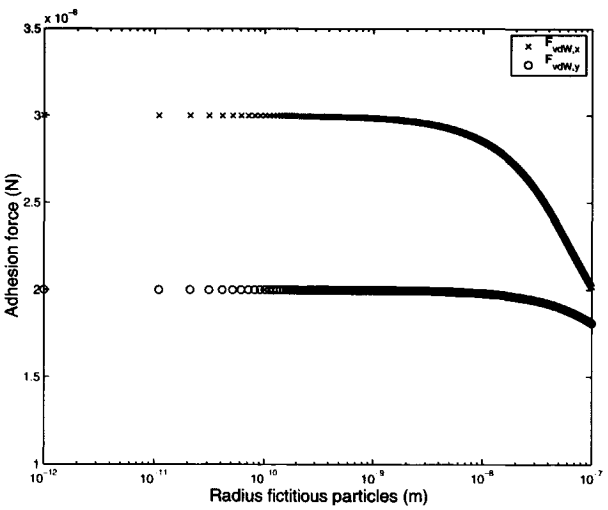

Figure 6.7: Calculated horizontal $F_{vdW,x}$ and vertical $F_{vdW,y}$ component of the adhesion force as function of the fictitious particle radius δ_i for the geometry given in Fig. 6.6

6.5 Numerical results

6.5.1 Introduction

In this section we study the cleaning by ultrasonic waves in detail. We do this by comparing the numerical results for the hydrodynamic force acting on the particles in a two-particles bridge (during the negative part of the wave when the particles are pushed away from the pore throat) with the adhesion force acting on these particles because of their interaction with the pore wall material. We will pay particular attention to the influence of different parameters such as the acoustic wave amplitude, the steady fluid flow rate, the aspect ratio and acoustic frequency. The results are expressed in terms of the ratio between the hydrodynamic force and the adhesion force as function of the different parameters. We assume that the particle bridge is broken when this ratio is above unity. It is possible that, in reality, a new bridge is formed during the subsequent positive part of the acoustic wave when the particles are again pushed in the direction of the pore throat. However, that possibility is not included in our calculations.

6.5.2 Criteria for particle bridge removal

Removal of a particle bridge can occur in two ways: either the bridge structure is removed as a whole from the throat or the bridge is broken due to rotation of the particles around the edge of the pore throat. In the first case the maximum drag force acting on the particles has to overcome the adhesion force in the direction of the pore axis. In the second case the torque (due to the hydrodynamic force) acting on a particle has to be larger than the adhesion torque acting on the particle. It turns out, that particle bridge removal due to rotation of the particles around the pore throat edge is easier than removal of the bridge structure as a whole.

6.5.3 Influence of acoustic wave amplitude

The magnitude of the detaching hydrodynamic force increases as the acoustic wave amplitude (so the acoustic power input) increases. As the adhesion force is constant, it can be expected that particle bridge removal will only take place above a certain value of the acoustic power input. This effect is shown in Fig. 6.8, in which the ratio between the hydrodynamic force and the adhesion force is given as function of the ratio $(U_A - U_S)/U_A$ for two values of the aspect ratio. U_A is the maximum fluid velocity generated by the acoustic wave and U_S is the steady fluid flow velocity (representing the oil flow rate through a reservoir during production). U_A is, of course, directly related to the acoustic wave amplitude. As expected particle bridge removal can only occur, when the fluid flow velocity (U_A) generated by the acoustic wave is sufficiently large. Hence when the acoustic wave amplitude or the acoustic power input is sufficiently large.

6.5.4 Influence of steady fluid flow velocity

As mentioned earlier there is a steady fluid flow (U_S) through the pore, which represents the oil flow rate through the reservoir during production. This steady flow pushes the particles against the pore throat. Therefore a larger hydrodynamic force from the acoustic wave is needed to remove the particle bridge than in the case that there is no steady flow. This effect is shown in Fig. 6.8, where the ratio between the hydrodynamic force and adhesion force is shown as function of the ratio $(U_A - U_S)/U_A$. It is clear from this figure, that the effect of the steady flow is to reduce the cleaning possibility of the acoustic wave. A larger acoustic power input is needed for cleaning. This effect is very special for fouling due to particle bridge formation. It has also be found experimentally by Poesio & Ooms (2004).

6.5.5 Influence of aspect ratio

We define the aspect ratio as the ratio between the diameter of the narrow part of the pore and the particle diameter. The particles used in our experiments have a rather narrow size distribution

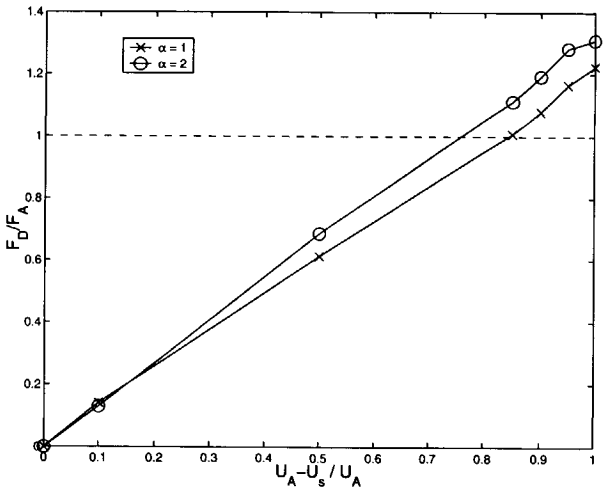

Figure 6.8: Influence of the fluid flow velocity generated by the acoustic wave (U_A) and of the steady fluid flow velocity (U_S) on the ratio between the hydrodynamic force and adhesion force for two values of the aspect ratio. Particle bridge removal will take place when this ratio is above 1.

with a peak around 0.8-1 μm. The pore size distribution depends, of course, on the type of sandstone and can be rather broad. The values for the aspect ratio that we investigate in this publication, are between 1 and 2. If the aspect ratio increases the hydrodynamic force on the particle bridge decreases. The reason is, that although the steady fluid flow velocity through the pore is kept constant the local velocity around the particle is smaller as the flow is less blocked before the entrance to the pore throat at larger values of the aspect ratio. The adherence force also decreases with increasing aspect ratio, because the average distance between the particles and the pore walls is larger. This last effect (decreasing adherence force) is considerably stronger than the first one (decreasing hydrodynamic force). So the net effect is, that with increasing aspect ratio the cleaning effect improves. This is shown in Fig. 6.8, where the ratio between the hydrodynamic force and adhesion force is shown as function of the ratio $(U_A - U_S)/U_A$ for two values of the aspect ratio (α =1 and 2). In Fig. 6.9 more details are given. In this figure the ratio between hydrodynamic force and adhesion force is shown as function of the aspect ratio (for three values of the relative acoustic input intensity I/I_0). An increase in aspect ratio at constant particle diameter means a larger pore diameter, which in its turn means a larger permeability of the porous material. So the conclusion is, that the cleaning efficiency improves with increasing permeability of the porous material.

6.5.6 Influence of acoustic frequency

The acoustic frequency influences the hydrodynamic force in two ways. As the frequency increases the hydrodynamic force acting on the particles increases too. However, with increasing frequency also the damping of the high-frequency acoustic wave in a porous material increases, see Biot (1956). For a particle in the porous material at a certain distance (say 0.1 m) from the acoustic source these two competing effects have to be taken into account. For low frequencies the particle bridge cannot be removed, as the hydrodynamic force is too small. For very high frequencies the particle bridge (at 0.1 m from the acoustic source) cannot be removed, because the acoustic wave has weakened too much due to the acoustic damping. The result can be seen in Fig. 6.10

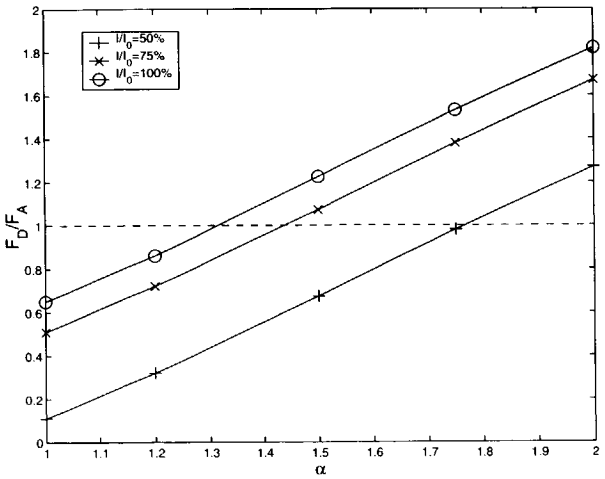

Figure 6.9: Influence of the aspect ratio α on the ratio between hydrodynamic force and adhesion force for three values of the acoustic input intensity I. ($I_0 = P_0/S$ is the reference intensity.) For values of F_D/F_A larger than 1, particle bridges are removed by the acoustic waves.

in which the ratio of the hydrodynamic force and the adhesion force is given as function of the (dimensionless) frequency for two values of the acoustic intensity and for two values of the aspect ratio. Only in a certain frequency interval particle bridge removal is possible. The frequency interval where acoustic cleaning is possible depends on parameters, such as acoustic input intensity and aspect ratio. The existence of a frequency interval for cleaning was found by Kuznetsov & Efimova (1983) during a field application. In their case the interval was between 5 and 50 kHz.

6.6 Up-scaling of the numerical pore-level results to the macroscopic permeability

In order to compare our numerical results with experimental data an up-scaling procedure, based on a physical model for the porous material, is developed. According to this model we assume that the porous material contains many pores with the shape sketched in Fig. 6.11. Each pore is characterized by four parameters: $r_{1,i}$, $r_{2,i}$, $l_{1,i}$ and $l_{2,i}$ (see Fig. 6.11). There are three types of such pores; each type is characterized by its own combination of $r_{1,i}$, $r_{2,i}$, $l_{1,i}$ and $l_{2,i}$ (so with i=1,2 or 3). It can be shown, that the contribution of each type of pores to the permeability is given by

$$K_i = \frac{N_i \pi}{8} \left[\frac{l_{1,i}}{l} \frac{1}{r_{1,i}^4} + \frac{l_{2,i}}{l} \frac{1}{r_{2,i}^4} \right]^{-1}, \tag{6.7}$$

where N_i is the number of pores of type i per unit surface area in a perpendicular cross-section of the porous-material model, as sketched in Fig. 6.11, and $l = l_1 + l_2$, see Kelder (1998). The total permeability K is calculated from the contributions of the three types of pores in the following way (Bear 1972)

$$\frac{1}{K} = \sum_i \frac{1}{K_i}. \tag{6.8}$$

The next step is to introduce fouling by particles into the model. This is achieved by assuming a certain number of pores to be blocked by particle bridges. This fraction can be different for

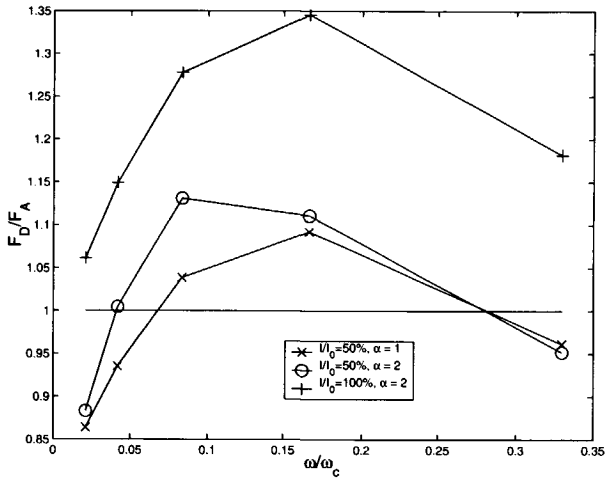

Figure 6.10: Influence of (dimensionless) acoustic frequency on the ratio between hydrodynamic force and adhesion force for two values of the (dimensionless) acoustic intensity I/I_0 and two values of the aspect ratio α. (The frequency ω_c is the critical frequency from the Biot theory.) When the ratio F_D/F_A is larger than 1, particle bridge removal occurs.

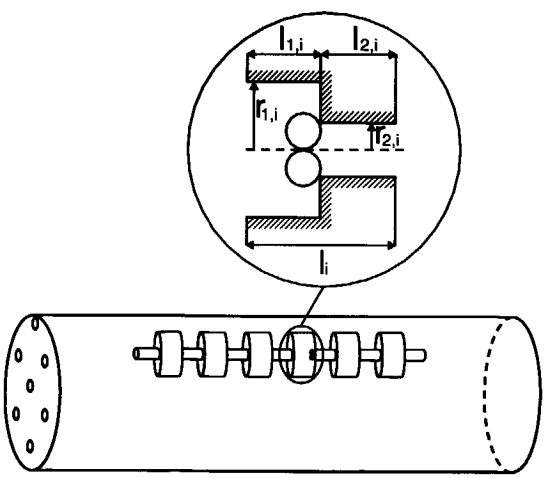

Figure 6.11: Conceptual model used for up-scaling of the numerical pore-level results to the macroscopic permeability.

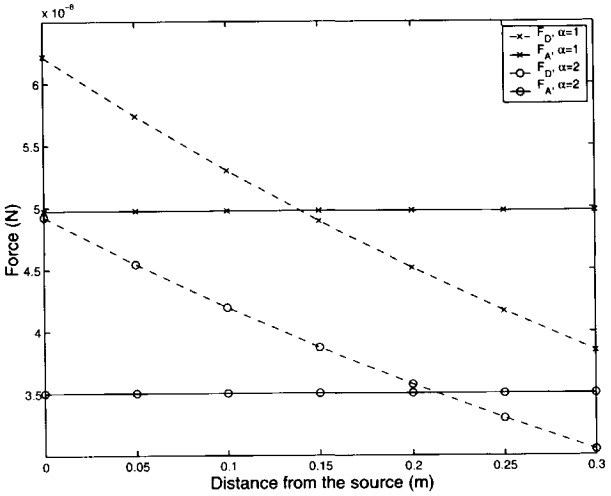

Figure 6.12: Comparison between colloidal adhesion force and hydrodynamic detaching force as function of the distance from the acoustic source.

the three pore types. So in the fouled area the numbers N_1, N_2 and N_3 are different from their original values for the clean porous material. The fouling is supposed to be uniformly distributed in the porous material. Using the Eq. 6.7 we can calculate the permeability for the fouled porous material.

The cleaning of the material by acoustic waves is then calculated at the pore level using the procedure explained earlier. For certain values of the relevant parameters (the acoustic intensity, frequency, steady fluid flow velocity, aspect ratio) the hydrodynamic force F_D is calculated as function of the distance from the acoustic source. A typical result is shown in Fig. 6.12. Where F_D is larger than the adhesion force F_A the porous material will be cleaned. We have assumed that the solid material behaves as a rigid frame, so that the velocity that determines the drag force is equal to the fluid velocity. A discussion of this hypothesis is given in Appendix A. In the other part the particle bridges are not removed by the high-frequency acoustic waves. As can be seen a typical value for the cleaned area is 0.1 m to 0.2 m from the acoustic source. After this pore level calculation we can use Eq. 6.7 again to determine the permeability distribution after the cleaning process.

The cleaning process is due, mainly, to the fast acoustic waves. Shear waves are assumed to be absent because of the perpendicular incidence of the waves onto the material. The slow wave is damped very quickly (first millimeters); it penetrates only a few millimeters. However, the fast wave can penetrate a larger distance. Dependent on the frequency it is of the order of 0.2 m. In earlier work we reported about measurements of the damping coefficient (Poesio, Ooms, Schraven & v. Bas 2002).

6.7 Comparison with experiments

We will now use the calculation procedure for the permeability improvement due to ultrasonic cleaning (as described in the foregoing paragraph) to compare permeability data obtained from cleaning experiments on Berea sandstone cores with their numerical predictions. The experiments have been described in detail by Poesio & Ooms (2004). We will not repeat these details here. We will only use some of the experimental results to check the reliability of the numerical calculation

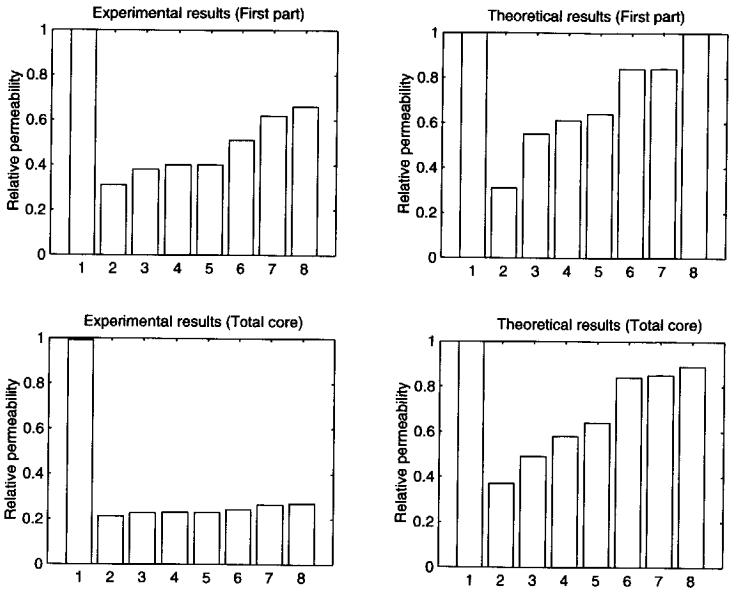

Figure 6.13: Comparison between experimental cleaning results and their model predictions. Step 1 gives the value of the relative permeability before fouling and step 2 the value after fouling. Steps 3, 4 and 5 show the relative permeability improvement due to an increase of the acoustic amplitude. Steps 6, 7 and 8 show the relative permeability improvement due to a decrease in net fluid flow rate.

procedure for the permeability improvement.

Using the known properties of the porous material and of the acoustic waves used during the experiments, the cleaning efficiency can be calculated and compared with the experimental data. During the experiments measurements were carried out over three parts of the sandstone cores: the first part (closest to the acoustic source), the second part (in the middle of the core) and the third part (furthest away from the acoustic source). The first part has a length of about 0.025 m. The total core length is about 0.2 m. It is clear that the cleaning process is in particular successful in the first part of the core, where the damping effect on the acoustic wave is not yet very strong. In Fig. 6.13 and Fig. 6.14 we present results for the first part and for the total core (part 1, 2 and 3 together, see Poesio & Ooms (2004)). In these figures the relative permeability is defined as the ratio of the permeability during the cleaning process and the initial permeability of the cores before fouling. Step 1 gives the value of the relative permeability before fouling and is by definition equal to 1. Step 2 gives the permeability after fouling of the core. The fouling procedure for the experiments is described in the publication by Poesio & Ooms (2004) and is, therefore, not repeated here. The fouling procedure for the numerical simulations has been described in the preceding section. Numerical fouling is achieved by assuming a certain number of pores to be blocked by particle bridges. As mentioned this fraction can be different for the three pore types. In this way we adapt the initial fouling for the numerical simulations to the initial fouling level of the experiments.

In Fig. 6.13 the influence of the acoustic amplitude and of the steady fluid flow rate on the cleaning efficiency is shown. Steps 3, 4 and 5 show the relative permeability improvement due to an increase of the acoustic amplitude. Steps 6, 7 and 8 show the relative permeability improvement due to a decrease in net fluid flow rate. The core cleaning improves with increasing amplitude as

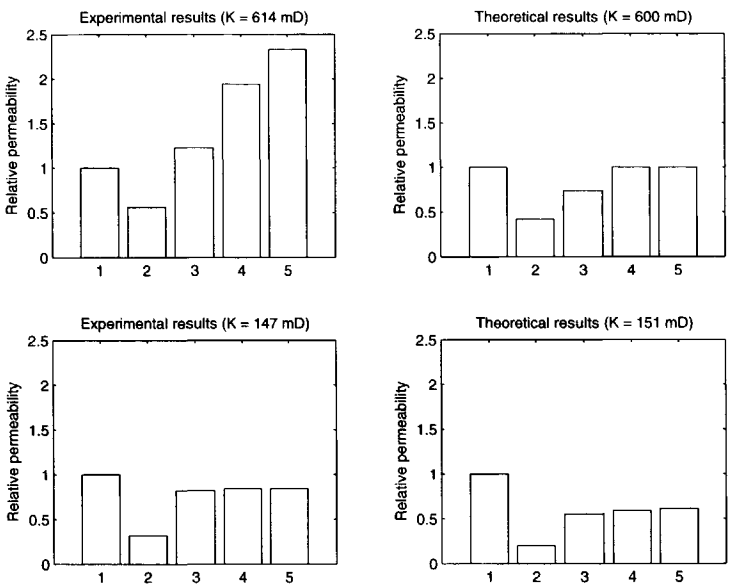

Figure 6.14: Comparison between experimental cleaning results and their model predictions for two values of the initial permeability of the porous material. Step 1 gives the value of the relative permeability before fouling and step 2 the value after fouling. Steps 3, 4 and 5 show the relative permeability improvement due to an increase of the acoustic amplitude.

the acoustic waves can penetrate deeper into the core material, before they are damped because of their interaction with the porous material. The cleaning improves with decreasing steady fluid flow rate, as the particle bridges can more easily be removed from the pore throat. The agreement between experimental data and model predictions is reasonable for the first part of the core. However, for the total core the cleaning efficiency is over-predicted by the model. The reason is not clear at the moment.

The effect of the absolute value of the initial permeability of the core material on the cleaning efficiency can be seen from Fig. 6.14. Experiments on cores with a permeability of 614 mD and 147 mD have been carried out. Step 1 gives again the value of the relative permeability before fouling and step 2 the value after fouling. Steps 3, 4 and 5 show the relative permeability improvement due to an increase of the acoustic amplitude. As can be seen the cleaning efficiency improves with increasing initial permeability of the porous material. Also the beneficial effect of a larger acoustic amplitude on the cleaning is again observed. The agreement between experimental results and model predictions is only qualitatively reasonable. A peculiar effect can be seen for the experiments on cores with a permeability of 614 mD. The relative permeability of the material can become larger than 1 during the cleaning process. This phenomenon can, of course, not be explained by our model. It is likely caused by a disintegration of the sandstone due to the acoustic waves.

6.8 Conclusions

We have studied the possibility of removing particle bridges from a porous material by high-frequency acoustic waves. To that purpose we have developed a numerical calculation procedure (based on the lattice-Boltzmann technique) to determine the hydrodynamic force on the particles in a two-particles bridge blocking a pore throat, and we have compared the hydrodynamic force with the adhesion force between the particles and the pore throat material. From this comparison follows, whether a particle bridge is removed from the pore throat, or not. The sensitivity of several relevant parameters, such as acoustic wave amplitude, acoustic frequency, aspect ratio and steady fluid flow velocity has been investigated. A calculation procedure has been developed to up-scale the numerical pore-level results to the macroscopic permeability. We have used this procedure to compare numerical predictions for the efficiency of the acoustic cleaning technique with experimental data derived from ultrasonic cleaning experiments on Berea sandstone cores. The agreement is only qualitatively reasonable.

Appendix A

In the up-scaling of the results, we have assumed that the skeleton is a rigid (incompressible) body at rest. The validity of this hypothesis depends on the properties both of the fluid and solid. By Biot's theory (Biot 1956), we can compute the ratio between the velocity of the fluid (U) and the velocity of the solid (u) due to the fast and slow wave:

$$\Gamma_{f,s} = \frac{U}{u} = \frac{-P\zeta_{f,s} + \rho_{11}}{Q\zeta_{f,s} - \rho_{12}} \tag{6.9}$$

where $\zeta_{f,s}$ are the wave numbers for the fast and slow wave respectively; the other symbols are defined as:

$$\begin{aligned} P &= K_p + K_f \tfrac{(1-\phi)^2}{\phi} \\ Q &= (1-\phi)K_f \\ \rho_{12} &= -(\alpha_\infty - 1)\phi\rho_f - i\tfrac{b}{\omega} \\ \rho_{11} &= (1-\phi)\rho_s - \rho_{12} + i\tfrac{b}{\omega} \\ b &= \tfrac{\phi^2\mu}{K} \end{aligned} \tag{6.10}$$

where K_p is the constrained modulus ($K_p = 26.1$ GPa), K_f is the fluid compressibility ($K_p = 2.2$ GPa), ϕ is the porosity ($\phi = 20\%$), α_∞ is the tortuosity ($\alpha_\infty = 2.8$), ρ_f is the fluid density

($\rho_f = 2650$ kg/m^3) and ρ_s is the solid density ($\rho_s = 2650$ kg/m^3). Those values have been taken from Kelder (1998). K is the permeability (K=200 mD) and μ is the fluid viscosity ($\mu = 1$ mPa s) We are, as already discussed, interested in the contribution of the fast wave. In this case, fluid and solid move in phase. We can evaluate this ratio for Berea sandstone saturated by water; this ratio is $\Gamma_f = 18.9$. So, at least in first approximation, our hypothesis is valid.

Removal of fouling due to internally generated particles was analyzed in the previous chapters. In the coming chapter fouling due to external particles (penetrated from outside into the porous material) is studied. This type of fouling is completely different from the previous one, since it does not penetrate deeper than a few millimeters into the material. It causes a sharp and localized drop in permeability, while the permeability reduction due to internally generated particles is uniform throughout the core. Accurate and detailed experiments are reported in the coming chapter about the fouling mechanism for external particles and about their removal by means of ultrasonic waves. Again the influence of the most relevant parameters is investigated. Special attention is given to the influence of the duration of the ultrasonic irradiation of the porous material.

Chapter 7

Fouling by external particles and ultrasonic cleaning of a porous material*

Abstract

The aim of this publication is to investigate experimentally the fouling of a porous material by external particles and the optimal way to clean it by means of high-frequency acoustic waves. We are in particular interested in the fouling by mud particles of the near wellbore region of an oil reservoir. Therefore we used in the experiments a natural sandstone as porous material and mud particles as fouling particles. To generate fouling mud particles were flushed through a sandstone core. Next the core was treated with very short bursts of ultrasound and the change in permeability was measured after each burst. (Earlier publications report only the end result after applying the total amount of acoustic energy.) Experiments were carried out under different acoustic-cleaning conditions to investigate the influence of the relevant parameters on the cleaning process. For instance, the amplitude of the acoustic waves, the duration of the bursts and the time between the bursts were varied. During the ultrasonic cleaning process brine flowed through the core. The influence of this flow was studied by changing the flow rate. Also the influence on the cleaning process of the temperature, pressure and initial core permeability was investigated. The experimental results show that short bursts of acoustic energy are more efficient for cleaning than long bursts (for the same total amount of acoustic energy). The overall conclusion is, that the optimal way of ultrasonic cleaning is by applying many very short bursts of low amplitude and a short rest time between the bursts while keeping the liquid (brine) flow at a very low velocity. More acoustic energy is needed to clean a core with a high initial permeability than a core with a low one. At low pressure cavitation occurs and prevents the generation of ultrasonic bursts. Cavitation can even have a negative effect on the cleaning process.

7.1 Introduction

Permeability reduction of the near wellbore region is a major problem for the oil industry. It causes a reduction in the oil production rate and in the total amount of oil that can be withdrawn from an oil reservoir. To solve this problem a number of techniques have been developed, such as hydraulic fracturing and acid injection. These techniques have negative side effects: they are expensive, environmental unfriendly, require production shut off, etc. New techniques are being developed, see for instance Tambini (2003), and, among them, ultrasonic stimulation is a very promising one. Field tests to investigate the applicability of ultrasonic cleaning were carried out

*P. Poesio, A. Jurrij and G. Ooms. "Fouling by external particles and ultrasonic cleaning of a porous material". *Submitted to J. Petroleum Sci. & Eng.*, 2004.

in Russia during the eighties and showed contradictory results: an increase in permeability was reported in 50% of the cases, while in the other 50% no improvement, or even a deterioration, was observed, for an overview see Beresnev & Johnson (1994). No explanation for this fact is available and, therefore, we think that a more fundamental investigation of the technique is necessary. As it is often difficult to make a satisfactory interpretation of field tests, laboratory experiments are of crucial importance. The first laboratory studies concerning the application of ultrasound to clean a porous material were performed by Venkitaraman et al. (1995) and Roberts et al. (2000). They investigated the cleaning of porous materials that were damaged by different fouling mechanisms: fouling by very small particles (fines) that were released from the porous material due to the flow of brine through the material (internal fouling), and fouling by mud particles and/or polymers from the outside into the porous material (external fouling). Poesio & Ooms (2004) and Poesio et al. (2004) performed a detailed study on the acoustic removal of fines from a porous material. In the present publication we focus our attention on the removal particles due to external fouling. We will pay particular attention to the effect of short acoustic pulses in order to find an optimal way to use the acoustic energy. Moreover the influence of many relevant parameters are reported. In Sec. 7.2 we discuss the experimental set-up and experimental procedure taken throughout the investigation. The fouling process and the measurement results for the level of fouling and for the penetration depth are given in Sec. 7.3. Ultrasonic stimulation results are discussed in Sec. 7.4. Conclusion will be drawn in Sec. 7.5.

7.2 Experimental set-up and procedure

In this section, a description of the experimental set-up, procedures and material used is provided.

7.2.1 Experimental set-up

The set-up used is described in this section and a sketch is given in Fig. 7.1. A Berea sandstone core is placed in a rubber sleeve, surrounded by a basin filled with water, that is enclosed on the other side by a metal casing. Adjacent to the front of the core a chamber is filled with brine and functions as inlet or exit of the core. The back surface of the core is closed off by a basin and a plunger, that also has an opening for inlet or exit use. The flow through the tubes is provided by a pump and ten valves make it possible to flow in different directions along different paths. In addition there is also a connection to a CO_2 network, which makes it able to flush CO_2 through the pores of the rock. The part of the drawing in the box is a new part added to the set-up to create damage by external particles. This part is used to circulate the mud through the chamber, in front of the core surface.

As mentioned before a system of valves makes it possible to flow in two directions and use different inlets and exits. The two directions are called production and injection mode. Production is flowing from the plunger to the horn, in Fig. 7.1 from right to left, also called back flowing in this publication. It is the direction in which oil is 'produced'. The injection mode is the direction opposite to this and is the way to 'inject' a liquid, for example acid.

Coreholder

The coreholder contains, from inside to outside, the sandstone core, a rubber sleeve, a water basin and a metal casing. From front to back: a metal wall with an opening for the horn, a metal ring that creates a chamber, the core, a diffuser, a plunger with a connection for the accelerometer, and a metal lid. The important parts and their purpose are described here.

Berea sandstone core is used and a full description will be given in a coming section. The cylindrical core has a diameter of 7.62 *cm* and a length of 20 *cm*. Around the core a rubber sleeve is placed: it has four openings to perform temperature and pressure measurements on the rock. The purpose of the sleeve is to pressurize and to seal off the core, to prevent any liquid flow through outside routes. The pressure transducers, embedded in the sleeve, allow measuring the

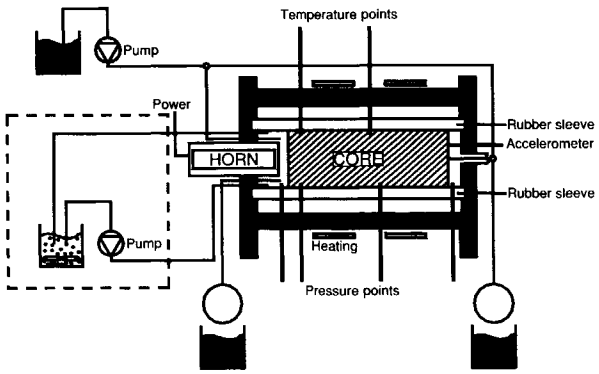

Figure 7.1: Set-up.

three pressure drops. There are two sleeves that can be used alternatively, the difference between them is the place of the first pressure point. The first pressure point has a distance of 1.04 *cm* from the front surface of the core in the first sleeve and a distance of 2.04 *cm* in the other. Apart from a few measurements, the first sleeve was always used, since it allows better accuracy on the permeability of the first part of the core. The second point is placed 11.46 *cm* further away in the first sleeve and 10.70 *cm* in the second one. These two points divide the core in three sections. The first section is 1.04 or 2.04 *cm* long. The short length makes it easy to detect particles that penetrate the rock. Section 2 is the middle part between the two pressure points. Section 3 is the back part of the core, behind the second pressure point. The water basin is put under pressure to press the sleeve against the rock. This confinement pressure is kept on 180 bars, which simulates the real well conditions as closely as possible. The casing encloses this whole system and assures a safe working environment for these extreme conditions of 180 bars and temperatures up to 80 ^oC. The diffuser/plunger combination creates easy access to the porous material for the liquid and serves as inlet/exit. The sides are closed off by the sleeve and it is pressed onto the core by the water behind it. In this way not only the exit of the rock is sealed off very well but good contact of the accelerometer is also ensured.

Ultrasonic equipment

The ultrasonic equipment consisted of:

- a converter, which converts electricity into mechanical vibrations of a piezo-electric element;
- an amplifier, which is used to set the amplitude of the vibrations;
- an ultrasonic horn, which concentrates the mechanical vibrations onto the front side of the core sample. Two acoustic horns were applied: a Branson Module PGA 220 (a 20 kHz horn with maximum power output of 2000 W) and a Branson Module PGA 470 (a 40 kHz horn with maximum power output of 700 W). The power output can be selected as a percentage of the maximum.

Temperature and pressure

One of the goals of this project is to look at the effect of temperature and pressure on the effectiveness of the ultrasound. For that reason, the sandstone core can be heated up to 150 ^oC by two metal bands around the casing. Heat exchangers, one in the front and one in the back to allow

flow in two directions, can preheat the liquid that is flown through the pores up to 80 ^{o}C. The temperature in the core is followed in two places and, moreover, the temperature of the liquid in the chamber and the liquid behind the back of the core are measured. The room temperature and the heating of the metal bands in two places in the liquid around the sleeve are also monitored. The pressure inside the core is set by the two exit pressure regulators. This pressure is called the pore pressure and varies during the experiments. The Leak-Off controls the outlet on the chamber side while the Production System puts pressure on the plunger side. The development of the pressure is followed by seven pressure transducers: three point measurements; one of the chamber, the back exit and the confinement pressure and four additional pressure difference measurements; the pressure drop over front and back of the chamber, the first part and second part of the core and over the total core. From these values the pressure drop over the third part is calculated.

7.2.2 Experimental procedure

The procedure consists of three parts: preparation of the core, creation of damages in the core (fouling of the core) and ultrasonic stimulation of the core.

Preparation of the core

The preparation of the core consists of removal of the air from the core, saturation and stabilization of the rock and it is rounded off by the measurement of the initial permeability. This permeability is used as a reference value, to express the amount of damage. The complete procedure is given in detail here. First, the core is flushed with CO_2 to get all the air out of the pores. The flow is, then, switched to brine (2% KCl in water). Brine is pre-filtered (by a 0.45 μm mesh filter) to remove dirt and avoid unwanted particles that may reduce the core permeability or, even, plug the tubing. The brine flow is kept for several hours; the set-up is then stabilized for one night to make sure that the rock is completely wet and fully saturated. Ultrasound is applied to remove fine particles that are attached to the pores. Poesio et al. (2004) showed that removal of clay particles attached to the wall can considerably increase the permeability. This pre-treatment is meant to remove those particles and to avoid an extra increase in permeability during the first acoustic treatment. A mixture of brine and 15% of HCl is flown to dissolve calcite and fines sensitive to it. Finally the core is fully saturated again with brine and the permeability measured. The permeability is determined by using different flow rates and two directions. The permeability (K) is prescribed by Darcy's equation:

$$\frac{\Delta p}{L} = -\frac{\mu Q}{KA}, \tag{7.1}$$

where Q is the imposed flow rate; A is the cross sectional area, Δp is the pressure drop measured over the core of length L. The pressure drop in all three sections of the core is measured at a fixed flow rate and that measurement is repeated for seven flow velocities while other conditions are kept constant. These measurements give a number for the permeability. To reach a higher accuracy a line is fitted through these permeabilities, to determine the final values.

Creation of formation damage

The creation of the fouling in the core with external particles consists of preparation and application of the mud particles, back-flowing of the rock to remove damage that is not permanent and it is round off by the measurement of the damage permeability. The difference between this permeability and the initial one is a measure for the amount of blocked pores. The process is described in more detail in the following. The mud is treated in an ultrasonic bath to detach particles that are sticking together and to keep them as small as possible. The mud is then put in the front vessel (see Fig. 7.1) and it is circulated in front of the core. It is sucked in by creating an under-pressure in the chamber. This procedure is very time consuming and lasts until no pressure drop changes are detected. A back flow (only brine) is applied in order to remove the particles from the tubes and to remove the loose particles. Permeability in the new condition is then measured; in the following we will refer to this permeability as damaged permeability.

Ultrasonic particle removal

In this part of the procedure the damaged core is stimulated by a treatment of short bursts of ultrasound. During and after each pulse, brine flows through the core and the pressure drop, induced by this flow, is measured. This pressure drop is used to monitor the response of the damage (fouling particles) to the ultrasonic treatment. The result is a cleaned core with a final permeability, that is compared to the initial one. The details will be discussed in a coming section. When the pressure drop does not change anymore due to the acoustic stimulation, the treatment is stopped and the burst by burst development of the permeability during the whole treatment is plotted. After this procedure the core is again damaged and cleaned with ultrasound. During the acoustic treatment the power used by the horn is measured. The objective is to determine the amount of supplied energy during the burst under the chosen conditions. The course in permeability development during the step by step particle-removal process is plotted for each set of conditions as a function of the cumulative energy needed for the creation of the ultrasonic waves. (Sometimes the course of the permeability development during the removal process is given as a function of the number of bursts.) Before fouling the core again for the next experiment a mixture of brine and 15% HCl is flown to dissolve $CaCO_3$ particles that may still be present in the rock. The flow of acid mixture is switched to brine and the permeability compared with the initial one. If the last value is different by more than 2% from the initial one, the core is replaced by a new one. More details on this acid treatment can be found in Jurrij (2003).

7.2.3 Material

Berea sandstone

The porous material is Berea sandstone with a permeability of 100 or 300 mD. It is a clay bearing and water sensitive rock, with a porosity of around 20% and it is representative for most oil containing formations. Illite, mica, kaolinite and chlorite are the types of clay present. The main constituent of the matrix is quartz, as can be seen in Tab. 7.1. The most important properties are given in Tab. 7.2. The pore size distribution can be compared with the size of the particles (described in the next section) to see which percentage of the throats would allow the particles to pass through.

Berea	300 mD
illite/mica	2%
kaolinite	2%
chlorite	3%
quartz	89%
feldspar	2%
ankerite	1%

Table 7.1: Composition of Berea sandstone.

Berea	100 mD
porosity	18.4%
tortuosity	2.9
fluid permeability	130 mD
grain density	2.66 $\frac{kg}{m^3}$

Berea	300 mD
porosity	19.8%
tortuosity	2.9
fluid permeability	295 mD
grain density	2.66 $\frac{kg}{m^3}$

Table 7.2: Properties of Berea sandstone.

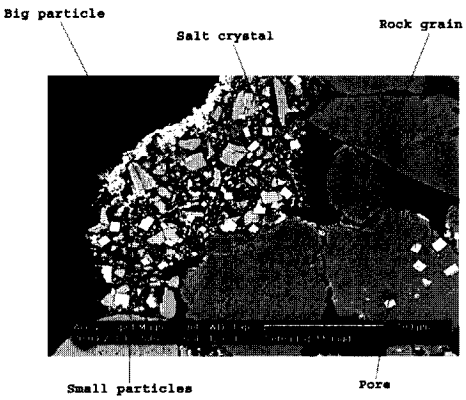

Figure 7.2: SEM-picture of a filter cake of Baracarb particles on Berea sandstone. The different components are indicated in the figure.

Particle properties

The particles that are flushed in from the outside to create damage are made of $CaCO_3$. This material is obtained by grinding marble or limestone. It is composed of two crystal forms, with the same chemical composition, Calcite and Aragonite. The density is 2900 kg/m^3. The brand name is Baracarb and attached to the name is a number that indicates the size of the particles in μm. The numbers are for example 2, 5 or 25. They point out the upper limit for the particle size. There are two reasons to use this material for the generation of damage:

- Baracarb is often used in drilling fluids. The Baracarb particles are the 'bricks' in the mud. In Fig. 7.2 a large bridge of Baracarb particles can be seen. In this SEM photo the shape of the $CaCO_3$ pieces can be seen quite clearly. They are obviously not spheres. In this case two different sizes of particles are being used, a large and a small size. The white squares are salt crystals, remains of the salty water, called brine, that has been pumped through the core.

- Baracarb particles are solvable in hydrochloric acid (HCl). That is a desirable property because it allows repeated use of one core of porous material. In between the successive experiments, the rock can be cleaned by using this acid.

To check whether the nominal size gives the right dimension for the particles, the size of the particles was measured in a solution (fluid with particles) with an optical particle sizer (Malvern). The measurement was done without ultrasonic agitation to have a situation as close as possible to the fouling experiments. It could be concluded that there were many particles with a size larger than the 2 μm. The range that has the highest probability was between 3 μm and 7 μm. These results were quite different from the expected size of 2 μm. A possible reason could be, that those colloidal particles tend to agglomerate in bigger flocks. This particle size information was compared with the pore size distribution of the core to estimate to which extent the particles were able to penetrate into the pores of the sandstone: 80% of the particles were smaller then 7 μm while 80% of the pore throats were larger than that same size. So the largest part of the particles could flow through most of the pores. From that information the conclusion could be drawn that this size of Baracarb was fit to create damage in the core. However, one should be aware that a

substantial amount of particles were relatively large. They could form a layer on the outer surface of the core and in that way close off the inlet for the other particles.

7.2.4 Parameters and objectives

The core was cleaned in different ways and under different conditions to compare the cleaning effect of the ultrasound for these different circumstances. The amplitude of the waves, the duration of the bursts and the time between the bursts was varied to find an optimal way of sound application, see Tab. 7.3. During the application of ultrasound, brine flowed through the core. The influence of this flow was established by changing its flow rate. The objectives are given in Tab. 7.4. The burst

APPLICATION OF SOUND	OBJECTIVES
burst time	Experience indicated that short pulses are most effective; test very short bursts; 0.4 sec - 3.6 sec
amplitude	Changing the amplitude of the waves changes the force on the particles; adjusted by 50, 75 or 100% of the max amplitude
rest time	Checking the removal effect of back flowing in comparison with removal during burst time (in combination with back flowing)

Table 7.3: Parameters for sound application.

time is the time during which the core was irradiated with ultrasound. The rest time is the time in between two successive bursts. That time can be important to cool down the liquid near the horn because dissipation of the ultrasonic energy raises the temperature. However such short pulses were used during these experiments, that this effect was negligible. In other experiments, different

BRINE FLOW	OBJECTIVES
flow rate	Back flowing during removal: for removal of particles deposited on pore walls acoustic waves and flow work together; for breaking of particle bridges in pore throats the flow opposes the acoustic wave action. Flows with a higher velocity can remove smaller particles from the walls and have a higher cleaning rate, but can cause formation of new bridges; 10 ml/min - 50 ml/min
no flow during burst	Venkitaraman et al. (1995) claim that sonic treatment under static conditions accompanied by subsequent back flowing gave good results

Table 7.4: Parameters for flow during acoustic treatment.

temperatures, pressures and permeabilities were used to come to a better understanding of the particles removal process. Their values and their possible influence are listed in Tab. 7.5. More information and the references can be found in the respective sections on experimental results.

OTHER	OBJECTIVES
temperature	Look into the influence of temperature on the removal effect. Temperature influences drag and bonding forces and transmission of sound; $30°C$ - $80\ °C$
pressure	Detect cavitation and measure its contribution to removal. Pressure has a slight influence on bonding forces but a clear effect on transmission of sound; 30 bars - 100 bars
permeability	The initial permeability and the amount of damage influence the transmission. Check if the amount of damage changes the course of the removal; 100 mD - 300 mD

Table 7.5: Other parameters.

7.3 Fouling induced by mud particles

In this section we analyze the procedure used to generate fouling by external particles. In a real mud polymer additives are present next to the particles. However, we wanted to investigate first the effect of ultrasound on particles alone. (In a next study a mixture of particles and polymer additives may be investigated.) We will discuss some experiments discussed in the literature, that are comparable to our experiments. Thereafter we present our own results.

7.3.1 Creating damage with external particles

During the experiments it was found that it is not easy to make particles penetrate deep into the formation. Drilling mud particle invasion into the wellbore formation has been investigated for years. An early study has shown that bridging of pores by particles is required to initiate external filter cake formation, which is a dense layer of particles on the outside of the rock. The same study also showed that an internal cake, which is a damaged area inside the rock, may also be formed inside the rock and that the invasion depth is around 2 cm, see Glenn & Slusser (1957). Researchers have looked into the main factors that determine formation damage due to particle and polymer invasion. These factors are: particle size distribution, permeability and pore size distribution, concentration of mud solids, over-balance pressure and mud circulation rate and rheology (Suri & Sharma 2001). Scientists have done investigations on all these different subjects. The problem with most of these investigations, concerning their application in this project, lies in the fact that always a combination of sized particles, drill solids and polymers was used. The few experiments that are comparable with our investigation (no use of polymer additives) are reviewed.

Jiao & Sharma (1992) tested a mud without polymers, 4% Bentonite/ 2% NaCl, on a 100 mD Berea sandstone core. The average particle size of the Bentonite suspension was much smaller than the Baracarb2, used in our experiments. Their results for the damaged permeabilities are given in Fig. 7.3. The injection direction of the mud was from section 1 to section 3 and back flowing, to clean again, had been done the other way around. The penetration depth that was realized in this way is very promising. Unfortunately, these desirable results cannot be reproduced in our set-up since they used a pump system that delivered a flow rate that was far to high for our pumps (10 times higher). That system was also able to circulate a much higher concentration of solids around 4%, compared to the 0.1% that our pump could handle.

Vetter, Kandarpa, Stratton & Veith (1987) focused on the use of particles smaller than 7 μm. They injected chrome oxide particles of 0.05, 1 or 7 μm and followed the developments in pressure drop during that flow. They gave some interesting results but the main drawback is that they

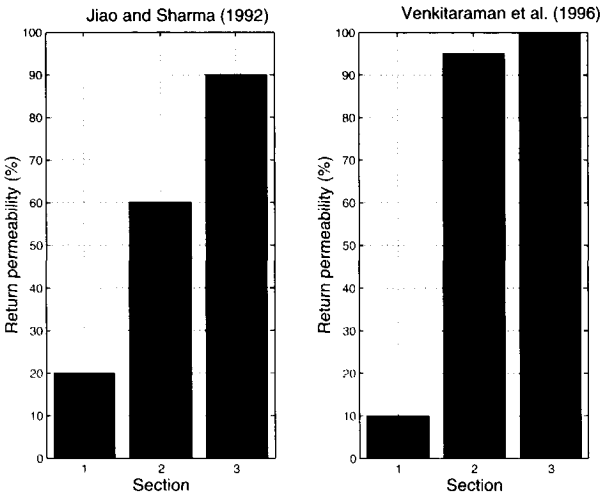

Figure 7.3: Permeability after injection of Bentonite particles in three different sections of the core. On the left the results by Jiao & Sharma (1992) are shown, on the right the results by Venkitaraman et al. (1995).

did not use back flow to remove the weakly bonded particles. So all their values hold for the situation directly after inducing the damage. This means that particles that bridged on the front of the core had not been removed at all. So Vetter et al. (1987)'s results hold for situations where a large external cake is present on the surface of the rock. The aim of our investigation was to look at damage that can withstand cleaning with back flow: the core was rinsed with brine until no particles were removed anymore. We monitored this phase by looking at the variation of the pressure drop across the first section of the core. Nevertheless, some general conclusions can be drawn from the experiments of Vetter et al. (1987). To begin with the fact that in a 100 mD core, particles of $1\mu m$ penetrate but the 7 μm cause filter cake build-up. Second, lower injection rates seem to damage the core more rapidly (as a function of injected pore volumes). They measured that the depth of their 1 μm particles was 2.2 cm. For the 1 μm particles a low concentration gave the best results and that concentration had a value of 0.025%.

Venkitaraman et al. (1995) did one test with Berea sandstone and a suspension of 4% Bentonite/ 2% NaCl. The materials were the same ones as used by Jiao & Sharma (1992) and they also used the same circulation time and overbalance pressure. Nevertheless these results were different and are, therefore, given in Fig. 7.3. It is worthy to note that the sections of the cores used by Venkitaraman et al. were much longer than in the experiments done by Jiao & Sharma (1992). The deviation from the results found by Jiao and Sharma can originate from a different circulation flow rate or a different initial permeability.

The conclusion is that the literature gives some useful information for inducing fouling with external particles but no real procedures for the use of a low concentration of $CaCO_3$. The outcomes of other experiments have to be adapted to values used in the current situation. The main factors that influence the damage formation are summarized here. First there is an interaction between concentration and overbalance pressure. Since the 4% concentration used in the successful experiments mentioned above is too much for the pump in our set-up, the problem is to set a value for the pressure drop over the core to suck in particles at a concentration of 0.1%. This overbalance pressure determines the flow rate of the particle suspension through the core and as mentioned above it's important to keep that rate low to avoid formation of an external filter cake. If the

particles are dragged toward the openings of the rock too fast, they are able to form bridges. On the other hand, that flow rate also determines the time that is needed to induce an amount of damage. So we want to keep it as high as feasible. Based on trial and error procedure, the circulation rate in the chamber is set at a maximum of 200 ml/min to ensure good operation of the pump.

The two main material factors are particle size distribution and pore size distribution. These two are restrained by the purpose of this research project: to look at a situation that occurs during oil exploration. Baracarb, $CaCO_3$ is the particle material, instead of Bentonite used in most experiments done by other people. Bentonite is a swelling clay and therefore used as a viscosifier in the mud. When the Bentonite particles have not been in contact with fresh water, they have a much smaller size than Baracarb2. The actual size of the Bentonite is not given in any of the papers, in which it is used to induce damage. For our experiments sandstone cores were available with two different permeabilities and the smallest size Baracarb, which is number 2 (see Sect. 7.2.3).

7.3.2 Experimental results of damage procedure

The procedure that was used to create the formation damage was already described in Sec. 7.2.2. As mentioned mud could be circulated in the chamber in front of the core. Due to the pressure drop over the core the mud in the chamber was slowly sucked into the rock and particles settled in the pores of the rock. During the damage experiments the first pressure point was situated at a distance of 1.04 centimeter from the surface adjacent to the chamber. This made possible to measure changes inside the core, like penetration of the particles, already after 1 centimeter. The first pressure drop was measured from a point in the chamber near the front surface to the first pressure point. This measurement included the pressure drop over the external filter cake. This made it impossible to use this pressure drop as an indication for the amount of damage in the core during injection of the mud. To be able to control the damage process it would be necessary to see a change in permeability in the second part of the core. This would require a substantial penetration beyond 1 cm in the core which was not realized in our experiments.

The concentration of the solids was varied from 0.01% to 0.1%. Higher concentrations were not possible because the pump could not handle a large amount of solids. The time that was needed to damage the core with the very low concentrations was very high and it did not visibly increase the depth of the damage. The pressure difference over the core, the over-balance pressure, was first kept at values around 4 bars. On one hand the formation of an external layer on the surface had to be prevented, while on the other hand the flow through the core had to be high enough to limit the amount of time that was needed for significant fouling. This overbalance pressure in combination with a circulation flow rate of 180 $\frac{ml}{min}$ induced a flow through the core with a velocity of 0.5 $\frac{mm}{s}$. After a few hours the overbalance pressure was slowly increased to 10 bars to make an attempt to drag in more particles.

Back flowing during the fouling process (to remove the external cake) or intermediate flushing of the chamber with brine (to remove the particles that may have deposited in the chamber) did not create any effect on the return permeability. After dragging in the particles for 5 hours, the core was flushed with brine, from the back of the core to the chamber. This was done to detach the particles that were not stuck on the surface or inside the rock. The core was rinsed at the highest velocity (3 $\frac{mm}{s}$) to remove the external cake as good as possible. In real practice the back flow velocity would only reach a value of 0.5 $\frac{mm}{s}$ and in that case less particles are removed by back flowing. This flow rate was used during the damage procedure in one of the experiments to check the difference in removal when this part of the particles was left in or on the core, see Sec. 7.4.8.

Observations during the experiments on a 100 mD core showed that it was not possible to reach the first pressure point with the particles. They were probably filtered out by the external cake and narrow pore throats in the first millimeter of the core. The penetration depth of the $CaCO_3$ was deduced from spectra that have been obtained by SEM analysis of different areas (at different depths) of the core. The results of the analysis of the penetration depth for the 100 mD

core after back-flowing with brine are given in Fig. 7.4 and 7.5. Figure 7.4 gives the amount of different chemical elements for comparison. In the second Fig. 7.5 the results for Calcium are given separately. The distances were measured from the front surface of the core. The Carbon was

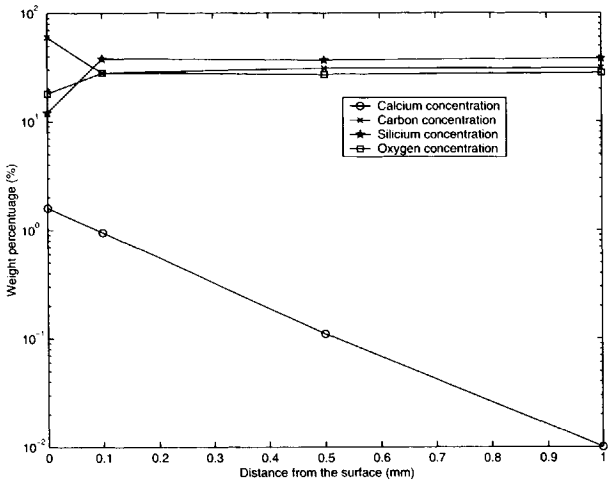

Figure 7.4: Concentration of chemical elements as function of the position inside a 100 mD core of Berea sandstone after $CaCO_3$ has been flown in. The concentrations are deducted from the spectrum measured by SEM.

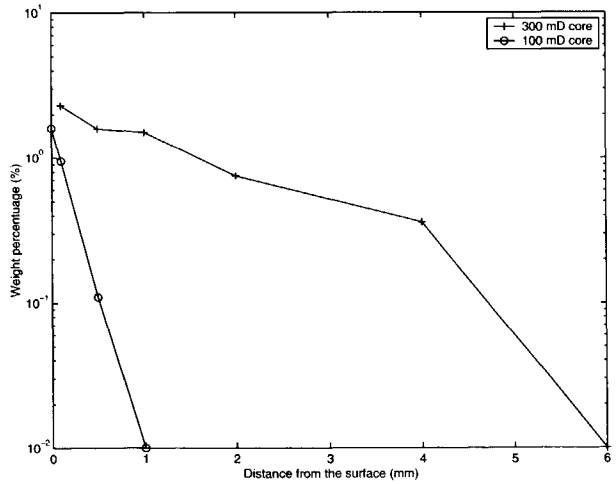

Figure 7.5: Concentration of Ca as function of the position inside a 100 mD and 300 mD core of Berea sandstone. The concentrations are deducted from the spectrum measured by SEM.

added in a part of the preparation process of the sample to increase the contrast in the material. The amount was so high on the surface because it was mostly present in void spaces and because

the front surface was very frayed which made it difficult to define the surface exactly. Silicon and Oxygen are elements of the solid matrix of the rock. There was no measurable amount of Calcium in Berea sandstone that was treated with hydrochloric-acid so this element was used to detect the damage material ($CaCO_3$). It is quite clear that the penetration was not very deep and that the amount was small. Nevertheless, the permeability dropped with 50% in the first section so even this small invasion can have an enormous effect. For that reason it is very important to investigate how ultrasound can remove this influential form of damage.

The amount and depth of Calcium in a 300 mD core is given in Fig. 7.5. The permeability of the first section was in this case less than 10% of the original permeability. This result comes closer to the measurements done by other people, mentioned in Sec. 7.3.1. The penetration in this core was much deeper since particles penetrated deeper because of the higher permeability, caused by larger pores. More research would be necessary to understand the details of the depth of the damage, but this is beyond the aim of this publication. The aim of this investigation is to look at ultrasonic removal of particle damage and for doing that an indication of the penetration depth is sufficient. The indication is a few millimeters.

Figure 7.6 is a SEM picture of the damage inside the core. The particles seem to be present more in bridge formations than in depositions on pore walls. Although both fouling mechanisms are visible. A distinction can be made between particles stuck in a particle bridge and particles that are deposited on a pore wall by using their different response to an increase in flow velocity. Deposited particles can be released because an increase in flow raises the drag on the particles, resulting in an increase of the permeability. The opposite is true for bridges. The enhancement of the flow makes new bridges or makes them stronger because the drag force pushes the particles together. Poesio and Ooms (2004) have shown that when the clays inside a sandstone are swollen, the fouling mechanisms is mainly based on formation of bridges. When they increased the flow rate, the permeability of the core dropped. The opposite occurred in the present experiments with fouling due to external particles. However, the effect was very small. The conclusion is that fouling of Berea sandstone cores by external particles in a reproducible way was more difficult than expected. However, after some testing a successful procedure was found. The permeability of the cores after fouling was always around 50% of the initial permeability. That amount of damage was extensive enough to perform and compare experiments with ultrasonic cleaning.

7.4 Experimental results of ultrasonic cleaning

In this chapter the results of the experiments on ultrasonic cleaning are presented. This section introduces the results generated during the treatment process and explains the numbers displayed in the graphs. This is followed by presenting the outcomes of the experiments on particle-damage removal under different conditions and for different ways of sound application. The results concerning the influence of the parameters are presented one by one.

7.4.1 Presentation of the results

The procedure for the ultrasonic fouling removal is already presented in Sec. 7.2.2. The core was stimulated in different ways and under different conditions to investigate the influence on the cleaning effect of ultrasound. The parameters were varied one by one in the experiments described here. To compare the effectiveness of the fouling removal the improvement in permeability was calculated after each burst. Darcy's law was used to calculate the permeability from the pressure drop induced by the flow of brine. The permeability at the end of the rest time was calculated to determine the improvement generated by the burst. The way it is presented here is by using the relative permeability:

$$K_{relative} = \frac{K}{K_0}, \tag{7.2}$$

where K_0 is the original permeability of the core (that is the permeability before the core was fouled). Only the removal in the first section of the cores is shown because of the limited pene-

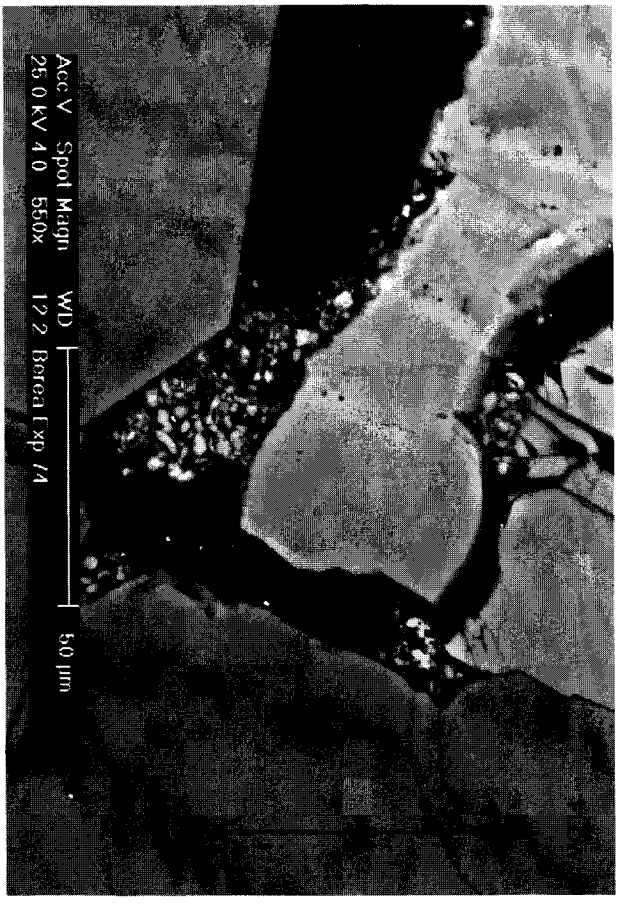

Figure 7.6: SEM picture of particle damage inside the sandstone (2 *mm* deep). The direction of the flow is indicated.

tration of particles into the core. The horn needed a certain amount of power to produce a burst. The acoustic power shown in the plots is defined as the electrical power times the horn efficiency. The efficiency is, however, not a constant value and depends on other parameters such as temperature. The acoustic power is set beforehand and the electrical power that needs to be provided to guarantee it is measured. The system stops automatically if it is not able to provide the acoustic power that has been set or if the working conditions are not safe (for instance overheating). So the graphs give the relative permeability (after each burst) as a function of the cumulative energy input. Often graphs that give the relative permeability as function of burst number will also be given. For example in Fig. 7.9, each point represents the new situation after a burst. The new situation is the relative permeability that is reached after the burst and the cumulative acoustic energy that was supplied so far.

7.4.2 Response to first burst

Before showing the experimental results the effect of the first application of sound (the first burst) is treated in more detail. The first burst generated contradictory responses with respect to the permeability. Sometimes a decline in permeability was induced, while other times a large increase was caused by the first burst. This may be the reason that field-tests with ultrasonic tools reported sometimes a deterioration in the permeability, as reported by Beresnev and Johnson (1994). The distribution of the response to the first burst in all the experiments that were carried out during this project is given in Fig. 7.7. In 15% of the cases there was a noticeable drop in permeability

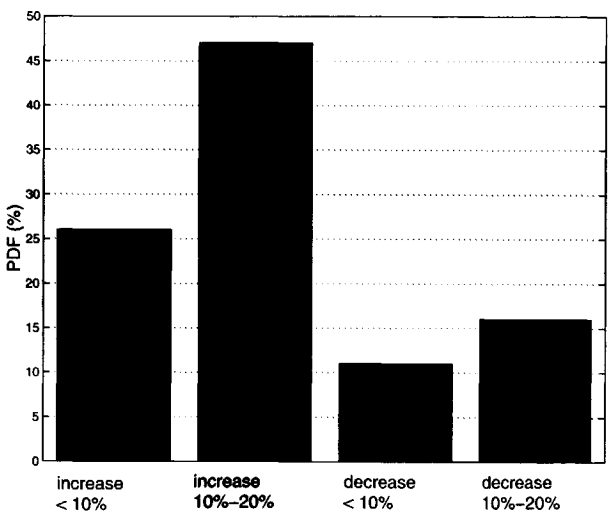

Figure 7.7: Statistics of the permeability response to the first acoustic burst. This statistics is based on 76 different experiments.

after applying one burst, while in 45% of the experiments there was a considerable improvement. It did not become clear during this investigation what the reason is for this phenomenon. A reason can be that the high concentration of released particles, induced by the first burst, creates the opportunity for the formation of new particle bridges. Those bridges decrease the permeability. We found that a certain burst time is necessary in order to avoid permeability decrease after the first burst. For a burst-time of 3.6 s no deterioration associated with the first burst application was found; so the negative part in Fig. 7.7 is mainly associated with 0.4 s and 1.2 s pulses. Poesio & Ooms (2004) did not report a negative first-burst effect for a burst time of 5 s. Also

Venkitaraman et al. and Roberts et al. did not report any first-burst deterioration effect during their experiments.

7.4.3 Influence of burst time

During the experiments it became clear, that very short pulses of acoustic energy are most efficient in removing particle fouling in sandstone. For that reason the duration of the bursts was changed and its effect studied. Burst times of 0.4, 1.2 and 3.6 seconds were used. In Figs. 7.8 and 7.9 experiments with short and long bursts are compared. The response to the first burst is

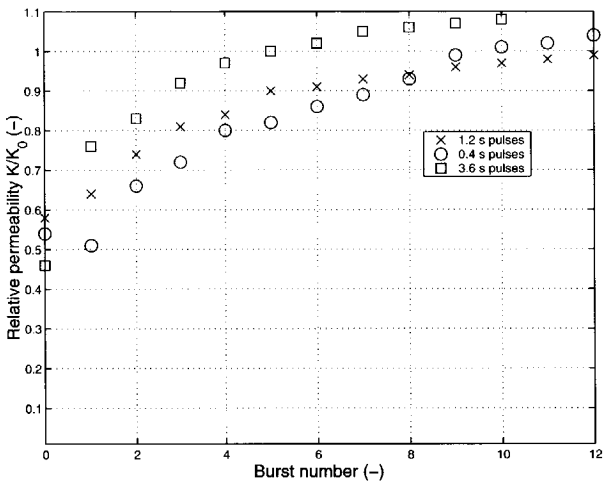

Figure 7.8: Influence of burst time on the relative permeability as function of the burst number (*355 mD, 100% input power, 50 ml/min*).

different in the three experiments (one case is shown with a permeability decrease after the first burst). As far as the number of bursts is concerned, the effectiveness of short and long bursts is more or less the same. However the total amount of energy that is needed to achieve the same result, is significantly less for the short burst time. When the permeability during acoustic cleaning approaches the initial permeability, it seems to be easier for the long bursts to remove the particles that are left. The increase from 80% to 99% demands nine bursts of 0.4 seconds, five of 1.2 seconds and only three when the 3.6 seconds are used. Obviously, when looking at the amount of supplied energy the short bursts are still preferable.

7.4.4 Influence of acoustic wave amplitude

Changing the acoustic input power (the acoustic wave amplitude) changes the force on the fouling particles. Better-connected particles or deeper-penetrated particles can be removed when the amplitude is larger. In our experiments acoustic waves with two different amplitudes were used. Figure 7.10 gives the course of the ultrasonic removal for the two experiments as a function of cumulative energy and Fig. 7.11 as a function of burst number. The course of the cleaning process as function of the number of bursts is more or less the same for the two cases. Apparently the low amplitude waves are already strong enough to move the particles so much that they are flushed out of the core. (In a situation where the fouling penetrates deeper into the sandstone and hence further away from the ultrasonic source, the wave amplitude will probably have a larger impact.)

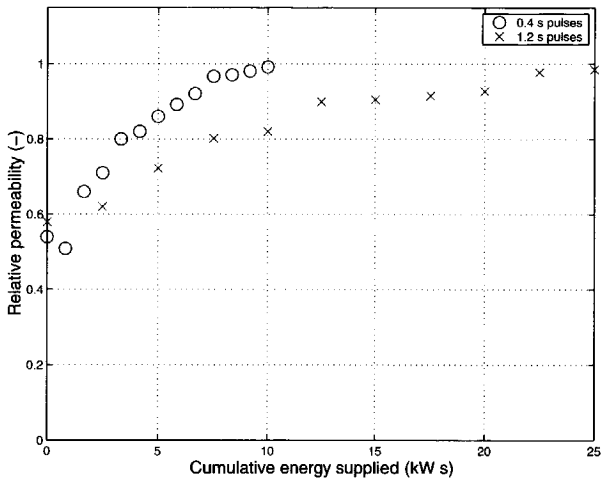

Figure 7.9: Influence of burst time on the relative permeability as function of the cumulative energy supplied (*355 mD, 100% input power, 50 ml/min*).

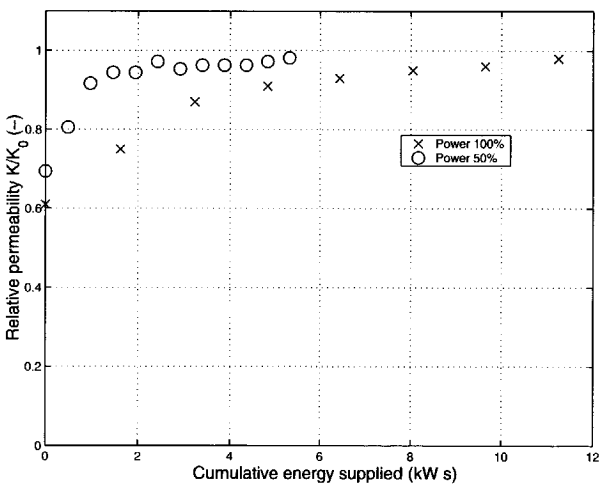

Figure 7.10: Influence of acoustic wave amplitude on the relative permeability as function of the cumulative energy supplied (*110 mD, 1.2 s sonification time, 10 ml/min*).

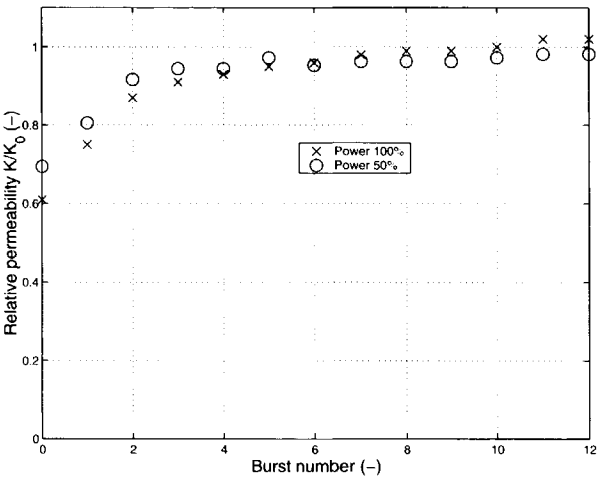

Figure 7.11: Influence of acoustic wave amplitude on the relative permeability as function of the burst number (*110 mD, 1.2 s sonification time, 10 ml/min*).

The conclusion is, that bursts with different amplitude are equally effective but the amount of energy needed is considerably smaller.

7.4.5 Influence of rest time

After the application of an ultrasonic burst brine was pumped through the pores for a certain amount of time (the rest time). We studied the influence of the rest time to find out whether the removal of the fouling particles takes place during the application of the ultrasonic burst or during the flow thereafter. We found that the permeability did not depend on the rest time between the bursts. The permeability increase seems to take place immediately at the start of the ultrasonic burst. It is an instant effect. To check this result also an acoustic treatment with zero rest time was executed, to see whether the total absence of an intermediate flow had an influence on the cleaning result. To that purpose the core was treated seven times with a group of three consecutive bursts of 0.4 seconds each. After a group of three bursts the core was back flowed to remove the detached particles and to measure the pressure drop. The result of this experiment was compared with the result of a 'normal' one with two minutes in between the bursts. Both results are plotted in Fig. 7.12. There is absolutely no difference between the two cases. So the conclusion is, that the rest time does not influence the amount of removed fouling particles. The permeability improvement takes place during the ultrasonic burst application and not during back flowing.

7.4.6 Influence of flow

As mentioned during the application of ultrasound the core was flushed with brine. This flow can influence the removal process in two ways. First it transports the particles that have been detached. From that point of view a high flow rate is preferable. Secondly a high flow rate can be responsible for the formation of new particle bridges and have a negative effect on the permeability. Calculations show that the fluctuating liquid velocity in the porous material due to the acoustic oscillations is considerably larger than the constant velocity due to the brine flow. So, from that point of view, it cannot be expected that the velocity of the brine flow has a significant influence on the cleaning process. However, Barake's experiments on damage induced by swelling clays clearly

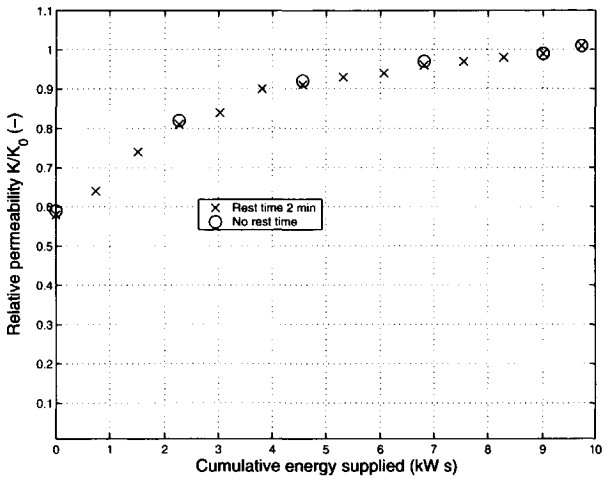

Figure 7.12: Influence of rest time on the relative permeability (*350 mD, 0.4 s sonification time, 50 ml/min*).

showed that the permeability increase due to ultrasonic cleaning is considerably larger when a very low brine flow rate was applied (Barake 2000). To investigate the influence of the flow rate we carried out some experiments under different flow conditions. Below we discuss the results of experiments with a continuous flow rate and without flow.

Flow during and after the application of ultrasound

The results for a back flow rate of 10 *ml/min* and 50 *ml/min* during and after the application of ultrasound are given in Fig. 7.13. For the case with a flow rate of 50 *ml/min* the first burst had a negative effect on the permeability. This response makes it difficult to compare the results for the two flow rates. For that reason the results are also shown without considering the first burst in the 50 *ml/min* case in Fig. 7.14. The last figure shows that the development of the permeability is roughly the same for both cases.

No flow during the application of ultrasound with flow thereafter

The extreme situation in which there is no brine flow during the acoustic treatment was also studied experimentally. Venkitaraman et al. (1995) claims that acoustic cleaning under static conditions accompanied by subsequent back flowing gave good results. During our experiments the flow of brine was stopped 20 seconds before the burst and recommenced directly after the burst with a flow rate of 50 *ml/min*. In Fig. 7.15 the results from this experiment without a flow during acoustic treatment is compared with the experiment with a flow rate of 50 *ml/min* during the treatment. It can be concluded that the acoustic treatment effect is about the same for the two cases, although the final permeability is a bit larger for the case without a flow during acoustic stimulation.

No flow during and after the application of ultrasound

The experiments carried out to study the effect of a brine flow during treatment and the effect of rest time indicated that it is not necessary to have a brine flow during treatment and that also the rest time between bursts has not much influence on the permeability improvement. To further

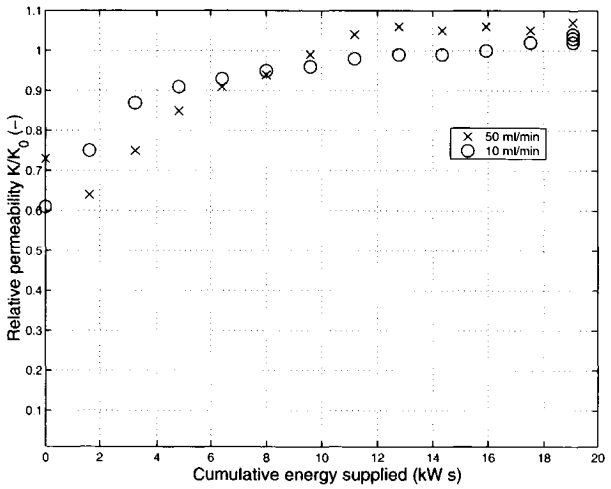

Figure 7.13: Influence of flow rate on the relative permeability as function of the cumulative energy supplied for two different flow rates (*100 mD core, 1.2 s sonification time, 100% power input, with first burst response*).

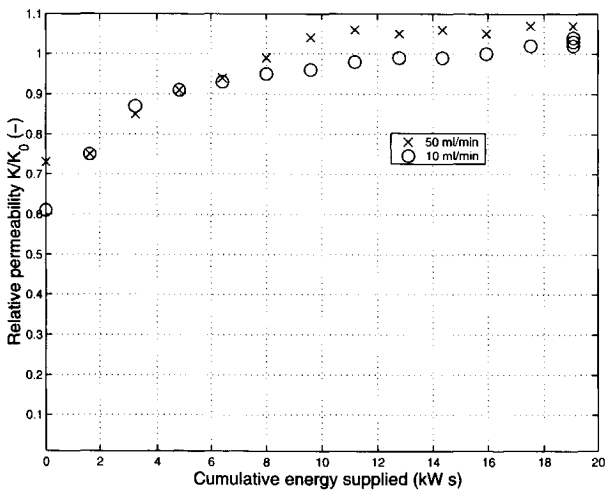

Figure 7.14: Influence of flow rate on the relative permeability as function of the cumulative energy supplied for two different flow rates (*100 mD core, 1.2 s sonification time, 100% power input, without first burst response*).

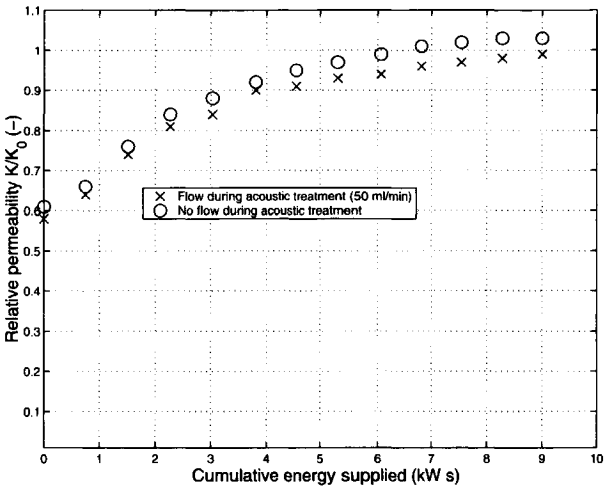

Figure 7.15: Influence of absence of flow rate on the relative permeability as function of the cumulative energy (*100 mD core, 1.2 s sonification time, 100% power input, without first burst response*).

investigate this remarkable result a core was ultrasonically treated without brine flow and with a rest time thereafter of one hour without flow. After the rest time of one hour a brine flow was started. From a practical point of view the advantage of such a treatment is that it would allow to close the well, treat it with ultrasound and make it ready for production again before the flow is started. From a scientific point of view it could give some information on the mechanism behind the damage removal.

To stimulate the core it was treated with 18 bursts of 0.4 sec in a few minutes. As mentioned during the application of the ultrasound and one hour thereafter there was no brine flow through the core. After that period the core was rinsed with brine at a rate of 50 ml/min. The course of the relative permeability during this process is given in Fig. 7.16. The arrow indicates the short period, during which ultrasonic stimulation took place. The figure shows that the improvement in permeability immediately after the flow is started, is around 20% of the initial permeability. The improvement during the subsequent back flow is an additional 10% of the initial permeability. The core needs to be cleaned for 40 minutes to reach the final permeability. That is much longer than for the experiments with a short rest time. This final permeability is almost 80% of the initial permeability. This is likely due to the fact that a part of the fouling particles gets stuck in the pores again when they are not flushed out of the core directly after stimulation.

7.4.7 Influence of temperature

The temperature has an influence on different aspects of the ultrasonic removal process. In an oil reservoir the temperature reaches values of $200°C$. To determine what the influence is of such a large temperature increase on the removal process, an experiment was done at $80°C$. It is known that the temperature has a large influence on the colloidal forces acting between particles and between particles and pore walls. Because the viscosity decreases with increasing temperature also the drag force on the particle decreases. On the other hand an increase in temperature, and therefore a decrease of the liquid viscosity, will decrease the acoustic wave attenuation in the porous material. To find out the result of these different influences experiments were performed at two temperatures. The data, retrieved from the experiments at $30°C$ and at $80°C$, are shown

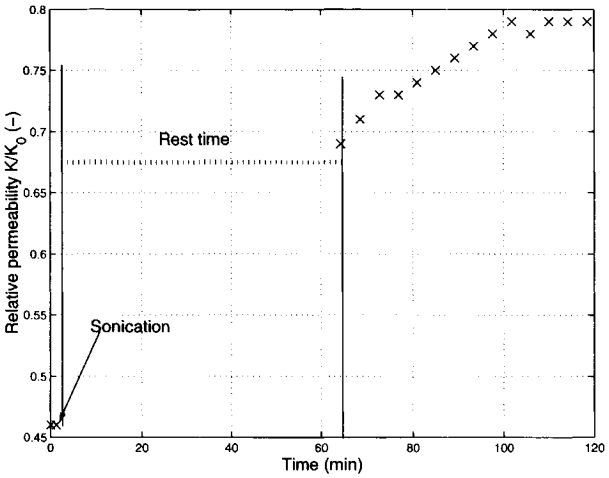

Figure 7.16: Effect of absence of flow during and after acoustic treatment as function of time. The arrow indicates the acoustic stimulation (*355 mD, 0.4 s sonification time, 100% power input*).

in Fig. 7.17. It can be seen that the rate of permeability improvement is the same for the two

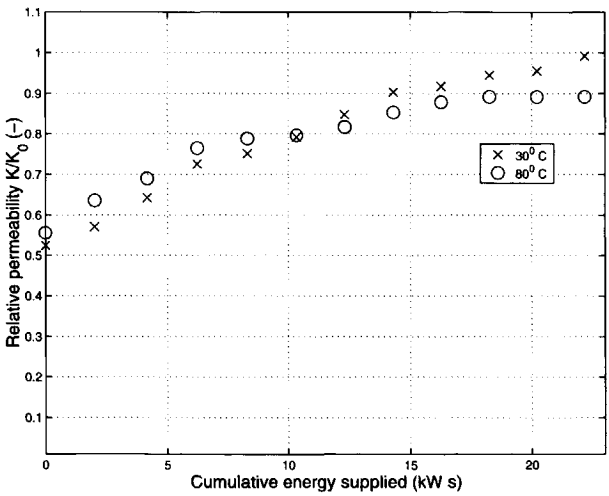

Figure 7.17: Influence of temperature on the relative permeability as function of the total energy supplied (*370 mD core, 1.2 s sonification time, 100% power input, 50 ml/min, 2 min rest time*).

temperatures when the amount of applied acoustic energy is taken as a reference. However, the acoustic horn needs less electrical energy to create acoustic waves of a certain amplitude at $80°C$. The reason is, that at this temperature the viscosity of the liquid, present in the chamber, is two times lower than at the lower temperature. This makes it easier for the oscillating part of the horn to move the adjacent liquid and therefore less electrical power is needed.

7.4.8 Influence of initial permeability and damage

The initial permeability (before damage) and the amount of damage influence the attenuation (inside the core) and reflection (at the core surface) of the acoustic waves, and hence also the acoustic cleaning efficiency. The wave attenuation in the sandstone increases with increasing permeability. Calculations with a model for the reflection of waves, made by Wu et al., predict a higher reflection for a larger permeability core (Wu et al. 1990). We have performed experiments to investigate the influence of the initial permeability and of the level of fouling on the acoustic cleaning efficiency.

Influence of initial permeability

First, the influence of initial permeability was investigated. We used two cores: one core with an initial permeability of 110 mD, the other one with 355 mD. In Fig. 7.18 the ultrasonic cleaning efficiency for these two cores are compared. This comparison between the two cases is difficult

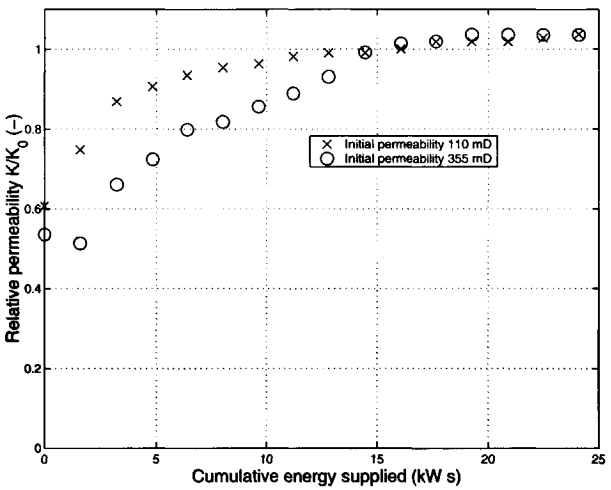

Figure 7.18: Influence of initial permeability on the relative permeability as function of the total energy supplied (*1.2 s acoustic treatment time, 100% input power, 2 min rest time, 50 ml/min, with first burst*).

since the response to the first burst is very different (discussed earlier). Therefore we used the Fig. 7.19 in which the first burst is not taken into account. As can be seen there is no large difference between the two cases in terms of cleaning efficiency as function of cumulative acoustic power. The reason is very likely the fact, that the penetration of fouling particles is not very large for both cases and so acoustic wave attenuation does not play an important role. (Nevertheless, a larger input of electrical power into the horn is needed for the high-permeability core. This is due to the stronger reflection of the waves at the front surface of the core in the 300 mD case.)

Influence of permeability after fouling

The influence of the permeability after fouling on the cleaning efficiency was also investigated. Cores with two different levels of fouling were achieved by applying different back flow velocities after the fouling process. Thereafter these cores were cleaned acoustically. The results are given in Fig. 7.20. As can be seen for the case with the lowest permeability after fouling the effect of the first three bursts is a 20% increase in permeability after each burst. For the other case the second

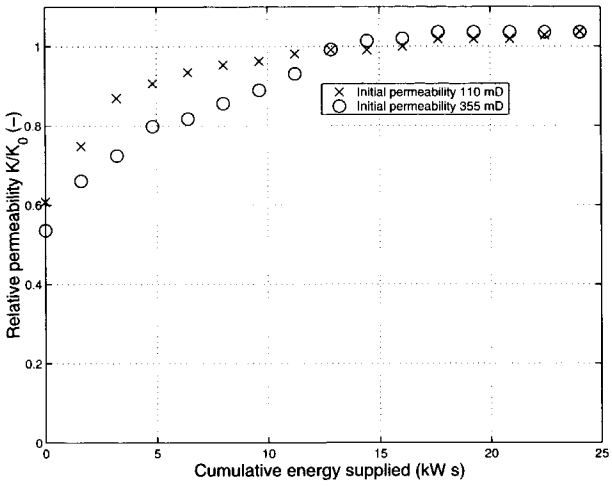

Figure 7.19: Influence of initial permeability on the relative permeability as function of the total energy supplied (*1.2 s acoustic treatment time, 100% input power, 2 min rest time, 50 ml/min, without first burst*).

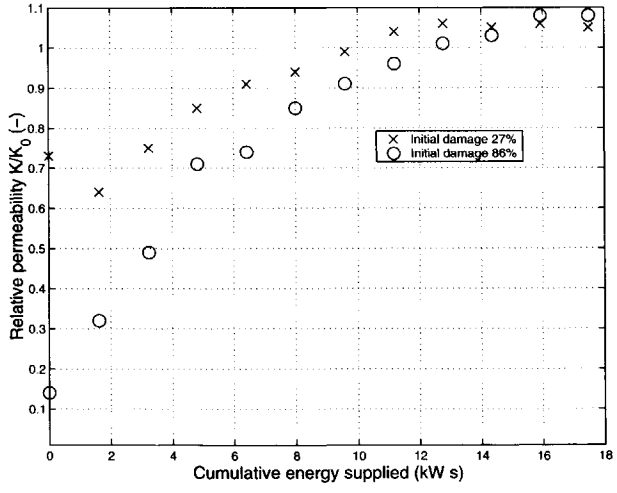

Figure 7.20: Influence of permeability after fouling on the relative permeability as function of the cumulative energy supplied (*110 mD core, 1.2 s sonification time, 100% input power, 2 min rest time, 10 ml/min*).

and third burst generate only 10% improvement. This seems logical since there are more particles to be removed when the level of fouling is higher. However it can also be seen from the figure, that there is not much difference in the cumulative energy needed to reach the final cleaning state.

7.4.9 Influence of pressure

The pressure has a slight influence on the colloidal forces, but a strong effect on the transmission of acoustic waves in the fluid. When the pressure increases the attenuation of the waves decreases and the waves will penetrate deeper into the core. However when the pressure is lowered too much, cavitation in the chamber will occur and a strong damping of the waves will take place in the chamber. According to Venkitaraman (1995) cavitation may contribute to the removal of near surface particles. We also studied the effect of the pressure on the cleaning efficiency. To that purpose the pressure inside the core was lowered to 30 bars. Unfortunately, the acoustic tool was not able to create bursts of a certain duration at 30 bars, because of suppression of the acoustic waves due to cavitation. Although the system was set to generate 0.4 s bursts, after about 0.2 seconds the horn automatically stopped generating waves. We think that the automatic arrest of the system was due to overheating: when the temperature of the horn exceeds a certain value, the system is stopped for safety reason. It seems that cavitation needs some time to develop. In the time that it was developing, the acoustic waves were generated in a normal way. However once the bubble implosions due cavitation became strong the horn was no longer able to generate acoustic waves. In Fig. 7.21 and Fig. 7.22 the cleaning results for the 30 bars experiment are compared with those for the 100 bars experiment. The relative permeability is given as a function of the number of bursts and as function of the cumulative energy. It is clear that cavitation has a

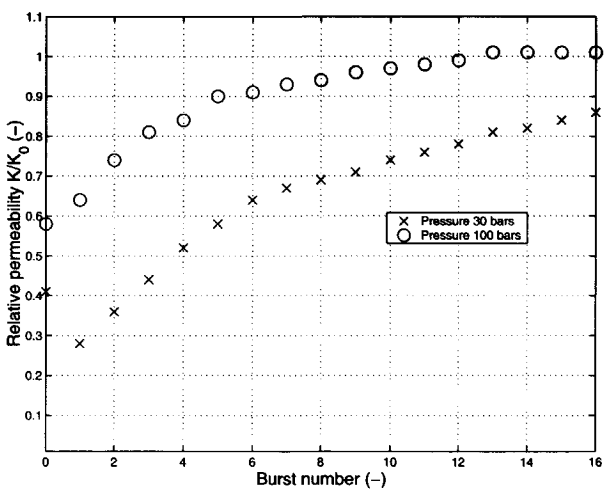

Figure 7.21: Influence of cavitation on the relative permeability as function of the number of bursts (*155 mD core, 100% input power, 2 min rest time, 50 ml/min*).

negative effect on the particle removal process, although this negative effect on the final relative permeability is rather small. Cavitation can effectively remove some of the near surface particles and this compensates for the suppression of the acoustic waves due to cavitation.

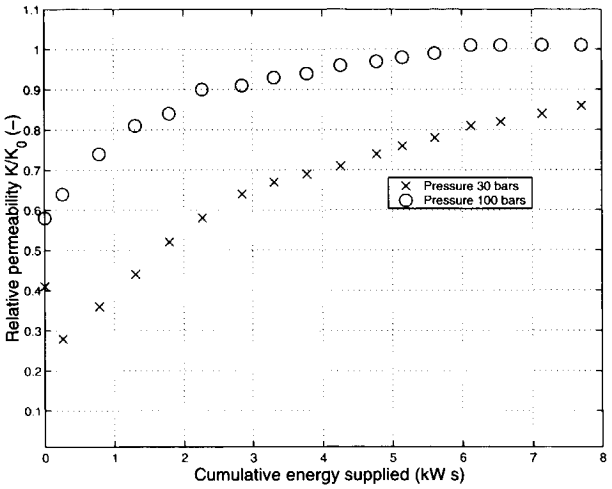

Figure 7.22: Influence of cavitation on the relative permeability as function of the cumulative energy (*155 mD core, 100% input power, 2 min rest time, 50 ml/min*).

7.5 Conclusion

Our experiments showed that ultrasonic stimulation is a very effective tool for removing fouling particles from a porous material. The ultrasonic waves are able to remove all the particles inside the core and, hence, to restore the permeability to its initial value. The development of the permeability shows that the cleaning process takes place during the acoustic treatment and not during the flow of brine after the treatment. The course of the cleaning process could successfully be followed by measuring the intermediate permeability changes after each acoustic burst. The repeatability of the experiments was good. The optimal way to carry out ultrasonic cleaning for this kind of fouling is by using very short bursts of acoustic waves with a low amplitude, a short rest time in between the bursts and keeping the flow of brine at a very low velocity. The results of the experiments concerning the influence of different parameters are summarized below.

- The number of bursts is important not their duration. Short bursts are equally effective as long ones, but they cost less energy. Long bursts are more capable of removing the last part of the fouling particles.
- Low amplitude waves are equally effective as waves with a high amplitude, but they cost less energy. (We think that this result is due to the rather shallow penetration of the particles during our experiments.)
- The rest time does not influence the cleaning efficiency. The permeability improvement takes place during the ultrasonic treatment and not during the period of back flowing of brine.
- A low flow rate during acoustic treatment makes it possible to obtain a larger final permeability than a high flow rate during treatment. Interrupting the flow during the acoustic treatment does not influence the cleaning process.
- At higher temperatures the treatment is less effective.
- Cavitation has a negative effect on the removal of particle fouling.

- In some cases a (strong) deterioration of the permeability is measured after the first burst. This phenomenon needs further study.

Finally we want to emphasize, that a precise interpretation of the results is difficult because of the variability and the complexity of the natural materials used. The physical insights of the experimental results are mostly qualitative. We think, however, that the experiments reported in this publication are a necessary first step for understanding the acoustic cleaning.

Chapter 8

Conclusion and perspectives

8.1 Conclusions

The aim of this project was to investigate experimentally and theoretically the influence of high-frequency acoustic waves on the flow of a liquid through a porous material and to study the possibility of such waves to remove small (fouling) particles from the porous material. The following conclusions, based on our study, can be drawn:

- The ultrasonic irradiation of a porous material decreases the viscosity of the liquid due to the (rather strong) damping of the acoustic waves. Therefore, the pressure drop over the flow through a porous material decreases at constant flow rate, or the flow rate increases at constant pressure drop.

- Due to the strong damping of the acoustic waves acoustic streaming can be observed in the porous material. This effect is interesting from a fundamental point of view. It is too small to be of importance for applications.

- Ultrasonic stimulation can be used to remove particles attached to pore walls. Experiments indicate that an increase in permeability can be achieved in the first ten centimeters of the porous material. A deeper cleaning effect can not be achieved due to the strong dissipation of the acoustic waves. The permeability of the porous material plays an important role, in the sense that a larger permeability allows a better cleaning.

- Particles bridge formation is a possible mechanism of permeability reduction. A key parameter for particles bridge formation is the fluid velocity: only at velocities higher than a critical value, bridges are formed and the permeability decreases.

- Particle bridges can be removed by ultrasound. Again the fluid velocity plays an important role. Lower velocities increase the effectiveness of the removal. This effectiveness increases with the (original) permeability of the porous material. There is an optimal frequency range that gives the best results.

- In the removal of particle bridges the sonication time plays an important role. It has seen that short (repeated) sonication times are more effective than long ones. However, if the sonication time is too short a decrease in permeability can be induced (at least during the first stages of the application).

- Filter cake formed by external particles can be removed by ultrasound. Since the penetration depth of external particles is very shallow, the acoustic intensity is not so important. However, again the sonication time is rather important in the sense that short sonication times give negative results.

8.2 Perspectives

The work presented here is based on a large number of experiments, during which particular emphasis was given to the influence of some relevant parameters. However, only two values of the acoustic frequency (20 and 40 kHz) were used. A useful extension of this study would be the application of more frequencies. This work can, also, be extended in other directions. The possibility to remove other type of damages, such as polymers and paraffins, needs to be accessed. The study of polymers is particularly challenging for a number of reasons:

- The propagation of sound through a porous medium saturated by a non-Newtonian fluid has not been properly investigated yet.
- The interaction between polymers chains and the solid skeleton is not at all properly understood.
- Polymers are common components of drilling muds.

In this investigation the porous material is always saturated by a single phase liquid (brine or water), while in practice a mixture of two- or three- phases is normally encountered. It could be extremely interesting to look into the effects of ultrasound on multiphase flow through porous material and to study the way in which ultrasound can effect the relative permeability. Few models exist that can perhaps explain the effect of ultrasound for such conditions, but a careful experimental investigation still needs to be done.

Appendix A

Interaction and collisions between particles in a linear shear flow near a wall at low Reynolds number*

Abstract

Flow fields around pairs of small particles moving and rotating in a shear flow close to a wall at low but finite Reynolds number are computed as a function of time by means of the lattice-Boltzmann technique. The total force and torque acting on each particle is computed at each time step and the position of the particles is updated. By considering the lift force and the disturbances induced by the particles the trajectories of the pair of particles are explained as a function of the distances from the wall and the Reynolds number. It is shown that when particles are positioned in a particular form, they collide. Collision maps are constructed for several values of the Reynolds number and distances from the wall. As we are interested in particle-bridge formation in shear flows similar calculations are also performed for a converging flow geometry.

A.1 Introduction

Clustering of small particles in a laminar or turbulent flow field occurs often in practice. In the clustering process hydrodynamic forces are dominant but colloidal forces play also an important role. We are particularly interested in the clustering of particles in the pores of a porous material because the particles can form bridges in the throat of the pores and reduce the permeability of the material. An example is given in Fig. A.1, where bridge formation by very small particles in a natural sandstone is shown; note that their size is less than 1/100 of the pore diameter. This type of fouling can cause severe problems during the exploitation of oil from an underground reservoir and it is important to understand better under which conditions bridge formation by particles can occur. During the movement of the particles through the pore of a porous material the Reynolds number Re is very low (10^{-3}-10^{-2}). Another important characteristic is that there is always a solid wall not far away from the particles. As the study of how particles form bridges is rather complicated, we begin studying the flow of a single particle in the vicinity of a wall. To that purpose the flow field around the particle is computed as function of time by means of the lattice-Boltzmann technique, Cate (2002), Cate, Nieuwstad, Derksen & van den Akker (2002) and Cate, Derksen, Portela & van den Akker (2004). The total force and torque acting on the particle

*P. Poesio, G. Ooms, J.C.R. Hunt and A. ten Cate. "Interaction and collisions between particles in a linear shear flow near a wall at low Reynolds number". *Submitted to J. Fluid Mech.*

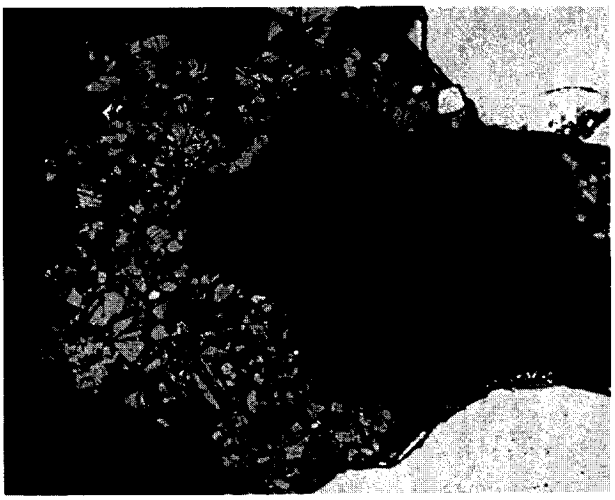

Figure A.1: Particles bridge formation in a pore throat inside a natural sandstone. Note that particles have a variety of sizes.

is computed at each time step and its position is updated. The trajectory and the particle induced disturbance are studied as function of the distance from the wall and for different values of Re. Next we extend the study by investigating the behavior of two particles. Particular attention is paid to the possibility that the particles collide and form the nucleus of a string of particles. In the final part of the paper, the possibility that two particles form a bridge in a converging flow configuration is investigated.

Several publications have been written about the hydrodynamic forces acting on a particle traveling in a shear flow at low, but finite, Reynolds number. The first to compute the inertial lift force on a spherical particle moving in such a shear flow was Saffman (1965). More recently Cherukat & McLaughlin (1994) computed the lift force acting on a spherical particle near a wall by means of a perturbation approach. Magnaudet (2003) calculated the drag force and the lift force on a sphere in a linear shear flow near a wall. Feng & Michaelides (2003) studied numerically the motion of a single particle near a horizontal wall in a linear shear flow. They investigated at which conditions the inertial lift force acting on a particle is large enough to overcome the gravity force, and the particle can move away from the wall. As the finite size of the particle is taken into account, also the disturbance of the particle on the flow field is calculated. The lift force on a rotating sphere in a shear flow was studied by Kurose & Komori (1999): they showed that at high Re the lift force change orientation. It is important to point out that Kurose & Komori (1999) computed the hydrodynamic forces acting on a spherical particle held in place with an imposed rotational speed, while we are interested in the case that the motion of the particle is driven by the flow. Patankar, Huang, Ho & Joseph (2002) studied the lift-off of a sphere in a two dimensional channel by means on direct numerical simulations. They paid particular attention at the role of the lift force for relatively high Re with the influence of gravity.

When two particles are moving in a shear flow close to a wall it is not immediately clear, in which direction they will move. For instance, it is possible that the trailing particle moves toward the wall due to the flow disturbance of the leading particle, while the leading particle itself moves away from the wall due to the inertial lift force. It is also possible that both particles move away from the wall because the inertial lift force dominates the movements of the particles. There is a competition between the viscous force and inertial force acting on the particles and at low, but finite, Re it is not directly clear which one dominates. The understanding of the

behavior of two interacting and colliding particles in a shear flow is fundamental to understand the formation of particle clusters (for instance in the form of strings) and particles bridges in such flows. Based on their recent work on the blockage of microtubes, Sharp & Adrian (2001) reported about shear induced arching (in this paper called bridging) as main mechanism causing the channel blockage. They base their conclusion on the observation of the geometrical configuration of the blockages; these blockages are very similar to the one we show in Fig. A.1. Their explanation is based on the likelihood of particles colliding when placed in a non-uniform laminar flow velocity profile. Collisions are then followed by formation of arches. They assume that when "particles are uniformly dispersed at the inlet of the channel, some mechanisms must bring the particles together in the channel". We show in this paper that this mechanism is correlated with weak (but not negligible) inertial forces, even at low Re.

In the formation of particle clusters or bridges colloidal forces (for instance the van der Waals force or electrical-double-layer force) can play a crucial role. The particles can be pushed together by hydrodynamic forces and particle cluster formation or particle bridge formation can then occur due to the colloidal forces. Here we limit ourselves (as a starting point) to the hydrodynamic interaction between two particles in a shear flow in the vicinity of a wall. Colloidal forces are taken into account in an indirect way. From the colloidal properties of the material (assumed to be clays) we can calculate at what distance the colloidal forces start playing a role. When the two particles get closer than this distance, we stopped the simulation and we recorded a "collision" Also the flow geometry is first simplified by studying the flow of two particles in the shear flow close to a plane wall. In the last part of the paper we investigate the movement and collision of particles in a convergent flow geometry, similar to the one shown in Fig. A.1. In such a way, first we understand the basic feature of particle collisions in a simplified geometry and later we will make use of this understanding to explain particle collisions and, hence, bridge formation in a more realistic, and more complex, geometry.

The practical relevance of this study in oil extraction and bioengineering are discussed in the conclusion.

A.2 Relevant parameters

The particles are released with an initial velocity $U_p(t=0)$ equal to the unperturbed local fluid velocity, given by $U_0 = \alpha y_i$; α is the shear rate. The instantaneous particle velocity is defined as $\mathbf{W}_p = (U_p, V_p) = d\mathbf{x}_p/dt$ and, hence, the relative horizontal velocity is $\Delta U_p = U_p - U_0(y_p)$ while the relative vertical velocity is $\Delta V_p = V_p$. The important parameters for our problem are the particle Reynolds number (Re) defined as

$$Re = \frac{\rho_f a \sqrt{\Delta U_p^2 + \Delta V_p^2}}{\mu}, \tag{A.1}$$

and the shear flow number

$$S = \frac{\alpha a}{\sqrt{\Delta U_p^2 + \Delta V_p^2}}, \tag{A.2}$$

where ρ_f is the density of the fluid and (as mentioned earlier) μ is the fluid viscosity.

Since Re=0 and $S \to \infty$ at t=0, we introduce two alternative dimensionless groups: the shear Re_s-number,

$$Re_s = \frac{\rho_f a^2 \alpha}{\mu}, \tag{A.3}$$

and the initial dimensionless distance from the wall,

$$\delta_i = \frac{y_i}{a}. \tag{A.4}$$

We believe that this set of parameters describe better the physics we are interested in. For a particle moving relatively to an unbounded fluid the size of the influence region of the particle is

given by ($l/a \sim 1/Re$). The influence region around a particle in a shear flow can be estimated by $l \sim \sqrt{\nu/\alpha}$ which can be shown to be given by $l/a \sim Re_s^{-1/2}$. We made calculations for the following two values of the shear Reynolds number $Re_s = 0.01$ and $Re_s = 0.1$. For the initial dimensionless distance from the wall for the leading particle we choose $\delta_i = 20$ (particle far away from the wall) and $\delta_i = 2$ (particle close to the wall). We expect that for the case $\delta_i = 2$ the wall will have a large influence on the behavior of the particles, while this influence will be reduced for the case $\delta_i = 20$. The initial position of the trailing particle relative to the leading one is of crucial importance for the behavior of the two particles and it is studied in detail.

A.3 Lattice-Boltzmann method

A.3.1 Numerical scheme

For our numerical simulations, the lattice-Boltzmann method was used. This method can treat moving boundaries with a complex geometry in an efficient way. Simulations with this method for the case of a single spherical particle settling in a confined geometry have shown very good agreement with experimental results, see Cate (2002), Cate et al. (2002) and Cate et al. (2004). The lattice-Boltzmann method uses a mesoscopic model for the fluid behavior, which is based on collision rules for the movement of hypothetical particles (not to be confused with the physical particles) on a grid. The grid is a uniform simple cubic lattice. It can be shown that, after averaging, the continuity equation and Navier-Stokes equation are satisfied. The lattice-Boltzmann method has been applied earlier to calculate a flow with particles by Ladd (1994*a*) and Ladd (1994*b*). Our method is based on the work of Eggels & Somers (1995); it is described in detail in Cate et al. (2004). The boundary condition at the surface of a particle is taken into account by means of an induced force-field method, similar to the one used by Derksen & van den Akker (1999). In this method a particle is represented by a number of points located in its surface. The surface points are evenly distributed with a mutual distance smaller than the grid spacing. The no-slip condition at the particle surface is satisfied in two steps. First the fluid velocity at each surface point is determined via a first-order interpolation of the fluid velocities in the surrounding grid points. Then (induced) forces are assumed to be present at the surface points of the particle of such a magnitude, that the fluid velocity in the surrounding grid points is changed in such a way that the no-slip condition at the surface points is satisfied. Thereafter the hydrodynamic drag force ($\mathbf{F_d}$) and also the torque ($\mathbf{M_d}$) acting on a particle by the fluid are computed and used to determine the particle motion. The particle movement is calculated with the aid of the following equations

$$m\frac{d^2\mathbf{x}}{dt^2} = \mathbf{F_d} \tag{A.5}$$

$$I\frac{d^2\theta}{dt^2} = \mathbf{M_d} \tag{A.6}$$

in which m is the particle mass, I the moment of inertia, $\mathbf{x}$ the space coordinate, θ the angle of rotation and t the time. This equation is integrated by using a simple Euler integration scheme where the forces are time-smoothed over two time steps. Very small time steps are used. We apply the Euler integration algorithm since we only consider particle pairs. (Although it might not be the best algorithm, see Aidun *et al.*). Time averaging is applied to the calculated forces obtained from the lattice-Boltzmann field, since these may contain fluctuations. For this purpose the time step is updated by integrating $m d\mathbf{v}/dt = 0.5 * (\mathbf{f}(t-1) + \mathbf{f}(t-2))$. This is a choice inspired by the paper of Ladd (1994a).

The computations were carried out on a three dimensional grid. We used particles of 10 lattice units (l.u.) radius. The length of the calculation domain is 400 l.u., the height is 400 l.u. and the perpendicular direction has a length of 200 l.u.. In a few cases we doubled the mesh size in each direction to investigate whether the results are independent of mesh size.

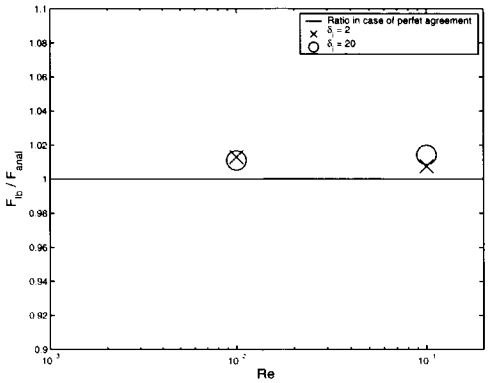

Figure A.2: Comparison between the lift force on a particle as calculated by our method (F_{lb}) and as calculated analytically F_{anal} by the procedure given in Cherukat & McLaughlin (1994). The definition of Re_s is given by Eq. A.3.

A.3.2 Calibration procedure for the particle radius

As discussed a particle surface is approximated in the lattice grid by means of particle surface points. It is known that this approximation causes the particle to experience a drag force that corresponds to a particle with a diameter larger than the real diameter. This effect can be compensated by ascribing to the particle a hydrodynamic radius that is smaller than the real radius. For the determination of this hydrodynamic radius a calibration procedure is applied. A well known procedure was proposed by Ladd (1994a). He calculated the drag force acting on a particle located in an array of particles with a periodic arrangement in two ways. He used his lattice-Boltzmann method and applied the analytical solution for this particular problem. From the comparison between the two results he found the hydrodynamic radius. The calibration procedure is based on the analytical solution of Hasimoto (1959) for the drag force on a fixed sphere in a periodic array of spheres at creeping flow conditions

$$\frac{6\pi\mu a U_u}{F_d} = 1 - 1.7601 C_\tau^{1/3} + C_\tau - 1.5593 C_\tau^2, \tag{A.7}$$

where $C_\tau = \frac{4\pi a^3}{3L^3}$; L indicates the size of the unit cell, U_u is the volumetric averaged fluid velocity across the unit cell, μ the fluid viscosity and a the particle radius. We used the same calibration procedure

The hydrodynamic radius was found for creeping flow conditions and one may wonder whether the result also holds at finite Reynolds number when inertial effects are important. Therefore, we have computed the lift force on a sphere held stationary in a linear shear flow in presence of a wall at low, but finite, Reynolds number. The results are compared with the analytical solution by Cherukat & McLaughlin (1994) in Fig. A.2 for two values of the dimensionless distance δ_i from the wall. ($\delta_i = y_i/a$, in which y_i is the distance from the wall and, as mentioned earlier, a the particle radius.) As can be seen the results compare well. The small difference between the analytical results and the theoretical ones can be explained by the finite size of the computation domain.

A.3.3 Lubrication force between two particles at a small distance

Ladd (1997) found that as pairs of particles approach particles, the lattice-Boltzmann method gives significant errors as the gap between the particles is less than the spatial resolution of the computational domain. He corrected the error by introducing an extra lubrication force that

accounts for the contribution to the hydrodynamic forces due to the unresolved part of the flow field. This lubrication force (acting along the centerline of two particles i and j) is given by

$$\mathbf{F}_{lub} = -\frac{3\pi\mu a}{s}\hat{\mathbf{x}}_{ij}\hat{\mathbf{x}}_{ij}\cdot(\mathbf{u}_i - \mathbf{u}_j) \tag{A.8}$$

where $s = R/a - 2$ is the dimensionless gap width (R is the distance between the centers of the particles) and $\mathbf{x}_{ij} = \mathbf{x}_i - \mathbf{x}_j$. $\mathbf{x}_i$ and $\mathbf{x}_j$ are the coordinates of the particles and $\hat{\mathbf{x}}_{ij} = \mathbf{x}_{ij}/|\mathbf{x}_{ij}|$. $\mathbf{u}_i$ and $\mathbf{u}_j$ are the particles' velocities. The lubrication force is assumed to be active, when the gap width between two particles is smaller than the distance between two lattice grid points. As the near field hydrodynamic force plays a critical role in our simulation, we used an improved version for the lubrication force given by Kim & Karilla (1991), in which a logarithmic correction is included

$$\mathbf{F}_{lub} = -\left(\frac{3\pi\mu a}{s} + \frac{27\pi\mu a}{20}\log\frac{1}{s}\right)\hat{\mathbf{x}}_{ij}\hat{\mathbf{x}}_{ij}\cdot(\mathbf{u_i} - \mathbf{u_j}). \tag{A.9}$$

It is not possible to compute the lubrication force at very small values of s, because it leads to numerical instability. At very small separation the particles experience colloidal forces. We define in this publication, that particles collide at the moment when the separation between the particles is so small that the van der Waals and the electrical forces become important. This occurs typically at $s = 10^{-2}$ for $R \sim 1\mu m$. At that moment the simulation is stopped and a collision event is recorded. If particles due to hydrodynamic interaction do not get that close, we assume that no collision occurs. Other definitions of a collision have been used in particulate flows, however we believe that the definition given above is the most suitable for our case.

In the lubrication force we have neglect the transverse component, assuming that it is small. The use of the transverse component of the lubrication force is a topic of ongoing research. Some preliminary computations, Derksen (2004), have shown that actually this component can be neglected in the case of low Re.

A.4 Single particle in a linear shear field

A spherical particle in a shear field at non-zero Reynolds number undergoes both a drag force and a lift force. The effect of these forces is to move the particle away from the wall. Initially the particle is released at a distance δ_i from the wall with the same velocity as the fluid. The particle begins to rotate leading to a lift force that causes the particle to move away from the wall. Then, the difference in velocity between the fluid and the particle generates the drag force. It is known that the inertial lift force is proportional to the Reynolds number. As in our case the Reynolds number is small, only a small movement away from the wall is observed. After an initial period during which the initial conditions play a role, the particle trajectory becomes linear. The relative velocity, defined as the fluid velocity at a certain position for the particle-free case minus the particle velocity at the same position, increases at the beginning and then gets a constant value. The initial increase of the horizontal velocity is due to the fact that the particle moves to regions where the fluid velocity is higher. The final relative velocity is very small (compared to the velocity of the unperturbed flow): the particle follows the fluid almost completely. Similar results have already been found by Feng & Michaelides (2003) (at higher Reynolds number and with gravity effect). Calculation concerning the motion of a single particle in a shear flow were also performed by Patankar et al. (2002). They studied the lift-off of a single particle in a two dimensional channel. Their conclusions and results are qualitative similar to ours, although the shear Reynolds number in their calculations is much higher than in our case. This similarity can be explained by the fact the in a shear flow the lift force is weakly dependent on the value of Re.

In order to understand the complicated flow field around a particle we discuss briefly the vertical fluid velocity component, shown in Fig. A.3. We will do that in some steps. First we consider the flow pattern around a single sphere moving in an unbounded fluid, then we discuss a particle moving in a shear flow without rotation, next we consider a rotating particle in a shear flow (without translation) and finally the complete flow pattern is discussed. The flow pattern

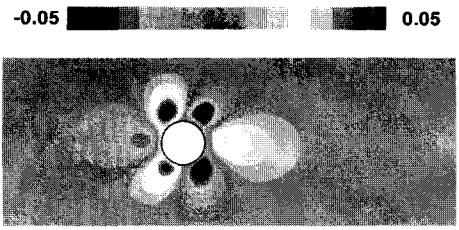

Figure A.3: Plot of the vertical component of the fluid velocity. $Re_s = 0.01$ ($Re = 6.4\ 10^{-4}$), initial position $\delta_i = 20$ and instantaneous position $\delta = 20.12$.

around a single particle in an unbounded homogeneous flow can be found in many textbooks on fluid mechanics, see for instance Batchelor (1965). In that case the asymmetry between the vertical fluid velocity components at the back and at the front of the particle originates from the non-zero Re condition. A particle translating in a linear shear has the tendency to start rotating. When this tendency is suppressed the two upper vertical-velocity lobes (that are positioned in the high-velocity region) are stronger than the two lower vertical-velocity lobes (that are in the low-velocity region). The asymmetry between the front of the particle and its backside is again due to the inertial forces at finite values of the Reynolds number. The vertical-velocity field around a rotating particle in a fluid (at rest at large distances) is determined by the fact that the fluid is dragged around to satisfy the no-slip condition. We can now try to understand the complete fluid flow pattern shown in Fig. A.3 in terms of the elementary "building blocks" we have just described. Very close to the particle there is a thin layer of positive vertical-velocity fluid on the left-hand side of the particle, and a negative one on the right-hand side. These two regions are a consequence of the rotation of the particle in clock-wise direction. The two lobes at the top of the particle and the two lobes at the bottom are also due to the rotation of the particle, as can be concluded from their sign. So the rotation of the particle is very important in the determination of the fluid flow field. The two middle lobes originate from the two upper lobes as in the case of a translating non-rotating particle, but they are deformed due to the particle rotation.

We now analyze the forces acting on a particle using the fluid flow field around the particle keeping in mind that ΔU_p and ΔV_p are horizontal and vertical relative velocities and Ω_p is the rotational speed. The force balance in vertical direction needs to account for the upward lift force ($\sim \rho_f \alpha a^3 \Delta U_p$, Saffman-like lift), the downward force due to the Magnus effect ($\sim \rho_f \Omega_p \Delta U_p a^3$), and the component of the drag force in vertical downward direction ($\sim \mu a \Delta V_p$). An order of magnitude analysis shows that the inertial lift force and Magnus force are both significant, while the vertical component of the drag force is negligible. In the horizontal direction there are two forces: the viscous drag ($\sim \mu a \Delta U_p$) (pointing forward as the particle travels slower than the fluid), and the horizontal component of the lift force ($\sim \rho_f \Omega_p \Delta V_p a^3$) (also pointing forward). Due those forces, the particle accelerates in the horizontal direction, as it rises in the shear flow.

The analysis of the flow field can now be used to understand the behavior of a trailing second particle, assuming that the trailing particle behaves as a point particle without influencing the fluid. In the next section this effect of the trailing particle is included. From Fig. A.3 we see that a trailing particle can respond to the flow field of the leading one in a variety of ways. When the trailing particle enters the back-side region of the leading particle where the vertical velocity of the fluid is positive, the trailing particle has the tendency to be pushed upward. When the trailing particle enters the region where the vertical velocity of the fluid is negative the trailing particle tends to move downward. However there is an inertial lift force acting on the trailing and leading particle, that want to push the particles upward. So while the leading particle will likely

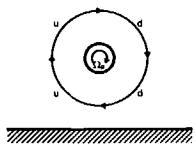

(a) Particle spinning with angular velocity Ω_p. $\Delta U_p = 0$, $\Delta V_p = 0$.

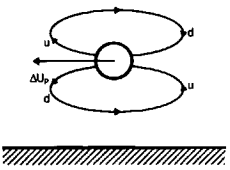

(b) Particle translating horizontally with relative velocity ΔU_p. $\Delta V_p = 0$, $\Omega_p = 0$.

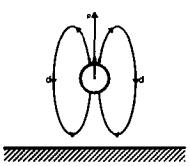

(c) Particle translating vertically with relative velocity ΔV_p. $\Delta U_p = 0$, $\Omega_p = 0$.

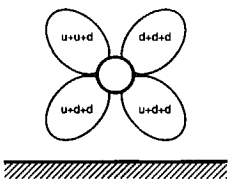

(d) Effect of the motion resulting from the superposition of (a), (b) and (c).

Figure A.4: *Mechanism* diagram for flow field around a particle. u: upward; d: downward.

rise, the trailing particle can move upward or downward depending on the competition between the two tendencies described above. We comment on these suggestions in the next section where the results of two finite-size particles are presented.

We can also give a "mechanism" diagram to explain the flow field around a particle in a shear flow and to explain the behavior of a trailing second (point) particle (see Fig. A.4). Again the flow field is considered to be built up from a number of basic elements. The flow disturbance due to the rotation of the particle is upward (u) on the left-hand side of the particle and downward (d) on the right-hand side (see Fig. A.4(a)). Because of its inertia the particle will move slower than the mean fluid velocity. This yields a flow disturbance with two recirculation regions, one above and one below the particle (see Fig. A.4(b)). Finally, due to the inertial lift force the particle moves upward and causes also two re-circulating regions, one at the left-hand side and one at the right-hand side of the particle (Fig. A.4(c)). The combination of all contributions is sketched in Fig. A.4(d). This diagram explains again, that a trailing second particle that enters the flow field at the backside of the leading particle at a larger distance from the wall than the leading particle will likely move upward. A trailing second particle that enters the flow field at the backside of the leading particle at a smaller distance from the wall than the leading particle will likely move downward.

The effect of *Re* on the vertical velocity of the fluid is analyzed. The flow field is qualitatively the same with the six lobes for the vertical component of the velocity. The fluid region around the particles that is influenced by the presence of the particles is reduced for the larger value of the Reynolds number. This feature is essential for understanding the possibility of collision between the particles. At low values of the Reynolds number the presence of particle is felt at larger distances from the particles than at high values. So at low values of the Reynolds number the particles start feeling each other at larger distances (than for large values of the Reynolds number) and they have more time to re-arrange their position.

The flow field around a particle is also influenced by the distance from the wall, as described before. As the particle gets closer to the wall, the flow field close to the wall starts interacting

with the wall itself (the region within which we expect that the particle interacts with the wall is of the order $Re_s^{-1/2}$). The region where the trailing particle is influenced by the leading particle is pushed upward and increases its size. The upper left lobe where the fluid is dragged upward is pushed against the particle. We expect that a collision is more likely for particles close to the wall than for particle far away from it. The trailing particle is not so easily pushed away from the leading particle as for the case that the particles are far away from the wall. The flow field is qualitatively similar in both cases, but a stronger interaction between the wall and particles close to the wall modifies more strongly both the size and the position of the six vertical-velocity lobes.

A.5 Two particles in a shear flow

We now study the hydrodynamic interaction and flow behavior of two finite-size particles in a shear flow close to a wall at small, but finite, Reynolds number. So the fluid flow disturbance due to both particles is taken into account. Particular attention will be paid to the possibility of a collision between the particles. We study the interaction between two equal-size particles (with radius a) in a shear flow (with shear rate α). The particles are assumed to have initially the local fluid velocity and they are free to move and rotate in response to hydrodynamic forces. We can find two different types of trajectories for the particles. The trailing particle can first move downward toward the wall and move upward later on, or the trailing particle can move upward from the start. The difference in behavior is determined by the difference in the initial position of the trailing particle. If the trailing particle is initially completely immersed in a flow region of the leading particle where the fluid velocity is pointing downward then it also starts moving downward. Whereas, if the trailing particle starts at a larger distance from the wall, where the influence of leading particle pushes the particle upward, then it will move upward. So the conclusion is that when the particles are close together, the particle-induced fluid flow field dominates the particle relative movement. When the particles are farther apart the shear flow field due to the presence of the wall becomes more important. When the particles do not collide, the distance between them increases and finally they behave as single particles and both move upward. In the final period also the velocity of the particles relative to the fluid is the same as in the case of a single particle. We do not treat here the case where the leading particle starts at a larger distance from the wall than the trailing one. In that case the leading particle travels faster than the trailing one and it never catches up.

In the trajectory map (Fig. A.5) we show the effect of the relative initial position on the initial stage of the trajectory of the trailing particle: a triangle means that starting from that initial position the particle initially move away from the wall, while an asterisk indicates particles initially moving toward the wall. As can be seen from the trajectory map the region of initial positions for the trailing particle that initially moves downward is not symmetrical behind the leading particle, the flow itself not being symmetrical. We found that the region of particles initially moving downward shrinks as the Re increases. The reason is, that the initial movement of the trailing particle is induced by the movement of the leading particle and (as mentioned) at high values of the Re-number this influence is weaker than at low values. The leading particle will move upward regardless the initial position of the trailing one because of the inertial lift force.

To summarize the results we build the collision maps, sketched in Figs. A.6, A.7, A.8 and A.9. As discussed the difference in flow pattern and particle trajectories depends on the way in which the two particles approach each other. The collision maps are made in the following way: we place the trailing particle at a certain initial position with respect to the leading particle, we release them with the local fluid velocity and we calculate the trajectories of both particles. We indicate on the collision map whether the initial positions of the two particles lead to a collision or not. So the map represents all the initial relative positions of the two particles that do or do not lead to a collision. This way showed the influence of the initial positions on the likelihood of collisions.

We investigated the influence of the Reynolds number and the initial distance from the wall on the form of the collision map. The results are shown in Figs. A.6, A.7, A.8 and A.9. The influence of Reynolds number can be seen from a comparison between Figs. A.6 and A.7, and

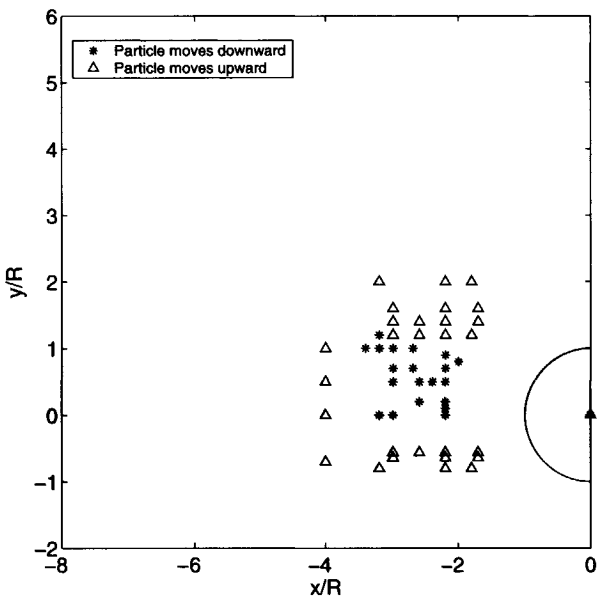

Figure A.5: Trajectory map giving an overview of the initial positions of the trailing particle with respect to the leading one, that lead to an upward ($\triangle$) or downward ($*$) movement of the trailing particle. $Re_s = 0.01$ and $\delta_i = 20$.

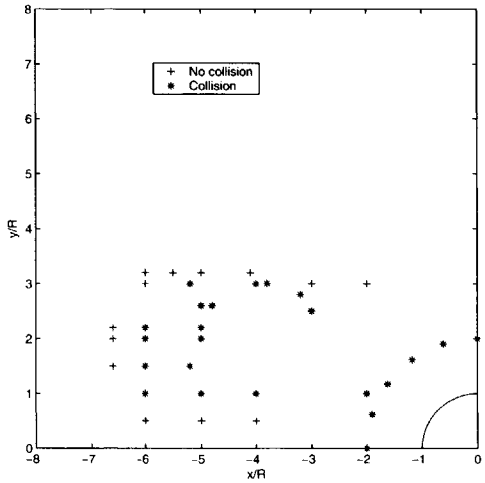

Figure A.6: Collision map for $Re_s = 0.1$ and $\delta_i = 2$.

from a comparison between A.8 and A.9. The collision region increases with increasing Reynolds number. This is due to the fact that the regions where the flow is disturbed reduce in size with increasing Reynolds number. The influence of the wall can be seen from a comparison between Figs. A.6 and A.8, and from a comparison between A.7 and A.9. As expected more collisions will occur for particles close to the wall. This effect is due to the strong deformation of the flow field around the particles close to the wall, because the particle rotation is greater near the wall. The deformation region behind the leading particle having a negative vertical component increases and at the same time the wall pushes the leading particle away from it. As a result more collisions occur. It can also be seen from the figures, that close to the wall the collision region is less influenced by the Re-number.

So far, we have analyzed only the case in which the initial positions of the two particles are in the same plane. It is interesting to look at possible effects of the offset in the out-of-plane direction. For the case $Re = 0.1$ and $\delta_i = 2$ we have carried out additional calculations for offsets (in the out-of-plane direction) equal to $a/4$, $a/2$, $3a/4$, and a. The results are shown in Fig. A.10. It is noted that the collision regions shrinks with increasing offset value. For an out-of-plane offset equal to a no collisions are found anymore. We carried out similar calculations at a lower value of the Reynolds number ($Re = 0.01$). Qualitatively the results are the same, although the collision region shrinks more quickly with increasing offset value.

In order to make a more quantitative description of the influence of the different parameters on the size of the collision region, we have calculated the area of the collision region (made dimensionless by the particle surface area) as function of the different parameters. These calculation are summarized in table 1. In the same table, we also show the volume of the collision region as function of the different parameters.

One may wonder, what type of particles clusters may develop due to collisions when many particles are present in the flow field. The calculation about the relative movement of two particles suggest, that a trailing particle tends to collide and cluster at the upper backside part of a leading particle.

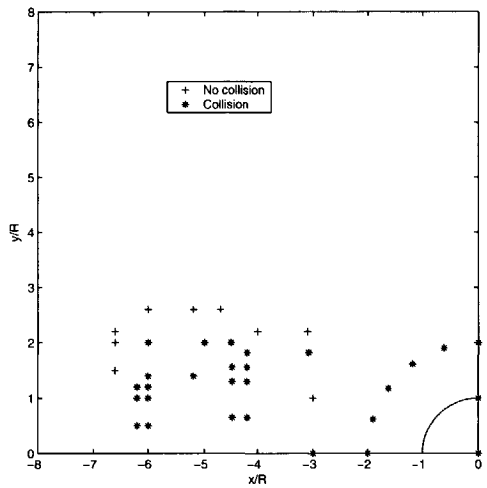

Figure A.7: Collision map for $Re_s = 0.01$ and $\delta_i = 2$. As can be seen from a comparison with Fig. A.6 the collision region decreases with decreasing Re_s-number.

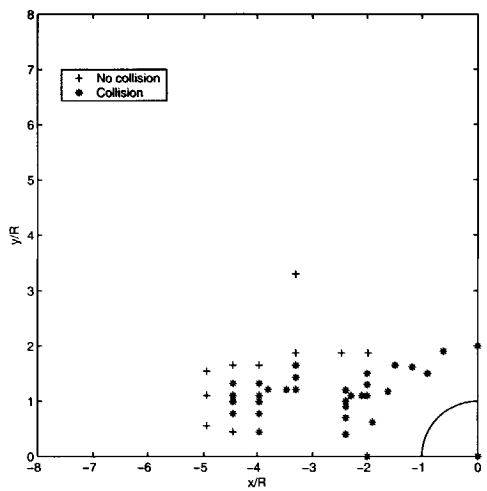

Figure A.8: Collision map for $Re_s = 0.1$ and $\delta_i = 20$. As can be seen from a comparison with Fig. A.6 the collision region decreases with increasing distance from the wall.

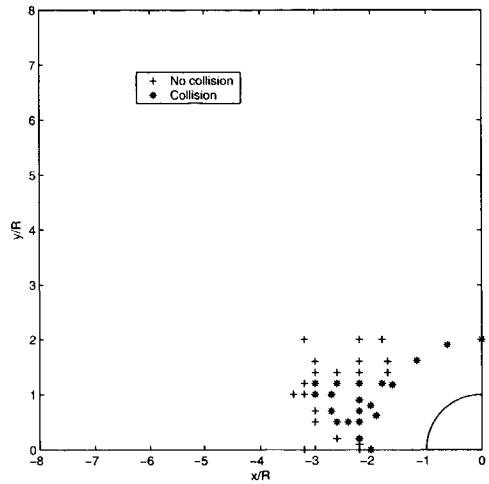

Figure A.9: Collision map for $Re_s = 0.01$ and $\delta_i = 20$

Out-of-plane offset	$Re = 0.01$ $\delta_i = 20$	$Re = 0.1$ $\delta_i = 20$	$Re = 0.01$ $\delta_i = 2$	$Re = 0.1$ $\delta_i = 2$
0	0.48	1.87	2.12	4.16
$a/4$	0.11	0.67	0.93	2.23
$a/2$	0	0.14	0.19	1.19
$3a/4$	-	0	0	0.44
a	-	-	-	0
Volume	0.12	0.71	0.93	1.43

Table A.1: Collision areas (made dimensionless by πa^2) for different out-of-plane displacement as function of Re and δ_i. Also the collision volume is given (made dimensionless by the $\frac{4}{3}\pi a^3$).

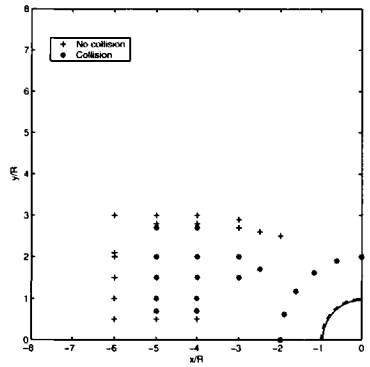

(a) Collision map for $Re_s = 0.1$ and $\delta_i = 2$, the out-of-plane offset is $a/4$. The dotted line is the sphere of radius a, while the continuous line represents the sphere in the plane of the trailing particle.

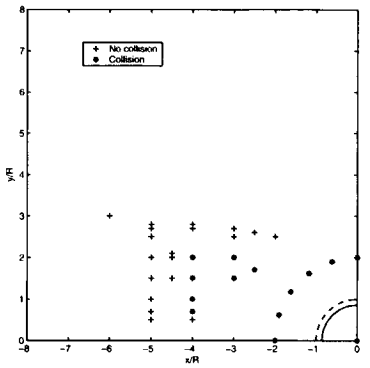

(b) Collision map for $Re_s = 0.1$ and $\delta_i = 2$, the out-of-plane offset is $a/2$. The dotted line is the sphere of radius a, while the continuous line represents the sphere in the plane of the trailing particle.

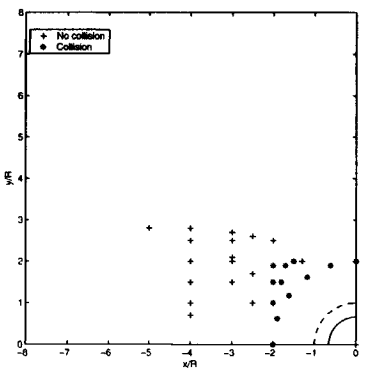

(c) Collision map for $Re_s = 0.1$ and $\delta_i = 2$, the out-of-plane offset is $3a/4$. The dotted line is the sphere of radius a, while the continuous line represents the sphere in the plane of the trailing particle.

Figure A.10: Influence of out-of-plane offset on the collision map for the case $Re_s = 0.1$ and $\delta_i = 2$. No collisions are recorded for an offset equal to a.

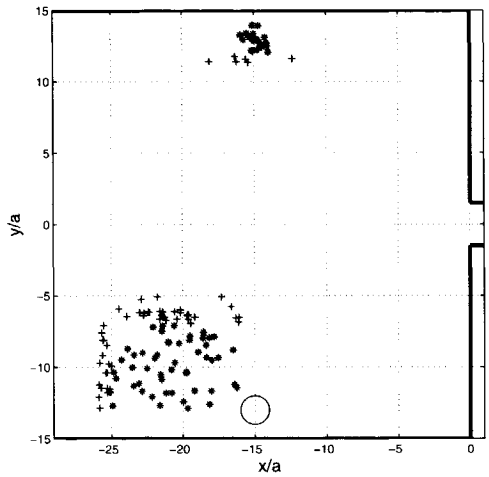

Figure A.11: Bridge formation map for $Re_s = 0.01$ and $\delta_i = 20$. The initial position of the leading particle is at $x/a = -15, y/a = -13$. The bridge formation area is considerably larger than the collision area shown in Fig. A.9. Moreover it consists of two parts. The total collision area is $23.8a^2$. The same trend is noted for $Re_s = 0.1$, in this case the collision area is $29.2a^2$.

A.6 Preliminary calculation of particles bridge formation

As mentioned in the introduction we are, in particular, interested in particles bridge formation in the pore throats of a porous material. To that purpose we have made a first preliminary calculation concerning the movement, possible collision and bridge formation of two particles in a converging flow at the entrance to a (suddenly) narrowing part of a two-dimensional channel (the throat). In Fig. A.11 a sketch of the flow geometry is given. For $x/a < 0$ there is a two-dimensional channel with solid walls at $y/a = -15$ and $y/a = +15$; for $x/a > 0$ the walls are at $y/a = -1.5$ and $y/a = +1.5$. Far upstream of the throat there is a parabolic fluid velocity profile, the flow is from left to right. Two particles can only pass simultaneously through the throat when they move behind each other through the throat; in other cases a particle bridge is formed at the throat entrance.

We have carried out additional lattice-Boltzmann calculation for two particles in the flow field with the geometry given in Fig. A.11. The simulations are similar to the ones as described in the preceding paragraphs for the movement of two particles in the vicinity of a flat solid wall, only the geometry is different. It is pointed out, that although the geometry consists of a two-dimensional channel the simulations are three-dimensional due the spherical geometry of the particles. In our simulations we fixed the initial position of the leading particle at $x/a = -15, y/a = -13$, and we varied the initial position of the second particle. For all these cases we calculated the trajectories of the particles and the possibility of a bridge formation by the two particles at the pore throat. We summarize the results in the bridge formation map also given in Fig. A.11. As can be seen from Fig. A.11 the bridge formation area (area of initial position of the second particle for which bridge formation occurs in the pore throat) is considerably larger than the collision area (area of initial position of the second particle for which collision occurs for the flow along a flat plate) shown in Fig. A.9. Moreover the bridge formation area consists of two parts. When the second particle starts in the vicinity of the wall on the opposite side of the pore, they can arrive simultaneously at the pore throat. This is, of course, due to the converging flow close to the pore throat.

To investigate the influence of the inertia forces on the collision mechanisms and hence on

bridge formation, we have carried out simulations at very low Re (i.e. $Re = 10^{-5}$). For this Re we could not detect any collision apart from the case that the trailing particle starts at the symmetrical position. So, it can be concluded that the inertia effect (although small) is responsible of the collisions. To further emphasize this point it is worth reminding that, for membranes Ramachandran & Fogler (1999) measured bridge formation at $Re = 6\,10^{-3}$, but not at $Re = 1.2\,10^{-4}$. Poesio & Ooms (2004) reported bridge formation in porous media at low (but not zero) Re. They measured bridge formation at $Re = 10^{-3}$, but not at lower values. It is pointed out, that much more work is needed to study particles bridge formation in pore throats. For instance in natural sandstones bridge formation usually occurs with many particles (see Fig. A.1). However, three-dimensional simulations with so many particles are not possible at the moment.

A.7 Conclusion

In this study of the behavior of two particles in a shear field in the vicinity of a wall detailed computations and order of magnitude results have been presented for the flow disturbances around the particles. Particular emphasis is given to the conditions for which a collision between the particles occurs. To that purpose collision maps have been calculated for two values of the Reynolds number and two values of the initial distance from the wall. In a collision map the area of initial positions of the trailing particle with respect to the leading particle that leads to a collision, is shown. This collision area increases with increasing Reynolds number and decreasing distance of the leading particle to the wall. This effect can be explained taking into account the region of influence around the particle. Also a first investigation has been made of particles bridge formation in a converging flow geometry. It turns out that the likelihood of collision by particles and hence the bridge formation area for a converging flow is considerably larger than the collision area for the flow along a flat plate. We have shown that at very low Re ($Re = 10^{-5}$) collisions do not happen, while they appear at higher Re and they are more probable (i.e. they happen for a larger number of initial position) as Re increases. This indicates that, in proximity to wall, collisions are dominated by weak inertia effects. This conclusion is in agreement with previous experimental works both on membranes, Ramachandran & Fogler (1999), and on natural porous material, Poesio & Ooms (2004). Of course, the particle shapes in reality may be different from the spherical one considered in this publication (see Fig. A.1). However, as noted in the paper the collision mechanism is dominated by the lift force acting on the particles. It has been shown by Auton, Hunt & Prod'homme (1988) that the lift force acting on a spherical-like particle in a shear flow is not sensitive to its precise shape.

Our analysis helps to understand the mechanism underlying collisions of particles in a shear flow at low Re in the presence of a wall. Collisions between pairs of particles are regarded as the first step for bridge formation. We have pointed that collisions, and therefore bridges, occur above a certain critical value for Re_s. The presence of a critical value for bridge formation is also confirmed experimentally by some previous work, see Ramachandran & Fogler (1999) and Poesio & Ooms (2004). This critical value, however, depends on several parameters such as particle concentration (this determines the probability to find particles in the relative position for collision), pore to particle diameter ratio, colloidal forces (neglected in this publication), and, very likely, on the length of the pore (for longer channel the probability for particles to get in the right position will increase). At this moment, however, there are no tools to predict whether bridge formation will occur.

The flow of particles in narrow tubes has several applications and it is of increasing importance. For instance, this study relates to acoustic stimulation of fouled porous media. Decline in permeability has a very dramatic effect on the near wellbore region of an oil reservoir and it leads to a reduction in productivity. Many techniques have been used to overcome this problem (for instance the use of acid), but they have negative side effects (being, for instance, environmental unfriendly). Recently the acoustic stimulation of the near wellbore region has been proposed as a possible remedy. This technique is very cheap and environmental friendly. The effectiveness of this technique is related to the cause of permeability reduction (particle deposition or particle bridge

formation). While particle deposition is a widely known mechanism, formation of particle bridges was not understood. Poesio et al. (2004) have already studied the possibility to remove particles attached on the pore walls by acoustics. Experiments, Poesio & Ooms (2004), have shown that particle bridges as well can be removed. Now that we have understood the phenomena involved in the bridge formation we are ready to take the next step and investigate the mechanisms involved in the removal of particle bridges.

Bio-engineers are also concerned by the flow of small particles in micro-devices as small as 1 μm up to 1 mm. Usually, those devices are made of small tubes within which chemical or biological reaction take place. A serious issue in these devices is the the clogging induced by small particles that may limit the use of such systems and hence may reduce the life expectancy.

Bibliography

Aarts, A. & Ooms, G. (1998), 'Net flow of compressible viscous liquids induced by traveling waves in porous media', *J. of Eng. Math.* **34**, 435–450.

Abad-Guerra, B. P. (1976), Methods for restoring productivity to gas wells in the Clinton sand of Ohio. A laboratory and field experiment, PhD thesis, Pennsylvania University State.

Auton, T., Hunt, J. & Prod'homme, M. (1988), 'The force exerted on a body in an inviscid unsteady non-uniform rotational flow', *J. Fluid Mech.* **197**, 241–257.

Barake, S. (2000), Ultrasonic well stimulation: experimental study on the effect of ultrasound on flow through porous media and ultrasonic damage removal, Master's thesis, Delft University of Technology.

Barake, S., v. Bas, F., Ooms, G. & Poesio, P. (2001), An experimental and theoretical investigation of the influence of high-frequency acoustic waves on the flow of a liquid through a porous material, *in* 'Rock Reservoir Workshop EAGE/SEG'.

Batchelor, G. K. (1965), *An introduction to Fluid Dynamics*, Cambridge University Press.

Batli, R. & Risnes, R. (1979), Stability and failure of sand arches, *in* 'SPE Ann. Tech. Conf.', Vol. SPE 8427.

Bear, J. (1972), *Dynamics of Fluid in Porous Media*, Elsevier Science Series.

Beresnev, I. & Johnson, P. (1994), 'Elastic wave stimulation of oil production: A review of methods and results', *Geophysics* **59**, 1000–1017.

Biot, M. (1956), 'Theory of propagation of elastic waves in a fluid-saturated porous medium. Low frequency range.', *J. Acoust. Soc. Am.* **28**, 168–191.

Cate, A. T. (2002), Turbulence and particle dynamics in dense crystal slurries, PhD thesis, Delft University of Technology.

Cate, A. T., Derksen, J., Portela, L. & van den Akker, H. (2004), 'Fully resolved simulations of colliding mono-dispersed spheres in forced isotropic turbulence', *J. Fluid Mech., in press.*

Cate, A. T., Nieuwstad, C., Derksen, J. & van den Akker, H. (2002), 'Piv experiments and lattice-Boltzmann simulation on a single sphere settling under gravity', *Phys. Fluids* **14**, 412.

Cherskiy, N., Tsarev, V., Konovalov, V. & Kuznetsov, O. (1977), 'The effect of ultrasound on permeability of rocks to water', *Transactions of the USSR Academy of Science, Earth Science Sections* **232**, 201–204.

Cherukat, P. & McLaughlin, J. (1994), 'The inertial lift on a rigid sphere in a linear shear flow field near a flat wall', *J. Fluid Mech.* **263**, 1–18.

Conway, M., Himes, R. & Gray, R. (2000), 'Minimizing clay sensitivity to fresh water following brine influx', *SPE 58748.*

Derjaguin, B., Churaev, N. & Muller, V. (1987), *Surface Forces*, Plenum Publishing Corporation.

Derksen, J. & van den Akker, H. (1999), 'Large eddy simulations on the flow by a rushton turbine', *AIChE Journal* **45**, 209–221.

Derksen, J. J. (2004), 'Private communication'.

Donaldson, E. C., Baker, B. A. & Carroll, H. (1977), Particle transport in sandstone, *in* 'SPE Ann. Tech. Conf.', Vol. SPE 6905.

Duhon, R. (1964), An investigation of the effect of ultrasonic energy on the flow of fluids in porous media, PhD thesis, University of Oklahoma.

Eggels, J. & Somers, J. (1995), 'Numerical simulation of free convective flow using lattice-Boltzmann scheme', *Int. J. Heat and Fluid Flow* **16**, 357–364.

Esipov, I. B., Fokin, A. V. & Ovchinnikov, O. B. (2002), Acoustic model of percolation development in granular medium, *in* O. Rudenko & O. Sapozhniko, eds, 'Nonlinear Acoustics at the Beginning of the 21st Century', Vol. 2.

Fairbanks, H. & Chen, W. (1971), Ultrasonic acceleration of liquid flow through porous media, *in* 'Chem. Eng. Prog. Symp. Ser.', Vol. 67, pp. 108–116.

Feng, Z.-G. & Michaelides, E. (2003), 'Equilibrium position for a particle in a horizontal shear flow', *Int. J. Multiphase Flow* **29**, 934–957.

Formation Damage (1990). Society of Petroleum Engineers, Reprint Series 29.

Gadiev, S. (1977), *Use of vibrations in oil production*, Nedra Press (in Russian).

Glenn, E. & Slusser, M. (1957), 'Factors affecting well productivity. ii: drilling particle invasion into porous media', *Petr. Trans.* **2**, 153–162.

Gorbachev, Y., Rafikov, R., Rok, V. & Pechkov, A. (1999), 'Acoustic well stimulation: theory and application', *First Break* **17**, 331–334.

Hasimoto, H. (1959), 'On the periodic fundamental solutions of the Stokes equations and their application to viscous flow past a cubic array of spheres', *J. Fluid Mech.* **5**, 317–328.

Higdon, J. & Muldowney, P. (1995), 'Resistance functions for spherical particles, droplets and bubbles in cylindrical tubes', *J. Fluid Mech.* **298**, 193–210.

Horblit, W. (1951), De-waxing oil in ultrasonic fields, PhD thesis, Colorado School of Mines.

Hubbe, M. A. (1984), 'Theory of detachment of colloidal particles from flat surface exposed to flow', *Colloids and Surface* **12**, 151–178.

Israelachvili, J. (1985), *Intermolecular & Surface Forces*, Academic Press Inc.

Jiao, D. & Sharma, M. (1992), 'Formation damage due to static and dynamic filtration of water based muds', *SPE 23823*.

Johnson, D., Koplik, J. & Dashen, R. (1987), 'Theory of dynamic permeability and tortuosity in fluid-saturated porous media', *J. Fluid Mech.* **176**, 379–402.

Johnston, H. (1971), Polymer viscosity control by the use of ultrasonics, *in* 'Chem. Eng. Prog. Symp. Ser.', Vol. 67, pp. 39–45.

Jurrij, A. (2003), Ultrasonic well stimulation: an experimental study into the step by step ultrasonic removal of damage induced by mud particles, Master's thesis, Delft University of Technology.

Kas'yanov, D. A. & Shaloshov, G. M. (2002), Acoustic stimulation on underground leaching, *in* O. Rudenko & O. Sapozhniko, eds, 'Nonlinear Acoustics at the Beginning of the 21^{st} Century', Vol. 2.

Kaviany, M. (1995), *Principles of heat transfer in porous media*, Springer Ed.

Kelder, O. (1998), Frequency-dependent wave propagation in water-saturated porous media, PhD thesis, Delft University of Technology.

Khan, A. & Fatt, I. (1965), 'A thermoelectric device for measuring the thermal conductivity of rock', *Society of Petroleum Engineers Journal* **5**, 113–116.

Khilar, K. C. (1981), Water sensitivity of sandstone, PhD thesis, The University of Michigan.

Khilar, K. C. & Fogler, H. S. (1998), *Migration of fines in porous media*, Kluwer Academic Publishers.

Kim, S. & Karilla, S. J. (1991), *Microhydrodynamics: principles and selected applications*, Butterworth.

Kim, Y. & Wang, M. (2003), 'Effect of ultrasound on oil removal from soil', *Ultrasonics* **41**, 539 542.

Komar, C. A. (1967), 'Effects of ultrasound on appalachian paraffin', *Pet. Eng.* **39**, 60–61.

Kurose, R. & Komori, S. (1999), 'Drag and lift forces on a rotating sphere in a linear shear flow', *J. Fluid Mech.* **384**, 183–206.

Kuznetsov, O. & Efimova, S. (1983), *Application of ultrasound in oil industry*, Nedra Press (in Russian).

Ladd, A. (1994*a*), 'Numerical simulation of particulate suspensions via a discretized Boltzmann equation. part 1: Theoretical foundation', *J. Fluid Mech.* **271**, 271–309.

Ladd, A. (1994*b*), 'Numerical simulation of particulate suspensions via a discretized Boltzmann equation. part 2: Numerical results', *J. Fluid Mech.* **271**, 311 339.

Ladd, A. (1997), 'Sedimentation of homogeneous suspensions of non-brownian spheres', *Phys. Fluids* **9**, 491–499.

Leighton, D. & Acrivos, A. (1985), 'The lift on a small sphere touching a plane in the presence of a simple shear flow', *Journal of Applied Mathematics and Physics* **36**, 148 174.

Lifshitz, E. M. & Landau, L. (1987), *Fluid Mechanics: Volume 6*, Butterworth-Heinemann.

Lighthill, J. (1978), *Waves in fluids*, Cambridge University Press.

Magnaudet, J. (2003), 'Small inertial effects on a spherical bubble, drop or particle moving near a wall in a time dependent linear flow', *J. Fluid Mech.* **484**, 167–196.

Maksimov, G. A. & Radchenko, A. V. (2002), Modeling of oil output intensification due to heating process in porous permeability medium at acoustical stimulation in a well, *in* O. Rudenko & O. Sapozhniko, eds, 'Nonlinear Acoustics at the Beginning of the 21^{st} Century', Vol. 2.

McDowell, L. M., Hunt, J. R. & Sitar, N. (1986), 'Particle transport through porous media', *Water Resources Research* **22**, 815 832.

Mikhailov, D. N. (2002), Changes of phase permeability due to microprocesses of water flooding under ultrasonic action, *in* O. Rudenko & O. Sapozhniko, eds, 'Nonlinear Acoustics at the Beginning of the 21^{st} Century', Vol. 2.

Mohan, K. & Fogler, H. (1997), 'Colloidally induced smectitic fines migration: existence of microquakes', *AIChE Journal* **43**, 565–575.

Morris, B. (1974), Sonic stimulation of marginal wells, *in* 'Select paper Pap. 9', Drill. and Prod. Institute.

Neretin, V. & Yudin, V. (1981), Results of experimental study of the investigation of acoustic treatment on percolation processes in saturated porous media, *in* 'Topics in non-linear geophysics', All-Union Research Institute of Nuclear Geophysics and Geochemistry (VNIIYaGG), pp. 132–137.

Nikolaevskiy, V. N. & Stepanova, G. S. (2002), Wave action on dynamics of two-phase flow in a pay-zone of oil reservoirs, *in* O. Rudenko & O. Sapozhniko, eds, 'Nonlinear Acoustics at the Beginning of the 21^{st} Century', Vol. 2.

Nosov, V. (1965), 'Soviet progress in applied ultrasonics', Vol. 2: Ultrasonics in the chemical industry: Consultant Bureau. New York.

Patankar, N. A., Huang, P., Ho, T. & Joseph, D. (2002), 'Lift-off o a single particle in newtonian and viscoelastic fluids by numerical simulation', *J. Fluid Mech.* **445**, 67–100.

Poesio, P. & Ooms, G. (2004), 'Formation and ultrasonic removal of fouling particles structures in a natural porous material', *J. Petroleum Sci. and Eng.* **xx**, xx–xx.

Poesio, P., Ooms, G., Barake, S. & v. Bas, F. (2002), 'An investigation of the influence of acoustic waves on the liquid flow through a porous material', *J. Acoust. Soc. Am.* **111**, 2019–2025.

Poesio, P., Ooms, G., Schraven, A. & v. Bas, F. (2002), 'Theoretical and experimental investigation of acoustic streaming in a porous material', *Phys. Rev. E* **66**, 016309.

Poesio, P., Ooms, G., van Dongen, M. E. H. & Smeulders, D. M. J. (2004), 'Removal of small particles from a porous material by ultrasonic irradiation', *Trans. Porous Media* **54**, 239–364.

Ramachandran, V. & Fogler, H. (1999), 'Plugging by hydrodynamic bridging during flow of stable colloidal particles within cylindrical pores', *J. Fluid Mech.* **385**, 129–156.

Rege, S. & Fogler, H. (1987), 'Network model for straining dominated particle entrapment in porous media', *Chem. Eng. Sci.* **42**, 1553–1564.

Risnes, R., Batli, R. K., Horsrud, P. & Baker, B. A. (1982), Sand arching - a case study, *in* 'European Petroleum Conf.', Vol. SPE 12948.

Roberts, P. M., Sharma, M. & Maki, V. (1998), 'Ultrasonic reduction of wellbore deposits and formation damage', http://eee4.lanl.gov/ultrasonic.

Roberts, P., Venkitaraman, A. & Sharma, M. M. (2000), 'Ultrasonic removal of organic deposits and polymer-induced formation damage', *SPE Drilling & Completion* **15**, 62046.

Russel, W. B., Saville, D. A. & Schowalter, W. R. (1989), *Colloidal Dispersions*, Cambridge University Press.

Saffman, P. (1965), 'The lift on a small sphere in a slow shear flow', *J. Fluid Mech.* **22**, 385 400.

Sharp, K. & Adrian, R. (2001), Shear-induced arching of particle laden flows in microtubes, *in* 'ASME International Mechanical Engineering Congress and Exposition', Vol. 2.

Shaw Resource Service Inc. (1992). Sona-Tool test information. Sonic Well stimulation research push. Indep. Petr. Montly, 40.

Sherbome, J. (1954), 'Recovery of hydrocarbons', *USA Patent 2670801.*

Simkin, E. & Surguchev, M. (1991), Advanced vibroseismic techniques for water flooded reservoir stimulation. mechanisms and field results, *in* 'Proc. 6^{th} Europ. Symp. on improved oil recovery', pp. 233–241.

Sokolov, A. & Simkiv, E. (1981), Study of the influence of acoustic treatment on rheological properties of some oils, *in* 'Topics in non-linear geophysics', All-Union Research Institute of Nuclear Geophysics and Geochemistry (VNIIYaGG), pp. 137–142.

Succi, S. (2001), *Lattice-Boltzmann Equation for Fluid Dynamics and Beyond*, Oxford University Press.

Suri, A. & Sharma, M. (2001), 'Strategies for sizing particles in drilling and completion fluids', *SPE 68964*.

Tambini, M. (2003), Beyond acidizing and fracturing, *in* 'SPE European Formation Damage Conference', Vol. SPE 82573.

Timoshenko, S. & Goodier, J. (1951), *Theory of Elasticity*, McGraw-Hill.

Tutuncu, A. & Sharma, M. (1992), 'The influence of fluids on grain contact stiffness and frame moduli in sedimentary rocks', *Geophysics* **57**, 1571–1582.

v. Bas, F., Zuiderwijk, P., Wong, S.-W., v. Batenburg, D., Birchak, B. & Yoo, K. (2004), 'Radial near wellbore stimulation by acoustic waves', *SPE 86492*.

Ven, T. V. D. (1989), *Colloidal Hydrodynamics*, Academic Press Inc.

Venkitaraman, A., Roberts, P. & Sharma, M. (1995), 'Ultrasonic removal of near-wellbore damage caused by fines and mud solids', *SPE Drilling & Completion* **10**, 27388.

Vetter, O., Kandarpa, V., Stratton, M. & Veith, E. (1987), 'Particle invasion into porous medium and related injectivity problems', *SPE 16255*.

White, F. M. (1991), *Viscous Fluid Flow*, McGraw-Hill.

Wong, S.-W., v. Bas, F., Groenenboom, J. & Zuiderwijk, P. (2003), 'Near wellbore stimulation by acoustic waves', *SPE 82198*.

Wu, K., Xue, Q. & Adler, L. (1990), 'Reflection and transmission of elastic waves from a fluid-saturated porous solid boundary', *J. Acoust. Soc. Am.* **87**, 2349–2358.

Zaytsev, S. & Aseyev, V. (1992), *Properties of Aqueous Solution of electrolytes*, CRC press.

Acknowledgment

This project was financially supported by FOM. The experimental set-up and the measurement apparatus were provided by Shell E. & P. (Rijswijk, The Netherlands). I am very grateful to this two institutions.

I would like to thank my supervisor prof. dr. ir. G. Ooms for his support and for his availability to provide me help whenever it was necessary. Gijs has been an excellent Teacher, not only for the scientific knowledge that he passed on to me, but also for my general development. I would also like to thank prof. dr. ir. M.E.H. van Dongen and dr. ir. D.M.J. Smeulders for the stimulating discussions and suggestions that greatly improved this work.

I am indebted to Ing. F. v. Bas for the discussions on the application of ultrasonic cleaning in the near wellbore region of oil reservoirs. These discussions were a continuous source of inspiration for my work.

I would like to thank dr. R.-E. Plessix for his support on a number of issues and for discussing with me the physics (and the mathematics) of wave propagation through porous media. I am grateful to dr. P.M. Roberts (Los Alamos National Laboratory) who invited me at his laboratory to give a lecture on ultrasonic stimulation of porous media. Peter was also so kind to share with me his deep understanding of the physics involved.

I am grateful to prof. dr. ir. F.T.M. Nieuwstadt for receiving me at the Laboratory for Aero- and Hydrodynamics at Delft University of Technology. Most of this research was carried out at Shell E.& P. (Rijswijk, The Netherlands) therefore I would like to acknowledge dr. Michiel Groeneveld for receiving me in his team.

Finally, I would like to acknowledge my parents, Angelo and Linda, and my girlfriend, Monica, for their support, love and encouragement during all those years and for all the coming ones.

About the Author

Pietro Poesio was born in Desenzano del Garda (Italy) on April 7^{th} 1975. He graduated with honors in July 2000 in Mechanical Engineering at Università degli Studi di Brescia with a thesis on the solidification of binary alloys. In October 2000, Pietro joined the Laboratory for Aero- and Hydrodynamics for his Ph.-D. project on the effect of ultrasounds on liquid fluid flow through porous media. The main part of this project was carried out in Shell E. & P. (Rijswijk, The Netherlands). He has published several papers in international journals and he has attended to many conferences all around the world. In February 2004, Pietro Poesio was invited to Los Alamos National Laboratory (USA) to give a lecture entitled *Removal of fine particles from porous media by ultrasonic irradiation. Experiments and Modeling.* He has also worked on liquid-liquid two phase flow in pipes.

Recently, he has started working as Assistant Professor at Università degli Studi di Brescia in the group of Thermal and Fluid Science. Currently, he is carrying his research on two-phase flows and spinodal decomposition.

Journal contributions

- P. Poesio, G. Ooms, S. Barake, and F.v. Bas. "An investigation of the influence of acoustic waves on the liquid flow through a porous material". *J. Acoust. Soc. Am.*, **111**(5):2019–2025, 2002.

- P. Poesio, G. Ooms, A.P. Schraven, and F.v. Bas. "Theoretical and experimental investigation of acoustic streaming in porous material". *Phys. Rev. E* **66**:016309, 2002.

- G. Ooms and P. Poesio, "Stationary core-annular flow through horizontal pipe", *Phys. Rev. E* **68**:066301, 2003.

- P. Poesio, G. Ooms, M.E.H. v. Dongen, and D.M.J. Smeulders. "Removal of small particles from a porous material by ultrasonic irradiation". *Transport in Porous Media*, **54**(3): 239-264, 2004.

- P. Poesio and G. Ooms. "Particle bridge formation and removal from porous media by ultrasonic irradiation". *Accepted for publication in J. Petroleum Sci. and Eng.*, 2004.

- P. Poesio, A. Jurrij and G. Ooms, Fouling by external particles and ultrasonic cleaning of a porous material. Submitted to Journal of Petroleum Science Engineering.

- P. Poesio and G. Ooms. Acoustic removal of clay particles from Berea sandstone. Submitted to SPE Production Facilities.

- P. Poesio, G. Ooms, J.C.R. Hunt and A. ten Cate. How particles interact and form strings and bridges in a shear flow. Submitted to J. Fluid Mech.

- P. Poesio and G. Ooms. Simulation of particle bridge removal by ultrasonic irradiation. Submitted to AIChE J.

Conference contributions

- S. Barake, F. van der Bas, G. Ooms and P. Poesio. An experimental and theoretical investigation of the influence of high-frequency acoustic waves on the flow of a liquid through a porous material. EAGE/SEG RESERVOIR ROCKS RES. WORKSHOP, in EXTENDED ABSTR. PAPER NO. PAU45SEG/EAGE, Pau (France), April 2001. ISBN 90-73781-16-7.

- P. Poesio and G. Ooms. Experimental investigation of the ultrasonic cleaning of the near well bore region of an oil reservoir. 16th International Symposium on Non-Linear Acoustics, in NONLINEAR ACOUSTICS AT THE BEGINNING OF THE 21^{st} CENTURY Vol.2, Editors Rudenko and Sapozhnikov, pp. 1229-1232, Moscow (Russia), August 2002. ISBN: 5-8297-0035-4.

- P. Poesio, G. Ooms, A. Schraven and F. van der Bas. Experimental and theoretical study of acoustic streaming in porous media. 2^{nd} Biot Conference on Poromechanics, in POROMECHANICS II, Editors: Auriault et al., pp. 763-768, Grenoble (France), August 2002. ISBN: 9-0580-9394-8.

- P. Poesio and G. Ooms. Theoretical and Experimental Study of the Removal of Small Particles from a Porous Material by Ultrasonic Irradiation. A.I.Ch.E. Annual meeting. Indianapolis (Indiana). November, 2002.

- P. Poesio and G. Ooms. Influence of ultrasonic waves on flow rate through porous media: experimental and theoretical study. IUTAM Symposium on Mechanics of Physicochemical and Electro-mechanical interaction in Porous Media. Eindhoven (The Netherlands), May 2003.

- P. Poesio and G. Ooms. Particle-bridges formation inside porous material. 5^{th} Euromech. Fluid Mechanics Conference, in Book of Abstracts, p. 232, Toulouse (France), August 2003.

- P. Poesio and G. Ooms. Acoustic removal of clay particles from Berea sandstone. International Symposium on Formation Damage Control. SPE86490. Lafayette (Louisiana), February 2004.

- P. Poesio and G. Ooms. The levitation force on the core in a stationary core-annular flow through a horizontal pipe. 3^{rd} International Symposium on two-phase flow modeling and experimentation. Pisa (Italy), September 2004.

- P. Poesio, G. Ooms, J.C.R. Hunt and A. ten Cate. How particles interact and form strings and bridges in a shear flow. 57^{th} Annual Meeting of APS Division of Fluid Dynamics will, Seattle, Washington, November 21-23, 2004.

- P. Poesio and G. Ooms. Simulation of removal of particle bridge formation by ultrasonic stimulation. 3^{rd} Biot Conference on Poromechanics. Norman (Oklahoma), May 2005.